

**Modeling and Simulation of Morphological
Phenomena in Discotic Mesophases subjected
to Extensional Flows**

by

Arvinder Pal Singh

**Department of Chemical Engineering
McGill University, Montreal**

August 1994

**A Thesis submitted to the Faculty of Graduate Studies and Research
in partial fulfillment of the requirements for the degree of
Master of Engineering**

© Arvinder Pal Singh, 1994

Abstract

Carbonaceous mesophases are naturally occurring discotic nematic liquid crystals which are used as precursor materials for the manufacture of high performance mesophase carbon fibers. The anisotropic structure of discotic mesophases imparts superior mechanical, thermal, and chemical properties to mesophase carbon fibers. To control the microstructure of discotic mesophases during the spinning processes a basic rheological understanding of these materials in extensional flows is required. The quantitative description and classification of the main morphological phenomena during the extensional flows of discotic mesophases is the central theme of this work.

In the first part of the present study, a phenomenological theory describing the microstructure of discotic mesophases under the influence of extensional flows is developed. The theory is then used to develop the governing equations for the uniaxial extensional flow of uniaxial discotic mesophases, which is the main type of flow encountered in the spinnline of the fiber-spinning manufacturing process. The driving forces for flow-induced morphological phenomena are identified. The unit sphere description is used to discuss and classify the analytical and numerical results. Parametric studies are performed using the alignment Deborah number, the nematic potential, and different initial microstructural conditions. The average orientation of the mesophase fluid is found to lie anywhere in a plane perpendicular to the extension direction, which agrees with existing experimental observations.

In the second part of this thesis, the theory is generalized to describe the microstructure of discotic mesophases in various types of extensional flows. A comprehensive flow classification based on the orienting strength and aligning strength of various industrially relevant flows is given.

In the last part of the thesis, the theory is extended to model flow-induced biaxiality in uniaxial discotic liquid crystals subjected to uniaxial extensional flows. Analytical and numerical solutions of the characterizing microstructural fields are given. The main flow-induced morphological phenomena is efficiently captured by projecting the results into orientation and alignment phase diagrams.

Résumé

A l'état naturel, les mésophases carboniques sont des cristaux liquides nématiques discotiques. Matériaux précurseurs, ils sont utilisés à la préparation de fibres de carbone mésophasique de haute performance. La structure anisotrope des mésophases discotiques augmente les propriétés mécanique, thermique et chimique, des fibres de carbone mésophasique. Pour contrôler la microstructure des mésophases discotiques pendant les processus de filage, une compréhension de base de la rhéologie de ces matériaux sous des conditions d'écoulements extensionnels est nécessaire. La description quantitative et la classification du phénomène morphologique principal, pendant les écoulements extensionnels des mésophases discotiques, constituent l'idée centrale de ce travail.

La première partie de cette étude développe une théorie phénoménologique décrivant la microstructure des mésophases discotiques sous l'influence d'écoulements extensionnels. La théorie est par la suite utilisée à développer les équations gouvernant l'écoulement extensionnel uniaxial des mésophases discotiques uniaxiaux, type d'écoulement principalement rencontré dans la ligne de filage du procédé de préparation des fibres. Les forces motrices des phénomènes morphologiques induit par l'écoulement sont identifiées. La description de sphère unité est utilisées afin de discuter et classer les résultats analytiques et numériques. Les études paramétriques réalisées utilisent le nombre d'alignement de Deborah, le potentiel nématique et les différentes conditions initiales des microstructures. L'orientation moyenne du fluide mésophasique se trouve n'importe où dans un plan perpendiculaire à la direction d'extension; ce qui est en accord avec les observations expérimentales existantes.

La théorie est généralisée dans la deuxième partie de cette thèse afin de décrire la microstructure des mésophases discotiques dans divers types d'écoulements extensionnels. Une classification compréhensive de l'écoulement, basée sur les tensions orientant et alignant les divers écoulements utilisés industriellement, est présentée.

Dans la dernière partie de cette thèse, la théorie est approfondie pour modéliser la biaxialité induite par l'écoulement dans le cas de cristaux liquides discotiques uniaxiaux soumis aux écoulements extensionnels uniaxiaux. Des solutions analytiques et numériques aux champs microstructuraux caractéristiques sont présentés. Le phénomène morphologique principal induit par l'écoulement est efficacement illustré en projetant les résultats sous forme de diagrammes de phase pour l'orientation et l'alignement.

Acknowledgements

I wish to express my deepest gratitude to my thesis supervisor, Professor A. D. Rey, for his help in understanding the problem considered in this thesis and for his encouragement, valuable guidance, support and especially for suggesting this interesting problem. I will always be indebted regarding what I learned from him about dedication and perseverance.

I would also like to thank all my colleagues in the Workman Wing, especially my officemates Won Hee Han and Philip Chan, for their helpful discussion and advice.

Lastly, I wish to thank my family for their love, support, encouragement and understanding.

Table of Contents

Abstract.....	1
Résumé.....	ii
Acknowledgements.....	iii
Table of Contents.....	iv
Nomenclature.....	viii

Chapter 1

Introduction

1.1.	Historical Note and Introductory Comments.....	1
1.2.	Types of Liquid Crystals.....	2
1.2.1.	Thermotropic Liquid Crystals.....	2
1.2.2.	Lyotropic Liquid Crystals.....	3
1.3.	Structural Classification.....	3
1.3.1.	Nematic Order.....	3
1.3.2.	Cholesteric order.....	4
1.3.3.	Smectic Order.....	4
1.4.	Discotic Phases.....	5
1.5.	Carbonaceous Mesophases.....	6
1.6.	Carbon Fibers.....	11
1.7.	Spinning of Mesophase Pitch.....	11
1.8.	Morphology of Mesophase Pitch-Based Carbon Fibers.....	14
1.9.	Nematic Ordering.....	15
1.10.	Extensional Flows.....	17

1.11.	Orientation Distribution Function.....	18
1.12.	Thesis Objectives.....	19
1.13.	Thesis Organization.....	20
1.14.	References.....	21

Chapter 2

Extension Dynamics of Discotic Nematics of Variable Order : Geodesic Flow and Viscoelastic Relaxation

2.1.	Abstract.....	22
2.2.	Introduction.....	23
2.3.	Governing Equations.....	25
2.3.1.	Definition of Coordinates, Orientation and Alignment.....	25
2.3.2.	Governing Orientation and Alignment Equations.....	28
2.3.3.	Governing Equations for Uniaxial Extensional Start-up Flow.....	34
2.4.	Results and Discussions.....	36
2.4.1.	Director Dynamics : Geodesic Flow and Viscoelastic Relaxation.....	36
2.4.2.	Alignment Viscoelastic Relaxation and Flow-Induced Melting.....	38
2.4.3.	Tensor Order Parameter Relaxation and Flow Birefringence.....	42
2.5.	Conclusions.....	46
2.6.	Appendix.....	46
2.7.	References.....	48

Chapter 3

Computer Simulation of Dynamics and Morphology of Discotic Mesophases in Extensional Flows

3.1.	Abstract.....	50
3.2.	Introduction.....	50

3.3.	Governing Equations.....	53
3.3.1.	Definition of Coordinates, Kinematics, Orientation and Alignment .	53
3.3.2.	Governing Orientation and Alignment Equations.....	57
3.4.	Analytical Results.....	61
3.4.1.	Director Dynamics.....	61
3.4.2.	Alignment Dynamics.....	64
3.5.	Numerical Results.....	66
3.5.1.	Orientation Relaxation.....	66
3.5.2.	Alignment Viscoelastic Relaxation.....	69
3.5.3.	Tensor Order Parameter Relaxation and Flow Birefringence.....	70
3.6.	Conclusions.....	72
3.7.	References.....	74

Chapter 4

Theory and Simulation of Extensional Flow-Induced Biaxiality in Discotic Mesophases

4.1.	Abstract.....	77
4.2.	Introduction.....	78
4.3.	Theory and Governing Equations.....	80
4.3.1.	Definition of Coordinates, Kinematics, Orientation and Alignment.....	80
4.3.2.	Governing Equations for Uniaxial Extensional Start-up Flow.....	86
4.3.3.	Analytical Results.....	91
4.3.3.1.	Director Triad Dynamics.....	91
4.3.3.2.	Uniaxial Alignment Dynamics.....	94
4.3.4.	Selection of Phenomenological Parameters.....	97
4.4.	Numerical Results.....	98
4.4.1.	Uniaxial and Biaxial Orientation Relaxation.....	98

4.4.2.	Uniaxial and Biaxial Alignment Relaxation.....	101
4.5.	Conclusions.....	107
4.6.	Appendix A.....	110
4.7.	Appendix B.....	113
4.8.	References.....	114

Chapter 5

Thesis Summary, Conclusions and Recommendations

5.1.	Thesis Summary.....	116
5.2.	Thesis Conclusions.....	117
5.3.	Recommendations.....	120

NOMENCLATURE

UPPER CASE LETTERS

A	Symmetric part of the velocity gradient tensor (rate of deformation tensor)
$\tilde{\mathbf{A}}$	Dimensionless rate of deformation tensor
A, B, C	Temperature dependent phenomenological coefficients
De	Alignment Deborah number (dimensionless extension rate)
F	External body force per unit volume
G	Excess free energy density
H(t)	Step function
I	Unit tensor
K	Boltzmann's constant
N	Co-rotational time derivative of the (uniaxial) director \mathbf{n}
N_d	Uniaxial discotic nematic phase
O(n)	Trajectory of director on the surface of the sphere
P	Projection operator
P	Biaxial scalar order parameter
$\dot{\mathbf{P}}$	Time derivative of biaxial scalar order parameter
Q	Tensor order parameter
$\dot{\mathbf{Q}}$	Time derivative of tensor order parameter \mathbf{Q}
$\hat{\mathbf{Q}}$	Co-rotational time derivative of \mathbf{Q}
R⁻ (R₁), R⁺ (R₂)	Representative regions on the surface of a unit sphere

S	(Uniaxial) scalar order parameter
S_c	Scalar order parameter corresponding to temperature T_c
$S^\#$	Scalar order parameter corresponding to temperature $T^\#$
S^*	Scalar order parameter corresponding to temperature T^*
S_0	Initial (uniaxial) scalar order parameter
S_{eq}	Equilibrium scalar order parameter
S_{ss}	Steady state scalar order parameter
\dot{S}	Time derivative of (uniaxial) scalar order parameter S
T	Absolute temperature
T_c	Nematic-isotropic transition temperature
$T^\#$	Absolute Temperature at the boundary of biphasic region and single isotropic region
T^*	Absolute Temperature at which the isotropic phase is metastable
U	nematic potential
W	Antisymmetric part of velocity gradient tensor

LOWER CASE LETTERS

a, b, d_1, d_2	Constants
e	Dielectric tensor
e_\perp	Element of the dielectric tensor e normal to (uniaxial) director n
e_\parallel	Element of the dielectric tensor e parallel to (uniaxial) director n
$\hat{i}, \hat{j}, \hat{k}$	Unit vectors along x, y, z axes in the Cartesian coordinate system
l	Biaxial director
l_0	Initial biaxial director l orientation
l_{ss}	Steady state biaxial director l orientation

l_x, l_y, l_z	Components of biaxial director l
l_{x0}, l_{y0}, l_{z0}	Initial components of biaxial director l
$l_{xss}, l_{yss}, l_{zss}$	Steady state components of biaxial director l
m	Biaxial director
\mathbf{m}_0	Initial biaxial director m orientation
\mathbf{m}_{ss}	Steady state biaxial director m orientation
m_x, m_y, m_z	Components of biaxial director m
m_{x0}, m_{y0}, m_{z0}	Initial components of biaxial director m
$m_{xss}, m_{yss}, m_{zss}$	Steady state components of biaxial director m
n	(Uniaxial) director
\mathbf{n}_\perp	Projection of (uniaxial) director n on y-z plane
\mathbf{n}_\parallel	Projection of (uniaxial) director n on x-axis
$\dot{\mathbf{n}}$	Time derivative of (uniaxial) director
\mathbf{n}_0	Initial (uniaxial) director n orientation
\mathbf{n}_{ss}	Steady state (uniaxial) director n orientation
n_x, n_y, n_z	Components of biaxial director
n_{x0}, n_{y0}, n_{z0}	Initial components of (uniaxial) director n
$n_{xss}, n_{yss}, n_{zss}$	Steady state components of (uniaxial) director n
p	Pressure
t	Time
u	Displacement vector; unit normal to the disc-like molecule
$\mathbf{v}(x, y, z)$	Velocity field
$v_{i,j}$	Velocity gradient tensor
x, y, z	Cartesian coordinates

GREEK LETTERS

λ	Reactive parameter or tumbling function
γ_1	Rotational viscosity
γ_2	Irrotational viscosity or irrotational torque coefficient
θ	(Uniaxial) director \mathbf{n} polar angle
ϕ	(Uniaxial) director \mathbf{n} azimuthal angle
ψ	Biaxial director \mathbf{m} polar angle
α	Biaxial director \mathbf{m} azimuthal angle
ω_1	Polar angle of the unit normal \mathbf{u} of the disc-like molecule
ω_2	Azimuthal angle of the unit normal \mathbf{u} of the disc-like molecule
$\dot{\epsilon}$	Constant extension rate
ϵ	Strain (dimensionless time)
Δ	Entropy production density
σ_i ($i=1,7$); τ_i ($i=1,6$)	Dimensional scalar phenomenological constants
$\sigma_4^*, \sigma_6^*, \tau_2^*, \tau_6^*$	Dimensionless phenomenological parameters
Λ	Free energy density
Λ^H	Entropic contribution to free energy density
Λ^F	Flow contribution to free energy density
λ_j^i ; $i=\mathbf{n}, \mathbf{l}$; $j=\mathbf{n}, \mathbf{l}$, mix	Set of reactive parameters
$\beta_{1,j}^i$; $i=\mathbf{n}, \mathbf{m}$; $j=\mathbf{S}, \mathbf{P}$	Set of ordering functions
$\beta_{2,j}$; $j=\mathbf{S}, \mathbf{P}$	Set of elastic functions

Chapter 1

Introduction

1.1. Historical Note and Introductory Comments

Many organic compounds do not undergo a single phase transition from the solid to the liquid phase, but assume one or more intermediate states called mesophases [1, 2, 3, 4]. The mesomorphic materials possess both liquid-like fluidity and solid-like molecular order. In solid crystals the centers of mass of the molecules are located on a three-dimensional periodic lattice, hence they have both orientational as well as positional order. In the case of isotropic liquids only short range order among the molecular centers of mass is present. The ordering in mesophases (or mesomorphic or anisotropic liquids) lies between that of a solid and that of an isotropic liquid. Based on the partial ordering two basically different types of mesophases have been observed [1, 2]. First, there are those in which the positional order is still present but the orientational order has disappeared or is strongly reduced, and are called disordered crystal mesophases or plastic crystals [1, 2]. Second, there are those in which the positional order is reduced or has even completely disappeared but exhibit long range orientational order, and are called ordered fluid mesophases or liquid crystals [1, 2]. A particular type of liquid crystal is investigated in this thesis.

The shape of the molecule is an important criteria for mesomorphism to occur. Since early investigations of liquid crystalline behavior the accepted fact, until recently, was that for thermotropic mesomorphism to occur the molecules have to be rod-like in shape. It was discovered in the last decade that compounds composed of disc-like molecules also show stable thermotropic mesomorphism and are generally known as discotic liquid crystals or discotic mesophases. The first discotic liquid crystal was prepared and identified in 1977 [5]. A number of synthetic [6, 7, 8] and naturally occurring [9, 10, 11, 12] discotic liquid crystals have been discovered.

Naturally occurring carbonaceous mesophases display discotic crystalline behavior and are derived from the pyrolysis of the coal or petroleum pitches [9, 10, 13]. This low cost mesophase is used as a precursor material for the manufacture of high

performance carbon fibers, which are currently competing with the more expensive carbon fibers derived from polymer textile yarns, such as PAN (poly-acrylonitrile) [14]. The basic knowledge of how to control the physical properties of high performance mesophase carbon fibers is lacking but is essential for their continuous commercial development. In particular, the process of melt spinning, in which planar disc-like molecules become oriented along the fiber axis [13, 14, 15, 16], is dependent on the rheological and the viscoelastic behavior of the material. In addition, it is known that the molecular arrangement in the cross section of fibers controls the mechanical properties such as tensile strength and the Young's modulus of fibers [9, 14, 15, 16]. To develop a basic scientific understanding of the mesophase carbon fiber spinning process, an understanding of the extensional rheology of discotic nematic liquid crystals is therefore essential. The general objective of this thesis is to elucidate, using theory and simulation, the fundamental couplings between processing and morphology, such as the effect of an extensional processing flow on the development of molecular orientation. This thesis considers, in addition to spinning flows, other frequently industrially used extensional flows, such as biaxial extension and planar extensional flow [17]

The rest of this chapter gives a brief presentation of the main quantities and phenomena required to quantitatively specify the flow-morphology relations of potential relevance to the mesophase carbon fiber spinning process. We start with a brief description of mesophase behavior and molecular ordering in liquid crystalline phases, and then focus our discussion on discotic mesophases, including the carbonaceous mesophases which are precursors for mesophase pitch-based carbon fibers. We next identify relevant issues concerning flow-microstructure-product properties, which motivate the practical utility of the present study. Then we define the quantitative tensorial measures of microstructure and morphology, which form part of the model equations presented and used in chapters 2, 3, and 4. Subsequently we present the kinematic quantities that specify various extensional flows, used in chapters 2, 3 and 4, and present the orientation distribution function. Finally we present the thesis objectives and organization.

1.2. Types of Liquid Crystals

1.2.1. Thermotropic Liquid Crystals

Single component systems that show mesomorphic behavior in a definite temperature range are called thermotropic liquid crystals. Every molecule in the thermotropic liquid crystalline phase participates in the long range ordering.

Thermotropics are of interest for applications in electro-optical display, temperature and pressure sensors, organic fibers, special materials of construction such as bullet proof jackets, etc. [1]. Most computer and watch displays use mixtures of low molecular weight rod-like nematic liquid crystals, such as 8CB(p-octyl-p'-cyanobiphenyl).

1.2.2. Lyotropic Liquid Crystals

Lyotropics show mesomorphic behavior in solution and are usually the solutions of rigid molecules in strong solvents [1, 2]. A well known example is Kevlar, which is a solution of (Poly(p-phenylene terephthalamide)) in sulphuric acid. The temperature range in which lyotropics exist is mainly determined by the concentration. The long range ordering is controlled by mainly the rod-like molecules (solute). Lyotropic liquid crystals are of great interest biologically and appear to play an important role in living systems [1].

1.3. Structural Classification

Based on the nomenclature proposed originally by Friedel in 1922, liquid crystals can be classified according to their molecular order into three major classes : nematic, cholesteric, and smectic.

1.3.1. Nematic Order

Figure 1 shows schematic representation of the nematic phase. The molecules tend to align parallel to each other and along some common axis called director \mathbf{n} . The director is a unit vector ($\mathbf{n} \cdot \mathbf{n} = 1$), and gives the average preferred orientation. Long range orientational order and cylindrical (or uniaxial) symmetry are exhibited by this liquid crystalline phase. The centers of gravity of the molecules are distributed at random. Thus, they possess orientational order like crystals and positional disorder like viscous phases [3, 4].

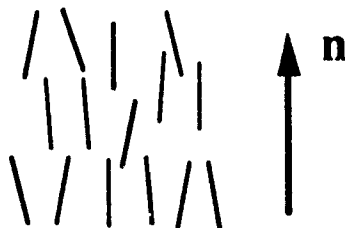


Fig. 1. Schematic representation of nematic order in liquid crystals.

1.3.2. Cholesteric Order

Figure 2 shows the schematic of the equilibrium structure of the cholesteric phase. The lack of long range translational order imparts fluidity to the cholesteric phase. On a local scale, the cholesteric order is similar to the nematic order, since the molecules tend to align along the director \mathbf{n} . On a larger scale, the cholesteric director follows a helical path given in a Cartesian coordinate system as [3]:

$$\mathbf{n} = (n_x, n_y, n_z) = (\cos(q_0 z + \Phi), \sin(q_0 z + \Phi), 0) \quad (1)$$

where q_0 is the wave vector and Φ is the arbitrary phase angle. The sign of q_0 correspond to left or right helices, and determines the magnitude the spatial period P [3] of the twisted planar cholesteric structure; the spatial period or pitch is given by :

$$P = \frac{\pi}{|q_0|} \quad (2)$$

Equation (2) shows that as $q_0 \rightarrow 0$ then $P \rightarrow \infty$, and the cholesteric liquid crystals becomes a nematic liquid crystals [3].

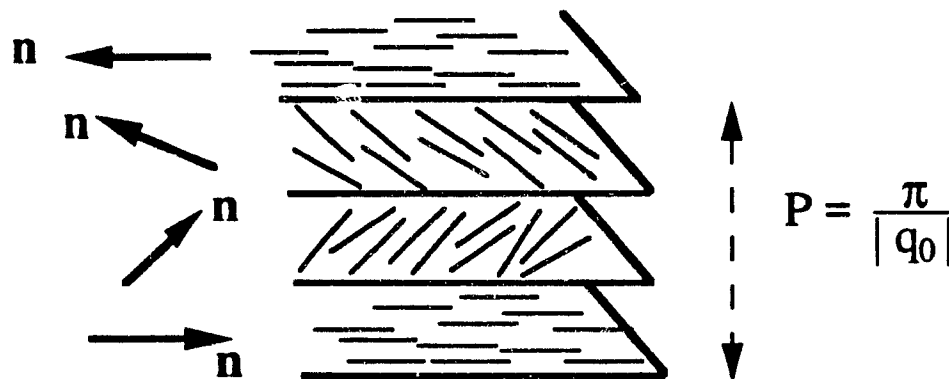


Fig. 2. Schematic representation of the cholesteric order.

1.3.3. Smectic Order

A smectic phase has, in addition to the orientation order of nematics and cholesterics, a single degree of translational order which results in a layered structure.

The various ellipses represent discs which are tilted with respect to the column axis. To summarize, the columnar phase has long range translational periodicity in two dimensions and liquid-like disorder in the third dimension. The columnar phase of discotic liquid crystals is not considered in this thesis, and therefore will not be discussed further.

Figure (5f) show a schematic of the nematic phase (N_d). This phase is found to be exhibited by relatively a few compounds (see figure 4b,e). The nematic phase of discotics has an orientationally ordered arrangement without any long-range translational order [4]. Discotic nematics, in contrast to the rod-like nematics, are optically negative and the director \mathbf{n} represents the preferred orientation of the short molecular axis (or the normal to the disc-like molecule). Only discotic nematics of the type shown in figure (5f) are investigated in this thesis.

1.5. Carbonaceous Mesophases

The carbonaceous mesophase is a uniaxial discotic nematic liquid crystalline thermodynamic phase, which forms during the liquid phase pyrolysis of coal or petroleum pitches, and is used as precursor in the manufacture of high performance mesophase carbon fibers [19]. Figure 6 shows the thermodynamic and structural changes brought about by heating a non-volatile organic compound, such as coal or petroleum pitch, in the absence of air [9]. The organic substance melts on heating and becomes an isotropic pitch or liquid. As the temperature rises over about 350° C, optically anisotropic spheres, known as spherules, appear in the isotropic matrix [10, 19, 20]. As the hydrogenative polymerization reactions continues the molecules get larger and the mesophase more viscous. When the molecules reach an average molecular weight of approximately 2000 they are, apparently, sufficiently large and flat to favor the formation of a liquid crystalline nematic phase called the carbonaceous mesophase.

The formation of the carbonaceous mesophase follows a nucleation and growth process, typical of metastable thermodynamic systems. The droplets or spherules are easily observed because of their optical anisotropy. Attractive forces among the spherules give rise to droplet coalescence and overall growth of the mesophase. The structure of the spherules and the molecular organization of the disc-like aromatic molecules within the spherules has been described by Brooks and Taylor (1965) [12]. The characteristic mesophase mechanisms that are involved in establishing the mesophase morphology are spherule precipitation, coalescence of spherules to form a bulk mesophase, and distortion of mesophase by mechanical deformation.

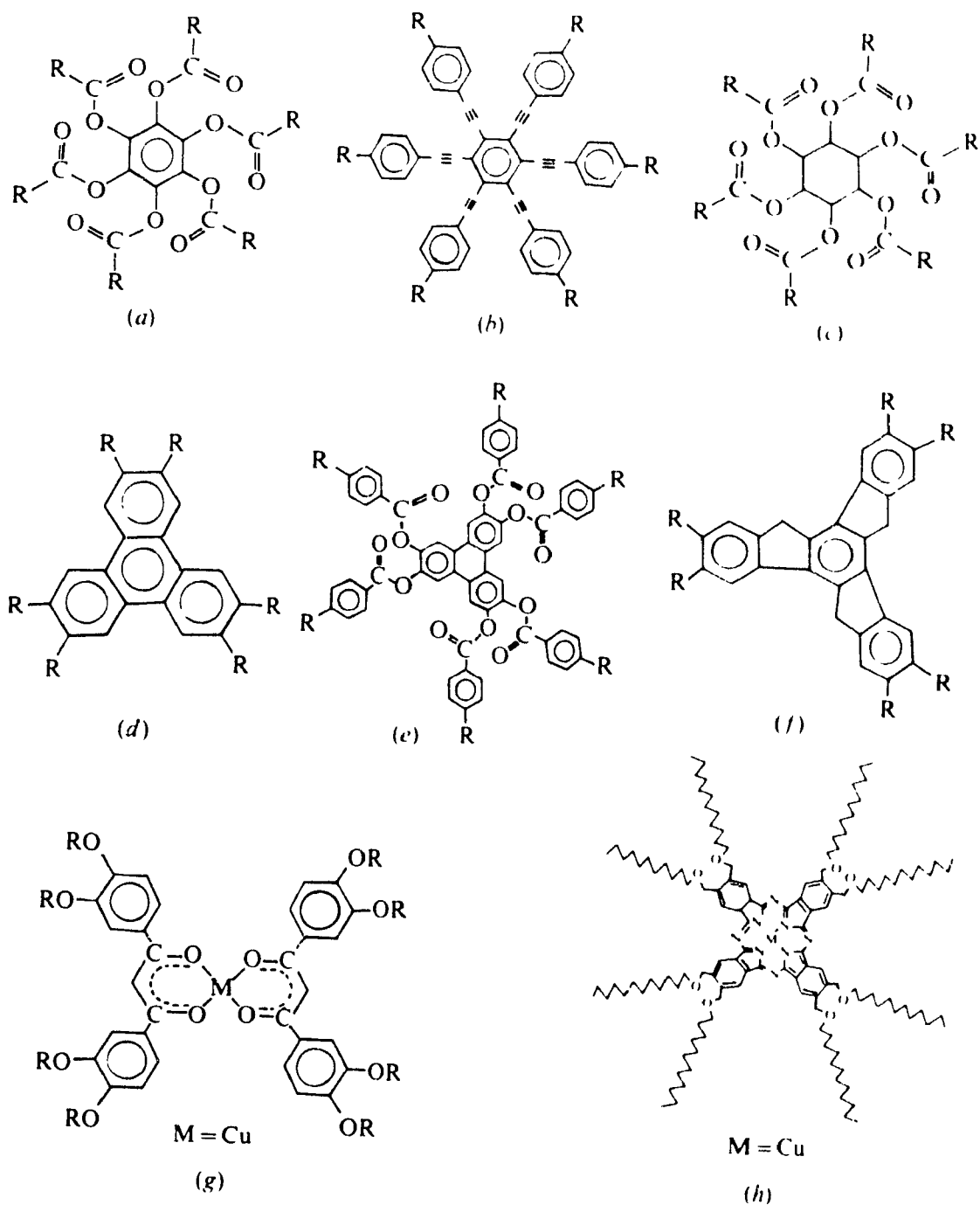


Fig. 4. Examples of disk-like molecules which display discotic mesophorism: (a) hexa-*n*-alkanoates of benzene, (b) hexakis ((4-octylphenyl)ethynyl)benzene, (c) hexa-*n*-alkanoates of scylloinositol, (d) hexa-*n*-alkanoates of triphenylene and hexa-*n*-alkoxytriphenylene, (e) hexa-*n*-alkyl and alkoxybenzoates of triphenylene, (f) hexa-*n*-alkanoates of truxene, (g) bis(3,4-nonyloxybenzoyl)methanato copper(II), and (h) octasubstituted metallophthalocyanine. Reprinted from [4].

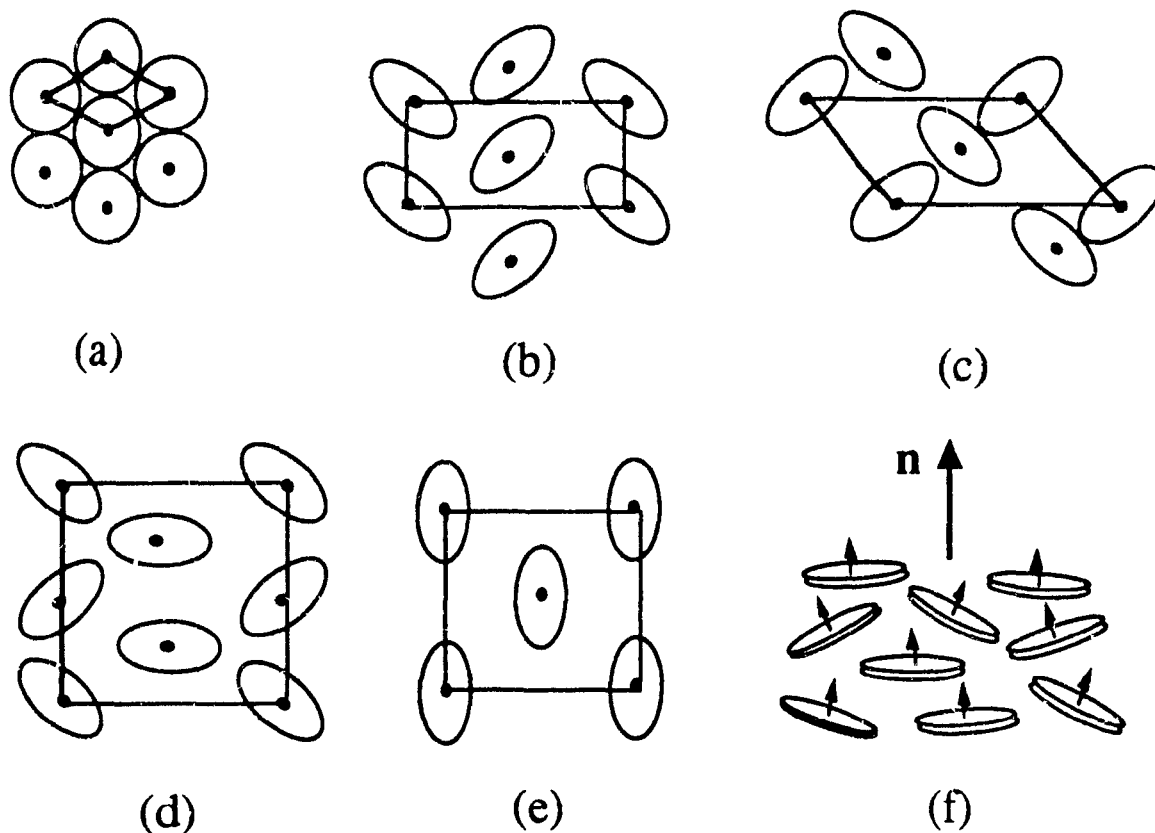


Fig. 5. (a)-(e) Top view of the columnar phases of disc-like molecules. The column axis is pointing out of the plane of paper, and the ellipses represent the discs which are tilted with respect to the column axis. (f) Side view of a typical discotic nematic liquid crystal.

The carbonaceous mesophase consists of disc-like molecules that display long range orientational order, such that the molecules lie approximately parallel to each other and there is no point-to-point registry between adjacent molecules. The orientation of each molecule is defined by its unit normal. The symmetry elements of the carbonaceous mesophase are [19]:

- (a) any translation;
- (b) any rotation about the unit normal to the disc-shape molecule;
- (c) a rotation of π radians about any axis parallel to the plane of the molecule.

Although the degree of symmetry is the same for a discotic nematic and conventional rod-like nematic crystal the fact that for the discotic nematic the axis of symmetry is normal to the long dimensions of the molecule has an important consequences for optical properties, the response to mechanical stress, and the alignment in external fields such as extensional flows, electric fields, and magnetic fields. In this thesis we focus on the distinguishing features of flow-induced orientation of discotic mesophases. A schematic model of carbonaceous mesophase formation is shown in figure 7 [19]. This model suggests that the stacking, size, and the possible shapes of disc-like molecules which may be quite irregular and have vacant sites or holes

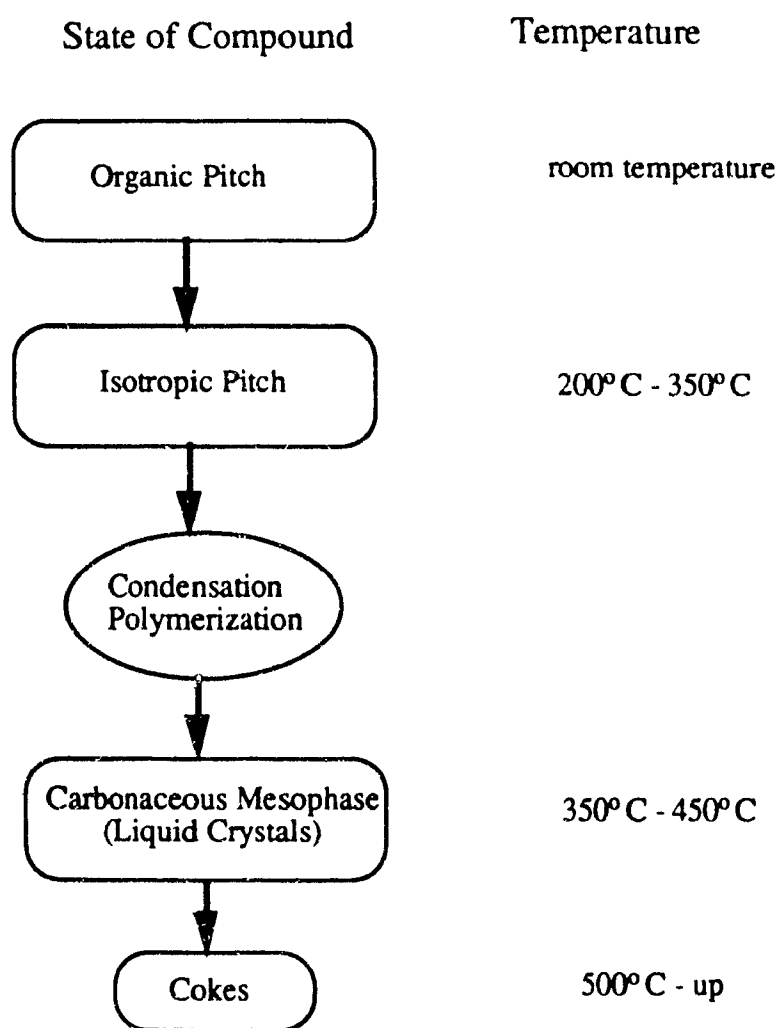


Fig. 6. Changes in the non-volatile organic compounds like coal or petroleum pitches brought about by heating in the absence of air [9].

The main microstructural features of the carbonaceous mesophases (uniaxial discotic nematic liquid crystals) are captured by the director \mathbf{n} , and by the degree of orientation order S . The director \mathbf{n} is a unit vector that describes the direction of the average molecular orientation of the unit normal to the disc-like molecules, and S is a measure of the average molecular alignment along \mathbf{n} . In discotic nematics the unit molecular normals are more or less aligned along \mathbf{n} . The dispersion of molecular orientation along \mathbf{n} is captured by the magnitude of S : when $S = 0$ the phase is isotropic, and when $S = 1$ all the molecules are perfectly aligned along \mathbf{n} . For normal discotic nematics the scalar order parameter S is restricted to the range $0 \leq S \leq 1$, and for abnormal discotic nematics to $-0.5 \leq S \leq 0$ [10, 11, 12]. The basic morphological and rheological phenomena have to at least include a description of temporal changes of (S, \mathbf{n}) . Below we show that in certain instances uniaxiality may be lost and a more complex description that includes biaxial ordering is necessary (see section 1.9.).

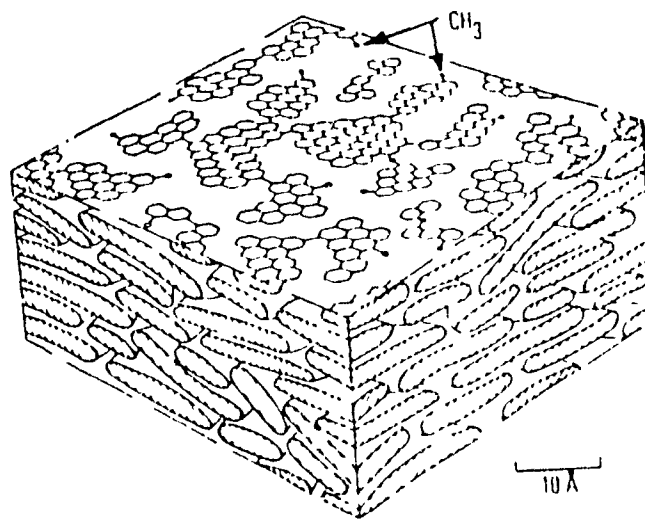


Fig. 7. Schematic model of the carbonaceous mesophase. Reprinted from [19].

1.6. Carbon Fibers

Three different types of commercial carbon fibers, manufactured from three different precursor materials, are : rayon carbon fibers, acrylic carbon fibers, and mesophase pitch based carbon fibers [21]. The rayon carbon fibers have relatively low tensile strength and low Young's modulus, and are used mainly as composites designed for use in rocket and space shuttle applications. The acrylic carbon fibers commonly known as PAN-based carbon fibers (poly-acrylonitrile) are copolymers of more than 85% of acrylonitrile and the rest are other comonomers which are used to improve processability. The PAN-based carbon fibers have high strength and high modulus and are used in a wide variety of applications[13, 15, 16, 21]. Pitch-based carbon fibers can be manufactured from two different states of the same precursor material (coal or petroleum pitches) . the liquid crystalline (discotic) state called mesophase, and the isotropic state. The isotropic pitch-based carbon fibers have low modulus and strength, and find applications as thermal insulations at high temperatures, gaskets and fillers in various plastics etc. [13]. The mesophase pitch based carbon fibers have ultrahigh strength and modulus and can be used for the same applications for which PAN-based carbon fibers are used. Table 1 compares the PAN-based carbon fibers and mesophase pitch-based carbon fibers on the basis of some selected properties of available manufactured carbon fibers [21]. The reason that mesophase pitch-based carbon fibers are preferred over PAN-based carbon fibers is the low-cost of the precursor material and processability in case of the former [22]. Also in addition, the structure and properties of mesophase based carbon fibers are unique and the fibers can thus be used for different purposes. The more graphitic structure of mesophase pitch-based carbon fibers leads naturally to the ultra-high moduli necessary for stiffness-critical purposes. The large negative coefficient of thermal expansion is particular attractive for metal composites which can be used for structures in outer space. The high thermal conductivity (approximately of the order of Copper) has put mesophase pitch-based carbon fibers in the fore front for the applications where rapid heat dissipation is important . PAN-based carbon fibers, rayon-based carbon fibers, and isotropic pitch-based carbon fibers are not considered in the present study.

1.7. Spinning of Mesophase Pitch

The mesophase pitches or carbonaceous mesophases are derived from the pyrolysis of the coal or petroleum pitches. Mesophase pitch consists of planar disc-shaped aromatic molecules which show, as discussed before, long range orientational

order. The highly ordered but deformable mesophase pitch is extruded in the conventional melt spinning process to form a precursor fiber. The planar aromatic molecules constituting the mesophase pitch become oriented along the fiber axis during the melt spinning and the orientation is preserved during the subsequent heat treatment by a chemical cross-linking or thermosetting process. Figure 8 shows the schematic of the alignment of the disc-shape molecules in the spinning process.

The fluid mechanical aspects of the carbon fiber spinning process include complex shear-elongational flows in the converging die (spinneret) and uniaxial extensional flow in the spinnline. In this thesis the effect of extensional flows on morphology is studied in detail.

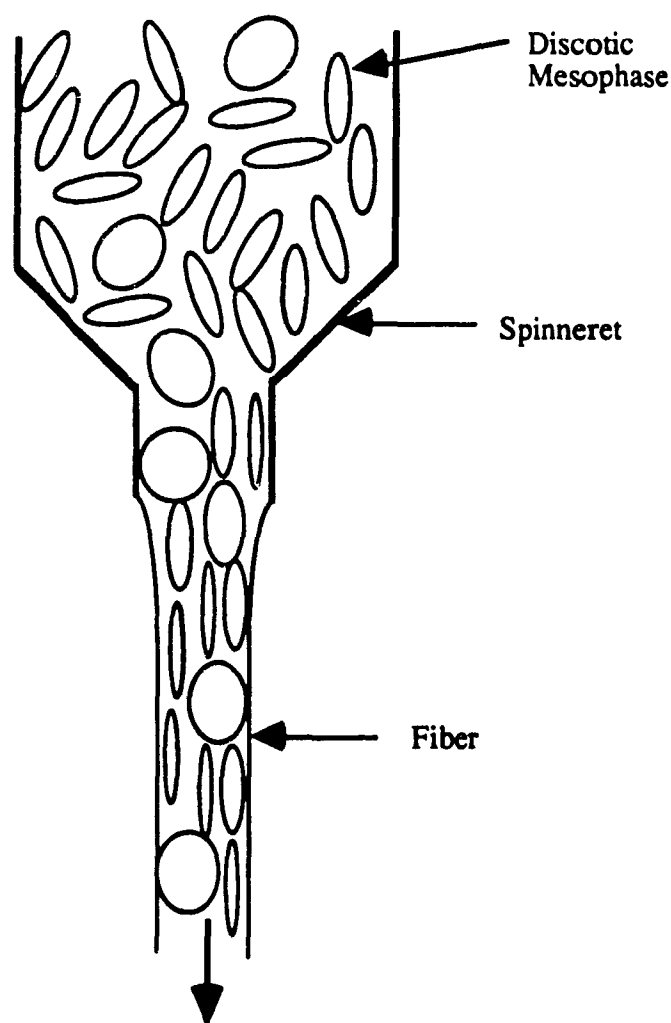


Fig. 8. Schematic of orientation process during the spinning process of carbonaceous mesophase (mesophase pitch). The various ellipses show the tilted discs orienting during the spinning process.

Table I : Selected properties of manufactured carbon fibers. Reprinted from [21].

Manufacturer	Fibre designation	Diameter, μm	Density, g cm^{-3}	Tensile strength (axial), GN m^{-2}	Youngs modulus (axial), GN m^{-2}	Strain at failure, $\epsilon_b, \%$	Thermal conductivity, $\text{W m}^{-1} \text{K}^{-1}$	Electrical resistivity, $\mu\Omega \text{m}$	Coefficient of thermal expansion (axial), 10^{-6}K^{-1}
PAN-type fibres									
Akzo	Fortafil 5(C)	7	1.8	2.76	345	0.8		9.75	
	Fortafil 3(C)	7.3	1.8	3.8	227	1.7	20	16.7	0.1
Amoco	T-50	6.5	1.81	2.90	390	0.7	70	9.5	1.13
	T-40R	6.5	1.78	3.45	290	1.2	43	10.9	0.3
	T-40	5.1	1.81	5.65	290	1.8	15	14.5	0.75
	T-650/42	5.1	1.78	5.03	290	1.7	15	14.2	0.75
	T-650/35	6.8	1.77	4.55	241	1.75	14	14.9	0.6
	T-300	7	1.76	3.65	231	1.4	8.5	18	0.6
BASF	Celion GY-70	8.4	1.90	1.86	517	0.36		6.5	1.1
	Celion G40-700	5	1.77	4.96	300	1.65		13	
	Celion G30-500	7	1.78	3.79	234	1.62		8.6	0.56
Hercules	Magnamite-HMS4	7	1.80	2.34	317	0.8			
	Magnamite-IM7	5	1.77	5.3	303	1.8			
	Magnamite-IM8	5	1.80	5.3	303	1.6			
	Magnamite-IM6	5	1.76	5.1	276	1.7		140	
	Magnamite-AS6	5	1.83	4.1	242	1.6		18.2	
	Magnamite-AS4	8	1.79	4.0	221	1.6		15.3	
Toray	Torayca-T300J	7	1.79	4.21	230	1.9		20	
Industries	Torayca-T300FT300	7	1.75	3.53	235	1.5		20	
	Torayca-T700S	7	1.82	4.8	230	2.1			
	Torayca-M40	6.5	1.81	2.74	392	0.6	85	8	-1.2
	Torayca-M50	6	1.91	2.45	430	0.5	89	8	
MP-type fibres									
Amoco	Thornel P-120	10	2.18	2.37	827	0.29	640	2.2	1.45
	Thornel P-100	10	2.15	2.37	724	0.32	520	2.5	-1.45
	Thornel P-75	10	2.0	2.1	520	0.4	185	7	1.4
	Thornel P-55	10	2.0	1.90	380	0.5	120	8.5	-1.3
	Thornel P-25	11	1.90	1.40	160	0.9	22	13	

1.8. Morphology of Mesophase Pitch-Based Carbon Fibers

It turns out that carbon fibers spun from carbonaceous mesophases have a spectrum of transverse textures, that are associated with various mechanical properties. The morphological features of the textures are defined by the spatial arrangement of the flat disk-like aromatic molecules in the cylindrical fibers. Some typical examples (see figure 9) found in the literature [13, 14, 15, 16] display radial, onion-like, and mixed radial and onion-like textures. In radial textures, the discotic molecules orient with their unit normals describing circles concentric with the fiber axis, while in the onion-like textures the discotic molecules themselves follow circular paths concentric with the fiber axis. In addition, the fiber cores may be isotropic or anisotropic, with the latter case giving rise to singular lines running along the fiber cores. For radial textures (or morphology) the presence of a singular line along the fiber axis introduces a potential fast failure mode by longitudinal crack propagation [16]; such failure modes are absent in the mesophase carbon fibers which have onion-like outer layers. The morphology or

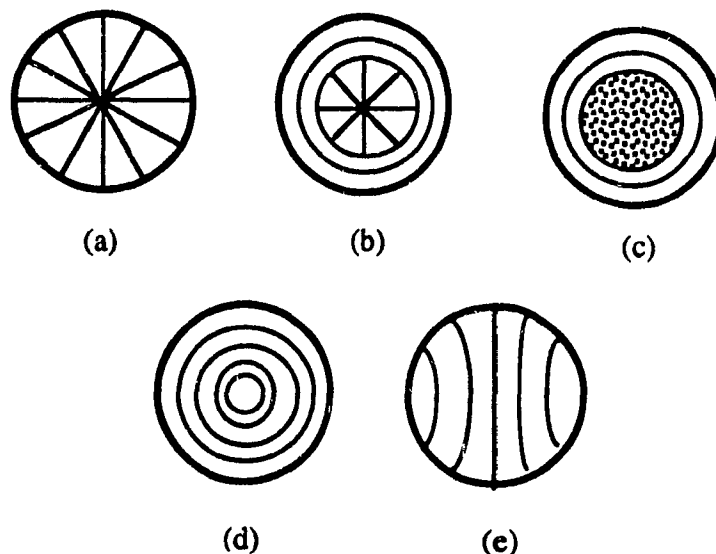


Fig. 9. Schematics of the various observed transverse textures of mesophase pitch-bases carbon fibers : radial morphology, (a), onion skin and mid-radial morphology (b), onion skin and mid-random morphology (c), onion morphology (d), and folded layer morphology (e). The lines indicate the molecular trajectories.

cross section texture of mesophase pitch-based carbon fibers is controlled by the pretreatment of the mesophase pitches, the constitution and spinnability of pitches, the spinning conditions, the fiber diameters, the spinnline tension, the temperature, and other factors [23]. In the present study the effect of constitution of mesophase prior to the processing (nematic potential U), spinning conditions (the effect of extensional flows) and the effect of different extension rate in the spinnline (the Deborah number) on the morphology of a model discotic mesophase are investigated.

1.9. Nematic Ordering

The term tensor order parameter is used to distinguish between the phases of different symmetry. It represents the extent by which the state of the molecules in a less symmetric phase differs from that in the more symmetric phase. The nematic phase has lower (higher) symmetry (order) than the isotropic phase. So the order parameter is defined so that it is non-zero in nematics and zero in the isotropic phase [2].

A second order, traceless, symmetric tensor order parameter Q is defined quantitatively by using a tensorial physical property such as the magnetic susceptibility, the electric polarizability or the dielectric constant, and by subsequently extracting the anisotropic part [24, 25]. The tensor order parameter Q is given as :

$$Q = S \left(nn - \frac{1}{3} \delta \right) + \frac{1}{3} P \left(mm - ll \right) \quad (3)$$

where the following restrictions apply:

$$Q = Q^T; \quad \text{Tr}(Q) = 0; \quad -\frac{1}{2} \leq S \leq 1; \quad -\frac{3}{2} \leq P \leq \frac{3}{2}; \quad (4)$$

$$n \cdot n = m \cdot m = l \cdot l = 1; \quad nn + mm + ll = \delta;$$

where $n, m, l (= n \times m)$ are unit vectors which form orthogonal director triad; n is known as the (uniaxial) director and m, l are termed as the biaxial directors. On the principal axes, the tensor order parameter is written as :

$$\mathbf{Q} = \begin{bmatrix} -\frac{1}{3}(S-P) & 0 & 0 \\ 0 & -\frac{1}{3}(S+P) & 0 \\ 0 & 0 & \frac{2}{3}S \end{bmatrix} \quad (5)$$

where $\frac{2}{3}S$, $-\frac{1}{3}(S-P)$, and $-\frac{1}{3}(S+P)$ are the eigenvalues corresponding the eigenvectors \mathbf{n} , \mathbf{m} , and \mathbf{l} respectively. If all the eigenvalues of the tensor order parameter \mathbf{Q} are zero (i.e., $S = 0, P = 0$) then the phase is defined as isotropic. If two eigenvalues of \mathbf{Q} are equal (i.e., $S \neq 0, P = 0$), the phase is termed as uniaxial nematic, and the uniaxial scalar order parameter S is sufficient to define the order of alignment of the molecules in the phase. If all the eigenvalues of \mathbf{Q} are different (i.e., $S \neq 0, P \neq 0$), the phase is called biaxial nematic [11, 12].

In the case of perfect axially symmetric molecules (for example rigid rods or rigid circular disks) no molecular interactions can result in a macroscopic ordering that is less symmetric than the molecules themselves. Thus an external cause, such as an external field perpendicular to \mathbf{n} , is necessary to produce ordering in a plane normal to \mathbf{n} . The biaxiality induced, in a phase containing axially symmetric molecules, due to the presence of an external field is referred to as field-induced biaxiality. In the absence of the external field, the biaxial nematic phase is expected only for molecules which are geometrically biaxial or those that do not possess axial symmetric. In chapter 4 of this thesis we characterize the extensional flow-induced biaxiality of a discotic that is uniaxial at rest.

S is known as the uniaxial scalar order parameter or uniaxial alignment, and is a measure of the degree of alignment of the unit normals to the disc-like molecules in the direction of director \mathbf{n} . The uniaxial scalar order parameter S is given as [1, 3] :

$$S = \left\langle \frac{3}{2} \cos^2 \theta - \frac{1}{2} \right\rangle \quad (6)$$

where θ is the angle of the unit normal to the disks with the director \mathbf{n} and $\langle \rangle$ represents the average over all the molecules in a particular region of space. For normal nematics S varies from 0 to 1; $S = 1$, for perfectly aligned molecules, $S = 0$ for isotropic liquid, and at the isotropic-nematic transition most theories predict $S = 0.5$. The biaxial scalar order parameter P is a measure of the degree of alignment of the projection of the molecular normals along the biaxial director \mathbf{m} , in a plane orthogonal to the uniaxial director \mathbf{n} . In other words, the biaxial scalar order parameter specifies the amount of transverse

ordering.

In the absence of biaxial ordering the uniaxial scalar order parameter S is simply termed as the scalar order parameter. This standard nomenclature is adopted in chapter 2 and chapter 3 of this thesis, whereas in chapter 4 while discussing the flow-induced biaxiality the two scalar order parameters, S and P , are referred as uniaxial scalar order parameter (S) and biaxial scalar order parameter (P), respectively. In the absence of biaxiality or where only the uniaxial behavior of the nematics is assumed, the biaxial directors \mathbf{m} , and \mathbf{l} are undefined and the uniaxial director \mathbf{n} is referred simply as the director. Following this standard nomenclature, in chapter 2 and chapter 3 (on uniaxial nematics), \mathbf{n} is called *director* and \mathbf{m} and \mathbf{l} do not appear; whereas chapter 4 of this thesis (on flow-induced biaxiality of uniaxial nematics) \mathbf{n} is called the *uniaxial director* and \mathbf{m} and \mathbf{l} are called the *biaxial directors*.

1.10. Extensional Flows

In this thesis the standard fluid flow terminology of [17] is adopted, and known kinematics are assumed. In Cartesian coordinates, the velocity field corresponding to the extensional start-up flow are as :

$$v_x = a \dot{\epsilon} x H(t); \quad v_y = -a(1+b) \dot{\epsilon} y H(t); \quad v_z = -a(1-b) \dot{\epsilon} z H(t); \quad (7)$$

$$H(t) = \begin{bmatrix} 0 & t < 0 \\ 1 & t \geq 0 \end{bmatrix}$$

where $\dot{\epsilon}$ is the constant extension rate, $a = +1$ or -1 , $0 \leq b \leq 1$ are parameters whose values captures the range of possible extensional flows. For uniaxial extensional flow $a = +1$, $b = 0$; for biaxial extensional flow $a = -1$, $b = 0$; for planar extensional flow $a = +1$, $b = +1$. Figure 1 in chapter 3 show the schematics of the deformations of a unit cube of nematics subjected to three representative extensional flows. The corresponding rate of deformation tensor ($A_{ij} = (v_{i,j} + v_{j,i})/2$, $i, j = x, y, z$), the symmetric part of velocity gradient tensor, is given as :

$$\mathbf{A} = \dot{\epsilon} \begin{bmatrix} a & 0 & 0 \\ 0 & -\frac{a}{2}(1+b) & 0 \\ 0 & 0 & -\frac{a}{2}(1-b) \end{bmatrix} \quad (8)$$

Extensional flows are encountered in many polymer processing operations such as fiber spinning, film blowing, sheet stretching, polymer foaming, and vacuum thermoforming etc. to name a few [17].

1.11. Orientation Distribution Function

The orientation distribution function $f(\mathbf{u})$ of a unit normal \mathbf{u} to the disc-shape molecule of a uniaxial discotic nematic liquid crystal represents the probability of finding a molecular unit normal in an infinitesimal solid angle of the unit sphere. From the definition of \mathbf{u} we have

$$f(\mathbf{u}) = f(-\mathbf{u}) \quad (9)$$

The Fourier representation of $f(\mathbf{u})$ has the following form [27]:

$$f(\mathbf{u}) = \frac{1}{4\pi} (f_0 + Q_j f_{ij}(\mathbf{u}) + Q_{ijkl} f_{ijkl}(\mathbf{u}) + \dots) \quad (10)$$

where Q_{ij} , Q_{ijkl} are the Fourier coefficients and f_0 , f_{ij} , f_{ijkl} are the surface spherical harmonics (or basis functions) which form an orthogonal basis such that

$$\int_{S^2} 1 \cdot f_{ij} \, d\mathbf{u} = \int_{S^2} 1 \cdot f_{ijkl} \, d\mathbf{u} = \int_{S^2} f_{ij} \cdot f_{ijkl} \, d\mathbf{u} = \dots = 0 \quad (11)$$

and are given as [27]:

$$f_0 = 1 \quad (12a)$$

$$\mathbf{f} = \mathbf{u}\mathbf{u} - \frac{\delta}{3} \quad (12b)$$

$$\begin{aligned} \mathbf{f} = & \mathbf{u}\mathbf{u}\mathbf{u}\mathbf{u} + \frac{1}{35}(\delta\delta + \mathbf{I} + \mathbf{I}^T) \\ & - \frac{1}{7}(\delta\mathbf{u}\mathbf{u} + \mathbf{u}\delta\mathbf{u} + \mathbf{u}\mathbf{u}\delta + {}^T(\mathbf{u}\delta\mathbf{u}) + (\mathbf{u}\delta\mathbf{u})^T + {}^T(\mathbf{u}\delta\mathbf{u})^T) \end{aligned} \quad (12c)$$

where from [27] :

$$\mathbf{I}^T (\mathbf{u} \delta \mathbf{u}) = \mathbf{I}^T : (\mathbf{u} \delta \mathbf{u}) ; \quad (\mathbf{u} \delta \mathbf{u})^T = (\mathbf{u} \delta \mathbf{u}) : \mathbf{I}^T \quad (13a,b)$$

The surface spherical harmonics are created by the even symmetric products of the components of the unit molecular normals \mathbf{u} , and are traceless. The unknown Fourier coefficients Q_{ij} , Q_{ijkl} are calculated using the orthogonality of the surface spherical harmonics as given in equation (11). The resulting approximated orientation distribution function, neglecting the Fourier coefficients of order higher than Q_{ij} , is given by :

$$f(\mathbf{u}) \approx \frac{1}{4\pi} \left(1 + \frac{15}{2} Q : \left(\mathbf{u} \mathbf{u} - \frac{\delta}{3} \right) \right) \quad (14)$$

Using equation (14) and the following parametrization of \mathbf{u} :

$$\mathbf{u} = \cos \omega_1 \mathbf{n} + \sin \omega_1 \cos \omega_2 \mathbf{m} + \sin \omega_1 \sin \omega_2 \mathbf{l} \quad (15)$$

the final truncated form of the orientation distribution function $f(\mathbf{u})$ is as given below:

$$f(\mathbf{u}) \approx \frac{1}{4\pi} + \frac{5}{8\pi} \left((2 \cos^2 \omega_1 - \sin^2 \omega_1) S + (\sin^2 \omega_1 \cos 2\omega_2) P \right) \quad (16)$$

where the three directors $(\mathbf{n}, \mathbf{m}, \mathbf{l})$ form a right handed orthogonal triad, and where ω_1, ω_2 are the polar and azimuthal angles of \mathbf{u} respectively. The orientation distribution function $f(\mathbf{u})$ is used (see figure 11 of chapter 4) to represent the density of the unit normals to the discs in the \mathbf{m} - \mathbf{l} plane.

1.12. Thesis Objectives

The main objectives of this thesis are : (a) to understand the flow-induced molecular orientation of idealized uniaxial discotic nematic liquid crystals subjected to extensional flows, which are the main flows encountered in fiber spinning and many other industrial processes, and (b) to establish the relevant qualitative features that describe the relations between extensional deformation inputs and orientation and alignment responses. The particular objectives of this thesis are :

- (1) To formulate an approximate phenomenological theory that describes the orientation and alignment of a model discotic nematic liquid crystal of variable

- alignment, during isothermal, incompressible, extensional flows;
- (2) To apply the developed phenomenological theory to isothermal, incompressible, irrotational, three dimensional extensional flows and to characterize the dynamic and steady state microstructure of model discotic liquid crystals;
 - (3) To characterize the effect of operating conditions (flow rate, initial thermodynamic state, temperature, initial orientation) and material properties (viscoelastic parameters) on transient and steady morphological phenomena;
 - (4) To rank and classify the different extensional discotic nematic flows according to their efficiency in producing typical patterns, and to provide a flow-morphology phase diagram for representative extensional flows;
 - (5) To identify the main extensional flow-induced phase transitions, such as uniaxial nematic-isotropic and uniaxial-biaxial;
 - (6) To provide a fundamental understanding of morphology development phenomena of discotic nematics in extensional flow, of direct use to the modeling of the carbonaceous mesophase spinning process.

1.13. Thesis Organization

The organization of the thesis is as follows. In chapter 2 an approximate phenomenological theory is developed and subsequently applied to describe the uniaxial extensional flow of a model discotic nematic liquid crystal. The sensitivity of the director paths, director steady states, and alignment relaxation along the director paths are analyzed with respect to the initial director orientation and to the extension rate. The minimizing principle that governs the director trajectories to the steady states are also determined in chapter 2. In chapter 3 the theory is applied to a range of extensional flows; the dynamics and microstructural response of uniaxial discotic nematics in these flows is simulated. A practical classification of various extensional flows based on orienting and alignment strength is given. In Chapter 4 the developed theory is used to simulate and analyze the flow-induced biaxiality in a uniaxial discotic nematic liquid crystal subjected to uniaxial extensional flow.

Chapter 2 of this thesis has appeared as an article in Journal de Physique II (France) 4 (1994) 645-665 and is identical with the reference '1' of chapter 3 and reference '14' of chapter 4. Chapter 3 of this thesis has been accepted as an article in Liquid Crystals (1994) and is identical with the reference '15' of chapter 4.

1.14. References

- [1] Priestley E.B., Wojtowicz P.J., Sheng P., "Introduction to Liquid Crystals", Plenum Press, New York, (1975).
- [2] Vertogen G., deJeu W.H., "Thermotropic Liquid Crystals", Springer-Verlag, Berlin, Heidelberg, (1988).
- [3] de Gennes P.G., "The physics of Liquid Crystals", Clarendon Press, Oxford, (1974).
- [4] Chandrasekhar S., Liquid Crystals, Second Edition, Cambridge Press, (1992).
- [5] Chandrasekhar S., Sadashiva B.K., Suresh K.A., Pramana, **9** (1977) 471.
- [6] Dubois J.C., Ann. Phys., **3**, (1978) 131.
- [7] Destrade C., Mondon M.C., Malthete J., J. Phys. France, **40**, (1979) C3-17.
- [8] Levelut A.M., J. Chem. Phys., **88** (1983) 149.
- [9] Otani S., Mol. Cryst. Liq. Cryst., **63**. (1981) 249.
- [10] Singer L.S., Faraday Discuss., Chem. Soc., **79** (1985) 265.
- [11] Destrade C., Mondon M.C., Melthate J., Mol. Cryst. Liq. Cryst., **71**. (1981) 111.
- [12] Brooks, J.D, Taylor G.H., Carbon, **3**, (1965) 185.
- [13] Singer L.S., Ind. Conv. of Coal and Carbon to Gas, Liquid, and Solid Products, London, (1981).
- [14] Singer L.S., Carbon, **16**, (1978) 413.
- [15] Honda H., Mol. Cryst. Liq. Cryst., **94** (1983) 97.
- [16] Singer L.S., Fuel, **60**, (1981) 839.
- [17] Bird R., Armstrong R.C., Hassager O., "Dynamics of Polymeric Liquids", Vol I, Wiley, New York, (1987).
- [18] Alben R., Phys. Rev. Lett., **30** (1973) 778.
- [19] Zimmer J.E., White J.L., In "Advances in Liquid Crystals Vol. 15, Academic Press, (1982) 157.
- [20] Gasparoux H., Mol. Cryst. Liq. Cryst., **63**. (1981) 647.
- [21] Peebles L.H. Jr., International Materials Review, **39** (1994) 75.
- [22] Edie D.D, Dunham M.G., Carbon, **27**, (1989) 647.
- [23] Rey A.D., 62nd Annual Meetings of Society of Rheology, New Mexico, (1990).
- [24] Lubensky T.C., Phys. Rev. A, **2** (1970) 2497.
- [25] Gramsbergen E.F., Longa L., deJeu W.H., Physics Reports, **135** (1986) 195.
- [26] Onat E.T., Leckie F.A., J. Applied Mechanics, **55** (1988) 1.
- [27] Bird R., Armstrong R.C., Hassager O., "Dynamics of Polymeric Liquids", Vol II, Wiley, New York, (1987).

Chapter 2

Extension Dynamics of Discotic Nematics of Variable Order : Geodesic Flow and Viscoelastic Relaxation ¹

2.1. Abstract

Variational methods are used to develop the governing equations that describe the flow of spatially invariant uniaxial discotic nematic liquid crystals of variable order; since the equations are based on a phenomenological truncated expansion of the entropy production, the equations are approximations. Restrictions in the phenomenological parameters appearing in the governing equations are imposed taking into account the ordering of the discotic phase. Numerical and analytical solutions of the director \mathbf{n} and alignment S are presented for a given uniaxial extensional start-up flow. The unit sphere description of the director is used to discuss and analyze the sensitivity of the director trajectories and the coupled alignment relaxation to the initial conditions (\mathbf{n}_0, S_0) and to the alignment Deborah number (De). The numerical results are used to characterize the relaxation of the tensor order parameter Q and to compute the steady flow birefringence. When the poles of the unit sphere are along the extension axis and the equator lies in the compression plane of the flow, it is found that the director trajectories belong to the meridians (great circles through the poles) and the dynamics follows a geodesic flow; when subjected to flow the director follows the shortest path that connects the initial orientation \mathbf{n}_0 and the equator (compression plane). As typical of geodesic flows, there is a strong sensitivity to initial conditions: when \mathbf{n}_0 lies on the poles no predictions on the eventually steady director orientation are possible. If the prior to flow orientation is close to the poles the coupled alignment relaxation along the geodesics is nonmonotonic and for large De the discotic may become temporarily isotropic. The couplings between \mathbf{n} and S are captured by the tensor order parameter relaxation. At steady state, the director lies on the equator, and the alignment and birefringence increase with increasing De .

¹ This chapter has been published as an article in Journal de Physique II (France) 4 (1994) 645-665.

2.2. Introduction

Discotic nematic liquid crystals are an important class of mesophases that occur naturally in carbonaceous mesophases [1, 2, 3]. These mesophases are formed by condensation of aromatic rings and tend to adopt a uniaxial discotic nematic phase Nd [4, 5], with the unit normals to the disc-like molecules more or less aligned along a common direction (see Fig.1 (b)), represented by the director \mathbf{n} , in what follows we use \mathbf{n} and orientation interchangeably. These materials find practical use in the spinning of high performance carbon fibers [2, 3, 6], and understanding their flow orienting behavior in the presence of uniaxial extensional deformations is of practical utility. As a first step in developing a basic qualitative understanding of such complex nonlinear problem, in this work we consider the flow orienting properties of a model incompressible discotic nematic liquid crystal of variable degree of order in isothermal uniaxial extensional flow.

Previous work [7, 8, 9, 10, 11] on the rheology and flow-induced orientation of uniaxial discotic nematics assumed that the scalar order parameter S remains unaffected by the flow; in what follows we use S and alignment interchangeably. The validity of this assumption for low molar mass materials justifies then the use of the Leslie-Ericksen (L-E) theory [12, 13] for uniaxial nematics with the proper values of the material parameters. The important differences in sign and magnitude of the material parameters corresponding to uniaxial rod-like and discotic nematics follow from the fact that rod-like nematics orient their longest molecular dimension along the director while disc-like nematics orient their shortest molecular dimension along the director. As is well known, the orienting properties of uniaxial nematics during shear flow are governed by the sign and magnitude of the tumbling (reactive) parameter λ : for aligning (non-aligning) rods $\lambda > 1$ ($0 < \lambda < 1$), and for aligning (non-aligning) discs $\lambda < -1$ ($-1 < \lambda < 0$); the tumbling parameter λ is given by the negative ratio of the irrotational torque coefficient (γ_2) and the rotational viscosities (γ_1), and represents the coefficient of the ratio of strain to vorticity torques acting on the director \mathbf{n} . Previous work [8,9] focused on the orienting properties of aligning uniaxial discotic nematics in steady shear, and it was found that shear orients the director in the shear plane and at a steady angle θ , lying in the $90^\circ \leq \theta \leq 135^\circ$ sector with respect to the flow direction. In steady shear-free uniaxial extensional flows, the orienting behavior of uniaxial nematics is again determined by the sign of λ : when $\lambda > 0$ the director aligns along the stretching (extension) direction, and when $\lambda < 0$ the director aligns somewhere in the compression plane, orthogonal to the stretching direction [11].

For materials of larger molecular weights the coupling between the director and the scalar order parameter should be retained [14]. This coupling introduces additional nonlinearities through the dependence of the generalized Leslie coefficients on the scalar order parameter, as shown in various works [14, 15, 16, 17, 18]. The nonlinear shear orienting behavior of rod- and disk-like nematics is now dependent on the shear rate, and flow-induced transitions involving aligning and non-aligning modes are triggered by varying the shear rate [18, 19, 20]. On the other hand, the behavior of rod-like nematics in extension is less dramatic since the competition between shear and vorticity is absent in an irrotational flow, and the effect of flow is to orient the director along the stretching direction with a concomitant increase in the scalar order parameter. A more complex situation presents itself for the uniaxial extension of discotic nematics, since they may orient anywhere in the compressional orthogonal plane, and may exhibit a nonlinear relaxation of S . The former observation explains the various observed cross section morphologies of mesophase carbon fibers, in which the normals to the molecular planes lie in the plane normal to the fiber axis [6, 21].

Our main objective in this work is to establish the relevant qualitative features that describe the relations between uniaxial extensional deformation inputs and orientation and alignment responses in an idealized discotic nematic liquid crystal. In the present paper the phenomenological properties of the particular model discotic nematic liquid crystal chosen for study are not fitted to those of any existing real material, and, as shown below, their choice is based on previous results. The particular objectives of this paper are :

- (1) To formulate and solve an approximate phenomenological theory that describes the orientation and alignment of a model discotic nematic liquid crystal of variable alignment, during isothermal, incompressible, uniaxial extensional flow ;
- (2) To characterize the sensitivity of the director paths to the compressional plane, to the initial conditions and to the extension rate by using numerical simulation;
- (3) To characterize the alignment relaxation along the director paths, to the initial conditions and to the extension rate by using numerical simulation;
- (4) To determine the minimizing principle that governs the director trajectories to the compression plane.

In this paper we use the unit sphere description of nematics [22, 23, 24, 25] only to facilitate the discussion and classification of the numerical results that pertain to the above mentioned objectives 2, 3, and 4.

The organization of this paper is as follows. In section 2.3 we define the coordinate system and the state variables, derive the governing equations, and briefly

present the elements of the unit sphere description used to discuss and classify the numerical solutions. A brief description of the numerical method used to integrate the governing equations is presented. In section 2.4 we present, discuss, and classify the solution vector, consisting of the time dependent director and alignment fields, obtained from numerical integration of the governing equations. Typical computations of the tensor order parameter relaxation and steady flow birefringence are presented.

2.3. Governing Equations

2.3.1. Definitions of Coordinates, Orientation and Alignment

In this paper we study the microstructural temporal and spatially invariant response of a model uniaxial discotic nematic subjected at time $t = 0$ to a constant uniaxial extension rate $\dot{\epsilon}$. In what follows we use cartesian tensor notation, repeated indices are subjected to the summation convention [26], partial differentiation with respect to the j th spatial coordinate is denoted by a comma (i.e., $v_{i,j} = \partial v_i / \partial x_j$) or by the symbol ∂_j (i.e. $v_{i,j} = \partial_j v_i$), and a superposed dot denotes the material time derivative (i.e. $\dot{S} = \frac{dS}{dt} = \partial S / \partial t + v_i \partial_i S$). The microstructure of the nematic is characterized by the uniaxial tensor order parameter $Q_{ij}(t)$ [13]:

$$Q_{ij} = S (n_i n_j - \delta_{ij} / 3) \quad (1a)$$

where the following restrictions apply:

$$Q_{ij} = Q_{ji}; \quad Q_{ii} = 0; \quad -1/2 \leq S \leq 1; \quad n_i n_i = 1 \quad (1b)$$

and δ_{ij} is the unit tensor. The magnitude of the scalar order parameter S is a measure of the molecular alignment along the director \mathbf{n} , and is given by $S = 3 (n_i Q_{ij} n_j) / 2$. Equation (1a) gives a proper description of the order in a discotic nematic phase if we identify the director as the average orientation of the unit normals to the molecular discs; see Fig.1(b); as explained in [27], with this identification, S is positive for both rod-like and disc-like uniaxial nematic liquid crystals, and no further distinction is required in this paper since rods are not considered here. Since uniaxial extensional flow will not induce negative values for the scalar order parameter S we further restrict its variation to the positive unit interval, $0 \leq S \leq 1$ [22].

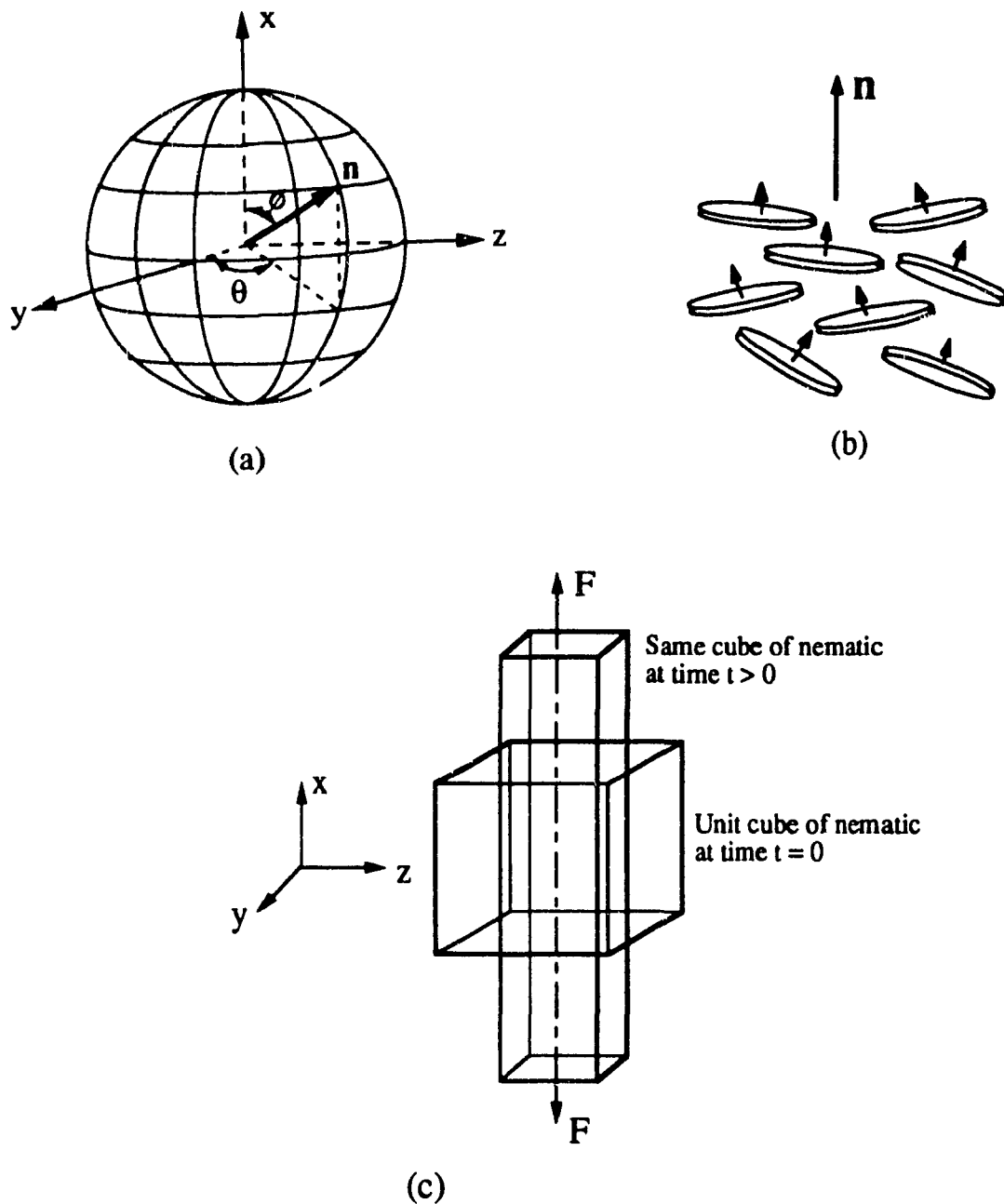


Fig. 1. Definition of (a) Coordinate systems, (b) Director orientation of a uniaxial discotic nematic liquid crystal, and (c) Uniaxial extensional flow deformation. (a) Director angles and unit sphere: θ ($0 \leq \theta \leq 2\pi$) is the azimuthal angle and ϕ ($0 \leq \phi \leq \pi$) is the polar angle. The north pole of the sphere is located at $\phi = 0$, the south pole at $\phi = \pi$, and the equator at $(\theta, \phi) = ([0, 2\pi], \pm\pi/2)$, \mathbf{n} denotes the director. (b) The director in a discotic nematic phase is the average orientation of the unit normals to the disc-like molecules. (c) Deformation of a unit cube, submitted to a uniaxial extension deformation along the x-direction.

To enforce the unit length constraint $\mathbf{n} \cdot \mathbf{n} = 1$ and to visualize the director orbits on the unit sphere, we parametrize the director with:

$$\mathbf{n} = (n_x, n_y, n_z) = (\cos \phi, \sin \phi \cos \theta, \sin \phi \sin \theta) \quad (2)$$

as shown in Fig. 1(a); θ ($0 \leq \theta \leq 2\pi$) is the azimuthal angle and ϕ ($0 \leq \phi \leq \pi$) is the polar angle. The north pole of the sphere is located at $\phi = 0$, the south pole at $\phi = \pi$, and the equator at $(\theta, \phi) = ([0, 2\pi], \pm \pi/2)$.

In the unit sphere description [22, 23, 24, 25] the director tip, in the presence of flow, defines a trajectory $O(\mathbf{n}_0)$ on the surface of the sphere :

$$O(\mathbf{n}_0) = \{ \mathbf{n} \in \Omega^2 ; \mathbf{n} = \mathbf{n}(t, \mathbf{n}_0), t \in \mathbb{R}^+ \} \quad (3)$$

where $\mathbf{n}_0 = \mathbf{n}(t=0)$, Ω^2 denotes the surface of the unit sphere and \mathbb{R}^+ the positive reals. To characterize the director orbits $O(\mathbf{n}_0)$ we need to define geodesics and meridians. A geodesic G is the shortest arc connecting two points on the sphere, and is given by [28]:

$$\sin(N_2) \cos \phi - (\cos N_2) \sin \phi \cos \theta - \frac{\sin \phi \sin \theta}{\sqrt{1/N_1^2 - 1}} = 0 \quad (4)$$

where N_1 and N_2 are constants that depend on the two points; the geodesic or great circle, is the intersection of the sphere with the plane containing the given points and the center of the sphere. When the two points are the poles ($N_2 = \pi$) the degenerate geodesics are the meridians M , which in terms of (θ, ϕ) and the director components (n_i) , are given by [28] :

$$\tan \theta = 1/b; \quad b^2 = 1/(N_1^2 - 1); \quad 0 \leq \phi \leq \pi \quad (5a,b,c)$$

$$n_y = b n_z; \quad -1 \leq n_y \leq 1; \quad -1 \leq n_z \leq 1 \quad (6a,b,c)$$

where a ($-\infty < b < \infty$) is a constant whose numerical value defines a particular meridian; a family of meridians is shown in Fig. 1 (a).

Figure 1 (c) shows the applied force F and deformations of a cube of discotic nematic subjected at $t=0$ to a uniaxial extensional flow; the applied extension and flow direction are along the x -axis (polar axis) and the compression (y - z) plane, that contains the equator of the unit sphere, represents the degenerate circle of stable steady director

orientation: $\mathbf{n}_{ss} = (0, n_{y_{ss}}, n_{z_{ss}}) = (0, \cos \theta_{ss}, \sin \theta_{ss})$, where the subscript ss denotes steady state.

To characterize the relaxation of the alignment as the director traverses the surface of the sphere, we divide the sphere into three characteristic regions: two equivalent spherical caps on which $|n_x| > 1/\sqrt{3}$, and the remaining spherical zone on which $|n_x| < 1/\sqrt{3}$. In an irrotational uniaxial extensional flow, the only flow effect on the orientation and alignment is due to the symmetric part of the velocity gradient tensor (v_{ij}), usually known as the rate of strain tensor or rate of deformation tensor and denoted by A , and whose ij and ji components are given by $A_{ij} = A_{ji} = (v_{i,j} + v_{j,i})/2$. An important observation, used below to classify the numerical results of alignment relaxation, is that a director whose tip lies in the spherical caps samples extensional strains ($A:nn > 0$), while a director whose tip lies in the spherical zone samples compressional strains ($A:nn < 0$).

2.3.2. Governing Orientation and Alignment Equations

A sufficiently general entropy production density Δ , similar to that proposed by [14], is given by [18]:

$$2D = \Delta = (\nu KT) [\sigma_1 (Q_{ij} A_{ji})^2 + \sigma_2 (A_{ij} A_{ji}) + \sigma_3 (Q_{ij} Q_{ji}) A_{lk} A_{kl} + 2\sigma_4 (\hat{Q}_{ij} A_{ji}) + 2\sigma_5 (Q_{ij} A_{jk} A_{ki}) + 4\sigma_6 (\hat{Q}_{ij} Q_{jk} A_{ki}) + 2\sigma_7 (Q_{ij} Q_{jk} A_{kl} A_{li}) + \tau_1 (\hat{Q}_{ij} \hat{Q}_{ji}) + 2\tau_2 (Q_{ij} \hat{Q}_{jk} \hat{Q}_{ki})] \quad (7)$$

where the ij components of the corotational time derivative of the tensor order parameter \hat{Q} , and of the vorticity tensor W are given by :

$$\hat{Q}_{ij} = \frac{\partial Q_{ij}}{\partial t} + v_k Q_{ij,k} - W_{ik} Q_{kj} + Q_{ik} W_{kj}; \quad W_{ij} = (v_{i,j} - v_{j,i})/2 \quad (8a,b)$$

and where v_k is the k th component of the linear velocity vector, σ_i ($i=1, \dots, 7$) and τ_i ($i=1, 2$) are scalar phenomenological constants with units of time that satisfy certain thermodynamic restrictions such that $\Delta \geq 0$ [14], $1/\nu$ is a molecular volume, T is the absolute temperature, and K is Boltzmann's constant. The most general expansion representing Δ is not closed, but the truncation given by equation (7) is sufficiently general and can be shown to reduce [18] to that of Leslie-Ericksen theory [12, 13].

In the absence of spatial gradients ($Q_{ij,k} = 0$) the Lagrangian density Λ is the sum of entropic $\Lambda^H(Q)$ [27] and flow $\Lambda^F(v, \nabla p, F)$ contributions:

$$\Lambda = \Lambda^H + \Lambda^F \quad (9a)$$

$$\Lambda^H = - \left(\frac{3}{4} A Q_{ij} Q_{ji} + \frac{3}{2} B Q_{ml} Q_{lk} Q_{km} + \frac{9}{16} C (Q_{lk} Q_{kl})^2 \right) \quad (9b)$$

$$\Lambda^F = - u_i (\rho \dot{v}_i + \partial_i p - \rho F_i) \quad (9c)$$

where A, B, and C are temperature dependent phenomenological coefficients, \mathbf{u} is the displacement vector, ρ is the density, p is the pressure, \mathbf{F} is external body force per unit volume. The negative of the entropic contribution Λ^H adopted here is known as the excess Landau-de Gennes free energy density [27], which is obtained from a truncated phenomenological expansion in terms of the two independent invariants $Q_{ij} Q_{ji}$ and $Q_{ij} Q_{jl} Q_{li}$. For uniaxial nematics equation (1a) holds and expression (9b) leads to the following excess free energy density $G(S, T)$ expansion :

$$G = \frac{1}{2} A S^2 + \frac{1}{3} B S^3 + \frac{1}{4} C S^4 \quad (10)$$

Usually, close to the nematic-isotropic transition, B and C are assumed to be independent of temperature, and it is further assumed that $A = a(T - T^*)$, where a is a constant. The cubic term ensures a first order transition at $T_C > T^*$, where T_C is the nematic-isotropic transition temperature and T^* is the temperature at which the free energy has zero curvature at $S=0$ ($@ S=0, \partial^2 G / \partial S^2 = 0$). For $B < 0$ and for the appropriate temperature range, equation (10) predicts the existence of the normal uniaxial discotic nematic phase, with the molecular unit normals oriented along the director. The minima predicted by equation (10) are :

$$S=0 \text{ (isotropic); } \quad S = -\frac{B}{2C} + \sqrt{\left(\frac{B}{2C}\right)^2 - \frac{A}{C}} \text{ (nematic)} \quad (11a,b)$$

Equation (10) predicts the existence of four temperature regions [27] : (i) $T > T^{\#}$: the stable phase is isotropic; (ii) for $T_C < T < T^{\#}$: there are two minima, the global one at $S=0$ (isotropic) and the other one for the superheated nematic phase; (iii) $T^* < T < T_C$: there are two minima, the global one corresponding to the nematic phase, and the local one corresponding to the supercooled isotropic phase; (iv) $T < T^*$: there is one minimum corresponding to the nematic phase. At the nematic-isotropic transition temperature $T=T_C$ the free energies of the isotropic and nematic phases are equal and from equation

(10) it follows that : (a) $T_c = T^* + 2 B^2 / (9aC)$, (b) the value of the order parameter at the transition is $S_c = -2 B / (3C)$, and (c) the latent heat per unit volume for the first order nematic-isotropic transition is $L = 2 a B^2 T_c / (9C^2)$. The temperature $T^\#$ divides the biphasic region from the single isotropic region and the following holds: (a) $T^\# = T^* + B^2 / (4aC)$, (b) $S^\# = - B / (2C)$. The temperature T^* is the lowest temperature for which the isotropic phase is metastable and at that temperature $S^* = -B/C$. Thus a characterization of G requires the specification of the four parameters a , B , C , and T^* . One common way to obtain values for the parameters is to use the Maier-Saupe molecular field theory and express the results in the form of equation (10). Here we use the following adapted results of Doi and Edwards [29] , for such parameter mapping between the phenomenological Landau-deGennes expansion and the molecular mean field theory :

$$\frac{3}{4} A = \frac{1}{2} \left(1 - \frac{U}{3}\right) vKT ; \quad \frac{3}{2} B = - \frac{U}{3} vKT ; \quad \frac{9}{16} C = \frac{U}{4} vKT \quad (12a,b,c)$$

where the nematic potential $U = 3 T^* / T$, and where vKT refer to the same quantities as in equation (7). The two parameters are now v and U . The resulting excess free energy density now reads:

$$G = \frac{2}{3} v KT \left[\frac{1}{2} \left(1 - \frac{U}{3}\right) S^2 - \frac{1}{9} U S^3 + \frac{1}{6} U S^4 \right] \quad (13)$$

The minima predicted by this free energy are [29]:

$$S=0 \text{ (isotropic)} ; \quad S = \frac{1}{4} + \frac{3}{4} \sqrt{1 - 8/(3U)} \text{ (nematic)} \quad (14a,b)$$

In what follows we use the symbol $S_{eq}(U)$, as given by the right hand side of equation (14b), to denote the equilibrium order parameter in the absence of flow. Comparing (11b) and (14b) it follows that if $B/C = -1/2$, which is generally consistent with nematics [27], both equations predict the same dimensionless temperature dependence of S , as embodied in the term A/C . In addition, equation (13) predicts the existence of four temperature regions with the same thermodynamic behavior as that predicted by equation (10) [29] . In terms of the nematic potential U , the boundaries of these four regions and the values of the alignment S in the nematic phase can be shown to be given by : (i) $U^\# = 8/3$, $S^\# = 1/4$, (ii) $U_c = 27/10$, $S_c = 1/3$, (iii) $U^* = 3$, $S^* = 1/2$. In this work we use the two parameter equation (13) to construct the Lagrangian Λ^H , since as shown

above (see also [29]), it is able to capture with two parameters the same qualitative thermodynamic behavior as the more general equation (10), and because it is consistent with our objectives.

The presence of a given flow field in a spatially invariant uniaxial discotic liquid crystal generates the following dynamical system :

$$\dot{y} = Y (y(t)); y = (n, S); y \in \Omega^2 \times [0,1]; y: \mathbb{R}^+ \rightarrow \Omega^2 \times [0,1] \quad (15a,b,c,d)$$

To find $Y (y(t))$, we use the following set of Euler-Lagrange equations [26,27]:

$$\frac{\tilde{\delta} \Lambda}{\delta n_i} - \frac{\delta D}{\delta \dot{n}_i} = 0; \quad \frac{\tilde{\delta} \Lambda}{\delta S} - \frac{\delta D}{\delta \dot{S}} = 0 \quad (16a,b)$$

$$\frac{\tilde{\delta} \Lambda}{\delta n_i} = (\delta_{ij} - n_i n_j) \left(\frac{\partial \Lambda}{\partial n_j} - \partial_k \frac{\partial \Lambda}{\partial (\partial_k n_j)} - \frac{\partial}{\partial t} \frac{\partial \Lambda}{\partial \dot{n}_j} \right) \quad (16c)$$

$$\frac{\tilde{\delta} \Lambda}{\delta S} = \left(\frac{\partial \Lambda}{\partial S} - \partial_k \frac{\partial \Lambda}{\partial (\partial_k S)} - \frac{\partial}{\partial t} \frac{\partial \Lambda}{\partial \dot{S}} \right) \quad (16d)$$

$$\frac{\delta D}{\delta \dot{n}_i} = (\delta_{ij} - n_i n_j) \left(\frac{\partial D}{\partial \dot{n}_j} - \partial_k \frac{\partial D}{\partial (\partial_k \dot{n}_j)} \right) \quad (16e)$$

$$\frac{\delta D}{\delta \dot{S}} = \frac{\partial D}{\partial \dot{S}} - \partial_k \frac{\partial D}{\partial (\partial_k \dot{S})} \quad (16f)$$

where $\tilde{\delta} \Lambda / \delta y$ is the projected total Euler-Lagrange derivative, and $\delta D / \delta \dot{y}$ is the projected space Euler Lagrange derivative [17]. The projection operator $(\delta_{ij} - n_i n_j)$ that appears in the director derivatives is required to eliminate the undetermined Lagrangian multiplier that arises from the unit length constraint on the director $n \cdot n = 1$; for the alignment no constraints are imposed and the projector operator is unity.

As shown in the Appendix, with the choices of Λ and Δ given in the equations (7, 9, 12), the dynamics of the director n and the alignment S are found to be :

$$\dot{y} = \begin{bmatrix} \frac{dn_j}{dt} \\ \frac{dS}{dt} \end{bmatrix} = \begin{bmatrix} W_{ij} n_j + \lambda (A_{ij} n_j - (A_{ik} n_i n_k) n_i) \\ \beta_1 A_{ik} n_i n_k + \beta_2 / \tau_1 \end{bmatrix} \quad (17a,b)$$

where $\lambda(S)$ is the tumbling function, $\beta_1(S)$ the ordering function, and $\beta_2(S,U)$ is proportional to $\delta\Lambda^H/\delta S$; these functions are given by :

$$\lambda = -\frac{\gamma_2}{\gamma_1} = - (3 \sigma_4^* + \sigma_6^* S) / (3S + \tau_2^* S^2) \quad (18a)$$

$$\beta_1 = - (9 \sigma_4^* + 6 \sigma_6^* S) / (6 + 4 \tau_2^* S) \quad (18b)$$

$$\beta_2 = (-3S + U S + U S^2 - 2 U S^3) / (3 + 2 \tau_2^* S) \quad (18c)$$

where the starred coefficients are scaled with the alignment relaxation time τ_1 .

To select numerical values for the three phenomenological parameters σ_4^* , σ_6^* , τ_2^* , we enforce the following constraints on the signs of λ and γ_1 [7, 8, 9, 10] and on the values of λ when $S=0$ and $S=1$ [7] :

$$\lambda = -\frac{\gamma_2}{\gamma_1} < 0 ; \quad \gamma_1 \geq 0 ; \quad \lim_{S \rightarrow 0} \lambda = -\infty ; \quad \lim_{S \rightarrow 1} \lambda = -1 \quad (19a,b,c,d)$$

The adopted values that satisfy the constraints are: $\sigma_4^* = 1/10$, $\sigma_6^* = 1.7$, $\tau_2^* = -1.0$, and the resulting λ and β_1 are shown in Fig.2. An indirect validation that the presently adopted values of the phenomenological coefficients, that appear in the dimensionless formulation of the governing equations for the idealized discotic nematic, may describe qualitatively some important features of the flow of real carbonaceous mesophases can be found by comparing the shear flow predictions of [32] with the experiments of [33]. In [32] the present model was solved for simple shear drag flow, using approximately similar values of the phenomenological coefficients (σ_4^* , σ_6^* , τ_2^*), and it was predicted that shear flow instabilities may set in at critical values of the shear rate; these instabilities are transitions between flow-tumbling and flow-aligning modes that characterize nematics of variable degree of orientation and mathematically are bifurcations between two types of periodic attractors and a steady state attractor. These shear flow instabilities were previously observed experimentally in a pressure-driven shear flow of a real carbonaceous mesophase by [33], where the observed pattern formation phenomena was explained using the tumbling-aligning transition, as calculated by [32]. Lastly, other set of parameters obeying the constraints (15a, b, c, d)

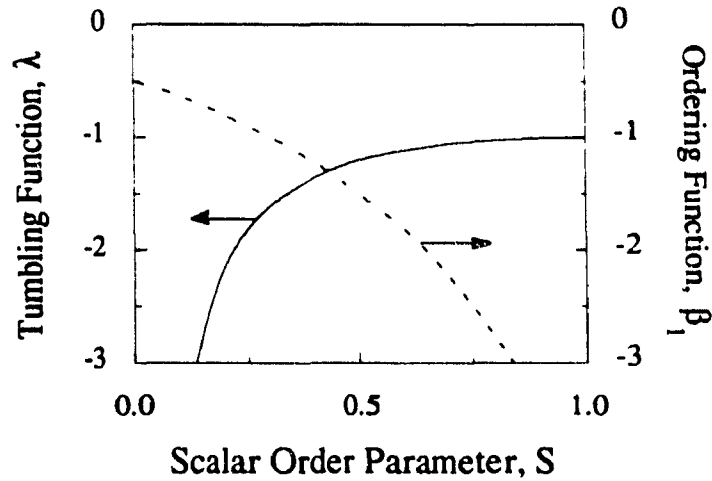


Fig. 2. Tumbling function λ and the ordering function β_1 as a function of the scalar order parameter S . The tumbling function is the ratio of the coefficient for strain and vorticity viscous torques, while the ordering function is the coefficient for the ambient strain rate $\mathbf{A}:\mathbf{nn}$ that governs the relaxation of S . For discotics (rod-like) nematics both are negative (positive).

were used in this work, but because the present flow is irrotational and all the attractors are steady states, the only differences in the computed solution vectors will be in the time scales, and hence, for brevity, these essentially similar results are omitted here.

If the alignment S is assumed to be constant, the present model is identical to the Transversely Isotropic Fluid (TIF) model of Ericksen [34] applicable to purely viscous nematic fluids:

$$\frac{dn_i}{dt} = W_{ij} n_j + \lambda (A_{ij} n_j - (A_{lk} n_l n_k) n_i) \quad (20a,b)$$

$$\lambda = \text{constant}; \quad \lambda > 0 \text{ (rods)}, \quad \lambda < 0 \text{ (disks)}$$

The constant alignment case was not studied in the present paper, but rigorous results for uniaxial extensional and biaxial extensional flows for rod-like nematics using the TIF model were obtained recently [35, 36]. A direct comparison of equations (17a) and (20a) shows that for irrotational flows ($\mathbf{W}=0$), the present model and the TIF model predict exactly the same director orbits $O(\mathbf{n}_0)$ and the only difference between the

predicted director fields is the time parametrization along the orbits; this difference is important in applications since it affects the number of strain units required to achieve a given orientation.

The following simplifying assumptions and approximations, have been made in deriving the mathematical model that describes the flow-induced alignment and orientation of an ideal discotic nematic liquid crystal, as given by equations (17, 18): (1) the fluid is incompressible and the flow is isothermal; (2) The orientation and alignment are space invariant; all elastic effects due to spatial gradients are neglected; (3) the entropy production has been arbitrarily truncated, such that it reduces to the Leslie-Ericksen expression; (4) The three coefficients of the Landau-de Gennes excess free energy have been fitted using two parameters; (5) Fluctuations that are important near the nematic-isotropic phase transition are neglected; (6) The velocity field is considered to be given, and therefore we dispense with solving the Cauchy equation of motion which involves the use of the nine parameters appearing in equation (7).

2.3.3. Governing Equations for Uniaxial Extensional Start-up Flow

The velocity field $v(x, y, z)$ corresponding to the uniaxial extensional start-up flow of the nematic sample, is given by [26]:

$$v_x = \dot{\epsilon} x H(t); \quad v_y = -\frac{\dot{\epsilon}}{2} y H(t); \quad v_z = -\frac{\dot{\epsilon}}{2} z H(t); \quad H(t) = \begin{cases} 0 & t < 0 \\ 1 & t \geq 0 \end{cases} \quad (21a,b,c,d)$$

where $\dot{\epsilon}$ is the constant extension rate. The non-zero components of the corresponding rate of deformation tensor A are: $A_{11} = \dot{\epsilon}$; $A_{22} = A_{33} = -\dot{\epsilon}/2$; this flow is irrotational and the vorticity tensor $W = 0$. A useful decomposition of the director field n and the rate of deformation tensor A is:

$$n = n_{\perp} + n_{\parallel}; \quad n_{\perp} = n_y \hat{j} + n_z \hat{k}; \quad n_{\parallel} = n_x \hat{i}; \quad A = \dot{\epsilon} \delta - \frac{3\dot{\epsilon}}{2} P \quad (22a,b,c,d)$$

where $\delta = \hat{i}\hat{i} + \hat{j}\hat{j} + \hat{k}\hat{k}$ and $P = \hat{j}\hat{j} + \hat{k}\hat{k}$. Replacing equations (21, 22) into equations (17a, 17b), we obtain the following dimensionless set of coupled nonlinear ordinary differential equations:

$$\begin{bmatrix} \frac{dn_1}{d\varepsilon} \\ \frac{dS}{d\varepsilon} \end{bmatrix} = \begin{bmatrix} \frac{3}{2} \lambda (n_1^2 - 1) n_1 \\ \frac{\beta_1}{2} (2 - 3 n_1^2) + De^{-1} \beta_2 \end{bmatrix} \quad (23a, b)$$

$$n_x = \text{sign}(n_x(t=0)) \sqrt{1 - n_1^2} \quad (23c)$$

where $\varepsilon = \dot{\varepsilon}t$ is the strain, $De = \dot{\varepsilon}\tau_1$ is the alignment Deborah number (dimensionless strain rate). When $De \rightarrow 0$ the alignment (S) relaxation is elastic, when $De \rightarrow \infty$ it is purely viscous, and for the intermediate values it is viscoelastic. At intermediate De the director relaxation is also viscoelastic, since it is coupled to S through $\lambda(S)$.

The initial conditions used to solve equations (23) are : @ $\varepsilon=0$: $\mathbf{n} = \mathbf{n}_0$; $S_0 = S_{eq}$, $\mathbf{n}_0 \cdot \mathbf{n}_0 = 1$, where $S_0 = S_{eq}(U)$ is given by equation (14b). In this paper we use two representative nematic potentials $U = 3$ and $U = 5$, and the corresponding initial conditions are: $S_{eq}(U=3) = 0.5$ and $S_{eq}(U=5) = 0.76$. All angles are reported in degrees.

Equations (23a, 23b) are integrated using an implicit corrector-predictor first order Euler integration method with an adaptable time step [37]. Application of the implicit corrector-predictor method transforms the set of coupled nonlinear ordinary differential equations (23a,23b) into a set of coupled nonlinear algebraic equations . For each time step the algebraic equations are solved using the Newton-Raphson iteration scheme [37] ; the predictor step generates a first guess for the iteration loop and the corrector step is the iteration loop itself. The adopted convergence criteria is that the length of the difference vector between the calculated solution vectors corresponding to two successive iterations is less than 10^{-6} . The transient solution vector obtained from the numerical solutions ($\mathbf{n}(\varepsilon)$, $S(\varepsilon)$), is used to calculate the tensor order parameter $Q(\varepsilon)$, and the converged steady state solutions (\mathbf{n}_{ss} , S_{ss}) are used to compute the steady flow birefringence. To facilitate the discussion and perform an analysis of the numerical solutions, some of the computed results are presented in reference to the unit sphere description of the director field.

2.4. Results and Discussions

2.4.1. Director Dynamics : Geodesic Flow and Viscoelastic Relaxation

Integration of equation (17) yields, for $\mathbf{W}=0$ and for \mathbf{A} as defined above, the following expression for the director relaxation $\mathbf{n}(\epsilon)$ for the uniaxial extension start-up flow :

$$n_i(\epsilon) = \frac{E_{ij} n_{j0}}{|\mathbf{E} \cdot \mathbf{n}_0|} ; n_i(0) = n_{i0} ; E_{ij}(\epsilon) = \exp \left\{ \tilde{A}_{ij} \int_0^\epsilon \lambda d\epsilon' \right\} ; \tilde{A}_{ij} = A_{ij} / \dot{\epsilon} \quad (24)$$

and in the component form:

$$n_x = \frac{E_{xx} n_{x0}}{|\mathbf{E} \cdot \mathbf{n}_0|} ; n_y = \frac{E_{yy} n_{y0}}{|\mathbf{E} \cdot \mathbf{n}_0|} ; n_z = \frac{E_{zz} n_{z0}}{|\mathbf{E} \cdot \mathbf{n}_0|} \quad (25a)$$

$$E_{xx} = \exp \left(\int_0^\epsilon \lambda d\epsilon' \right) ; E_{yy} = E_{zz} = \exp \left(-\frac{1}{2} \int_0^\epsilon \lambda d\epsilon' \right) ; E_{ij}=0 \text{ for } i \neq j. \quad (25b)$$

where n_{j0} is the j th component of the initial director orientation ($\mathbf{n}(0)$). From (25a, 25b) it follows that $n_y = a n_z$ ($a = n_{y0}/n_{z0}$), and comparing with equations (5,6) it follows that the director orbits belong to the meridians, and the director dynamics belong to the class of geodesic flows. Therefore the present problem should exhibit the characteristic sensitive dependence on initial conditions, that is typical of geodesic flows [30]. Equations (25a, 25b) shows that the stable director steady states are $\mathbf{n}_{ss} = (0, n_{y0}/n_{z0}, n_{z0}/n_{z0})$.

The director orbit follows a geodesic flow due to the inherent symmetry in the uniaxial extensional flow. This result is also predicted by the TIF equation (20a), since as mentioned above, for irrotational flows the geometry of the director orbits are insensitive to variations in the magnitude of the alignment.

Figure 3(a) shows that the unit sphere with representative meridians, Fig.3 (b) shows the computed polar angle ϕ as a function of azimuthal angle θ , and Fig. 3 (c) shows the corresponding computed scientific visualization of the average disc's relaxation, for $U=5$ and $De=1$, and the following director initial orientations (θ_0, ϕ_0): $A=(88.72, 2.56)$, $B=(63.4, 2.56)$, $C=(45, 2.56)$, $D=(26.56, 2.56)$, $E=(1.28, 2.56)$. Figure 3(a) shows that when starting on the poles, the director steady states, depicted by the

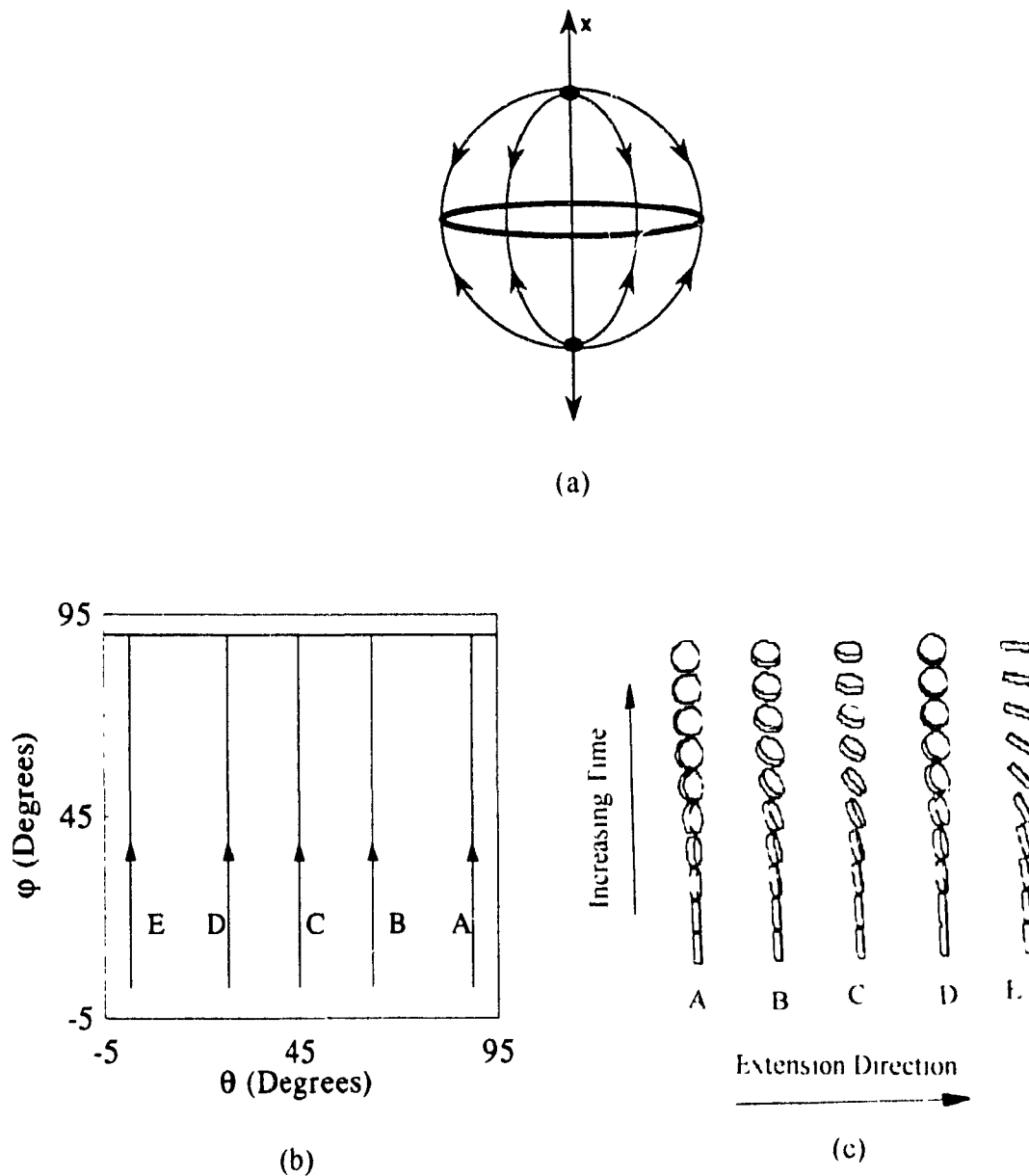


Fig. 3. Sensitivity of the director orbits to the initial conditions. (a) Schematic of the unit sphere and several meridians (great circles through the poles); the x-direction is along the extension direction and the equator represents the degenerate circle of stable steady director orientations. (b) Polar angle ϕ as a function of the azimuthal angle θ for $U=5$ and $De=1$, and for the following director initial orientations (θ_0, ϕ_0) : A = (88.72, 2.56), B = (63.4, 2.56), C = (45, 2.56), D = (26.56, 2.56), E = (1.28, 2.56). (c) Corresponding computed scientific visualization of the director relaxation, represented by the normals to the shown discs. Predictability is lost when the initial orientation is on the poles; close to the poles there is high sensitivity to \mathbf{n}_0 .

equator, are unpredictable. The (θ, ϕ) plot shows that the final steady state, denoted by the upper horizontal line, is highly sensitive to small variations of the initial orientation when the initial director tip is next to the poles. The computed director orbits follow the meridians defined by equations (5, 6). The visualizations shows the director (normal to the shown discs) relaxation, along the five different paths, exhibiting different combinations of tilting and twisting along the time axis, but eventually leading to a stable orientation on the plane (y-z), normal to the extensional direction.

Figure 4 shows the polar director angle ϕ as a function of strain ϵ , for $De=1$ (a), 0.5 (b), and 0.1 (c); $U=3$ (dash-dot line), $U=5$ (solid line), and $(\theta_0, \phi_0) = (45, 2.56)$. The figure shows that the director relaxation is viscoelastic, and that it is faster at higher De and at lower U , since for these conditions λ samples larger absolute values.

2.4.2. Alignment Viscoelastic Relaxation and Flow-Induced Melting

The alignment $S(\epsilon)$ relaxation depends on \mathbf{n}_0 through the ambient strain rate $\mathbf{A}:\mathbf{nn}$. Fig. 5 (a) shows the three representative regions for $\mathbf{A}:\mathbf{nn}$ in the two equivalent spherical caps R_1 the rate is positive ($\mathbf{A}:\mathbf{nn} > 0$), and in the spherical zone R_2 the rate is negative ($\mathbf{A}:\mathbf{nn} < 0$). The initial alignment relaxation characteristics are given by:

$$\begin{aligned} \mathbf{n}_0 \text{ in } R_1 : \left(\frac{dS}{d\epsilon} \right)_{\epsilon=0^+} < 0 ; \quad \mathbf{n}_0 \text{ in } R_2 : \left(\frac{dS}{d\epsilon} \right)_{\epsilon=0^+} > 0; \quad (26 \text{ a,b,c}) \\ \mathbf{n}_0 \text{ in } \partial R_1 = \partial R_2 : \left(\frac{dS}{d\epsilon} \right)_{\epsilon=0^+} = 0 \end{aligned}$$

Figure 5 (b) shows the three representative regions for $\mathbf{A}:\mathbf{nn}$, where the upper and lower rectangles represent R_1 , and the middle rectangle represents R_2 , and three characteristic initial orientations (θ_0, ϕ_0) : $P_1 = (45, 2.56)$ in R_1 , $P_2 = (0.9, 54.7)$ in $R_1 \cup R_2$, and $P_3 = (2.56, 89.9)$ in R_2 . Figure 5(c) shows the corresponding initial alignment S relaxation for $De=0.1$ and $U=5$. It follows that for any De , a sufficient condition for increasing S is that \mathbf{n} is in R_2 .

Figure 6 shows the alignment relaxation $S(\epsilon)$, corresponding to the conditions of the director relaxation of Fig. 4. The figure shows that at higher De ($De=1$), the viscous mode dominates the viscoelastic relaxation at all the times, and the effect of the relative magnitude of U is small. At lower De ($De=0.1$), the elastic mode dominates at all times if $U=5$, and negligible changes occur since $S_0=S_{eq}$, while for $U=3$ the viscous mode dominates the initial response, but the elastic mode dominates the later stage. Since in

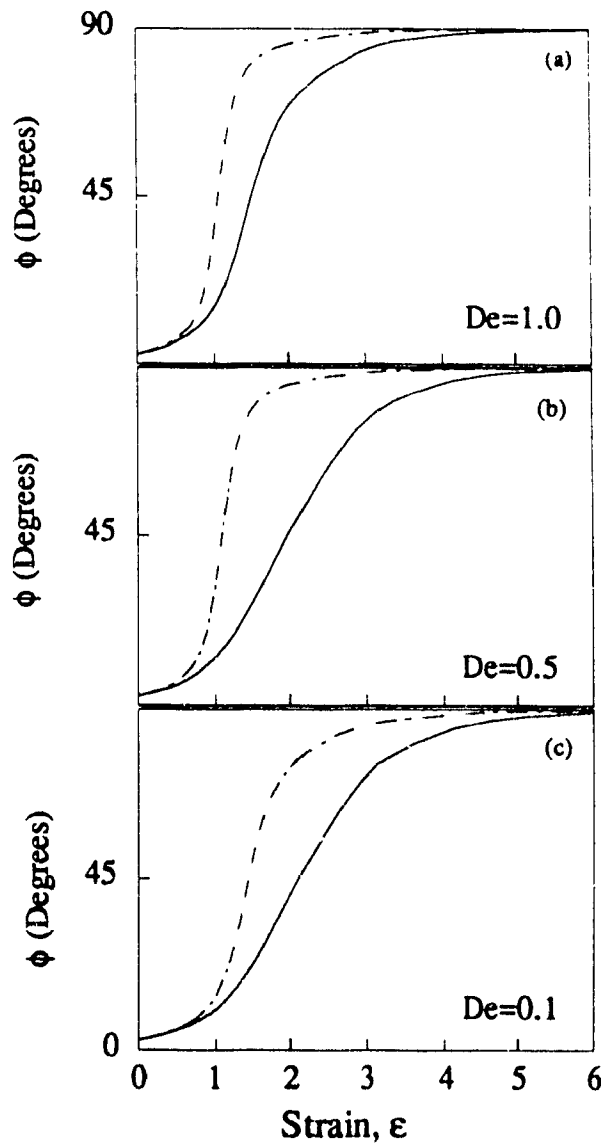


Fig. 4. Polar director angle ϕ as a function of strain ϵ , for $De=1$ (a), 0.5 (b), and 0.1 (c); $U=3$ (dash-dot line), $U=5$ (solid line), and the initial director orientation $(\theta_0, \phi_0) = (45, 2.56)$. The director relaxation is viscoelastic, and it is faster at higher De and at lower U .

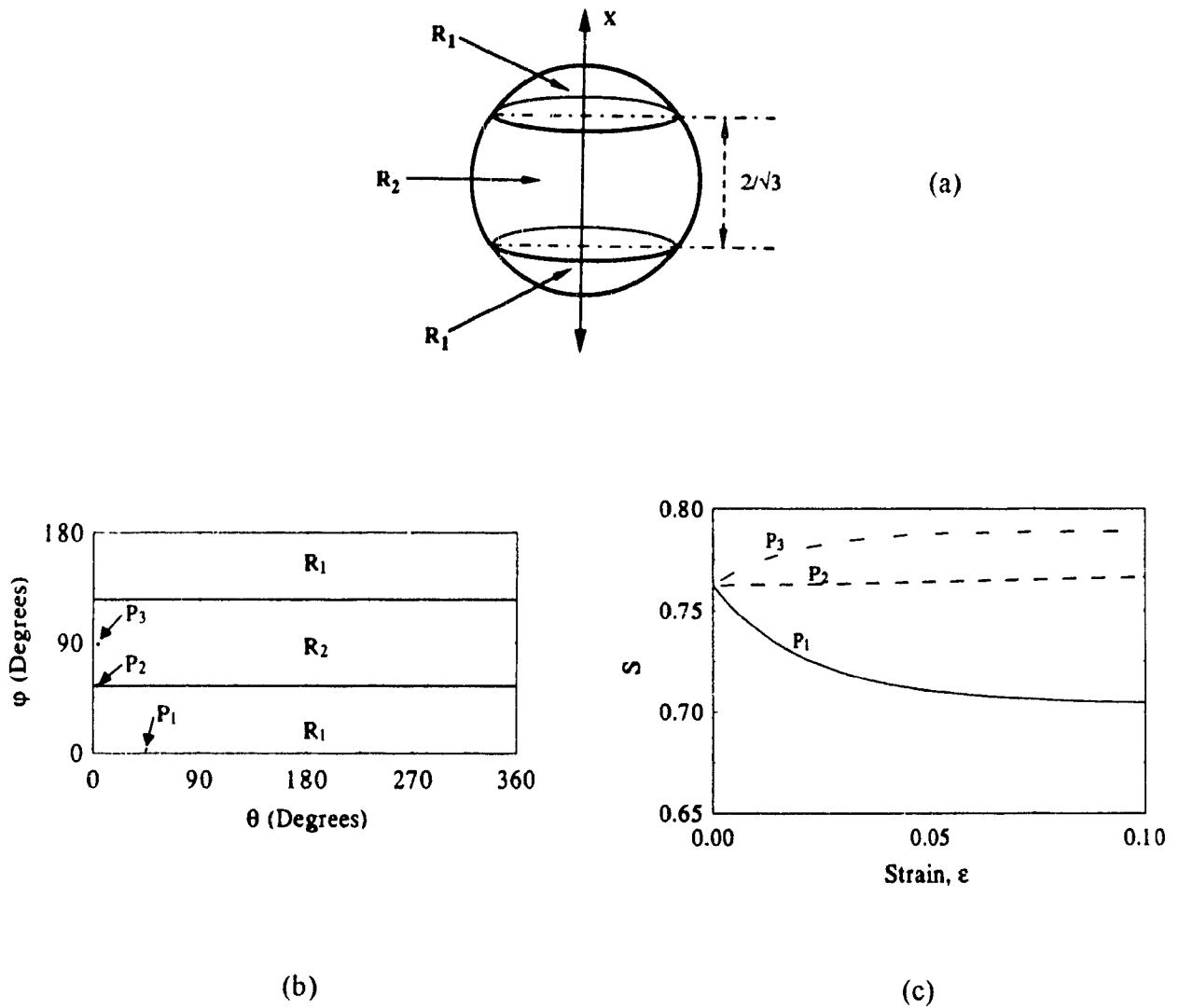


Fig. 5. Sensitivity of the initial alignment S relaxation to the initial director orientation. (a) The three characteristic regions for the ambient strain rate $\mathbf{A}:\mathbf{nn}$. (b) Planar (θ, ϕ) representation of the three representative regions for $\mathbf{A}:\mathbf{nn}$: where $\mathbf{A}:\mathbf{nn} > 0$ on the two equivalent upper and lower rectangles (R_1) and $\mathbf{A}:\mathbf{nn} < 0$ on the middle rectangle (R_2) to the two closed curves, and three characteristic initial orientations (θ_0, ϕ_0) : $P_1 = (45, 2.56)$ in R_1 , $P_2 = (0.9, 54.7)$ in $\partial R_1 = \partial R_2$, and $P_3 = (2.56, 89.9)$ in R_2 . (c) initial alignment S relaxation for $De=0.1$ and $U=5$.

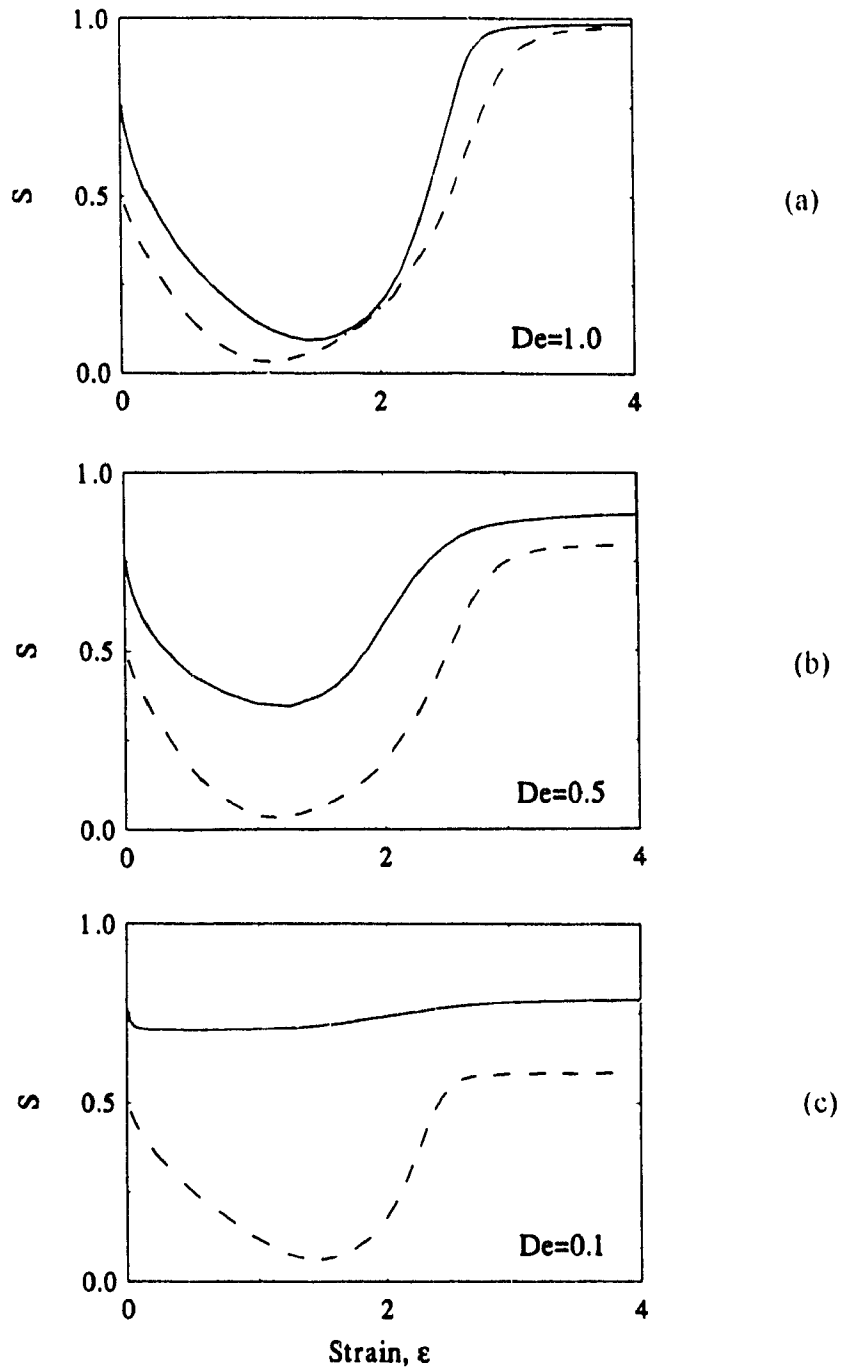


Fig. 6. Alignment relaxation $S(\epsilon)$, corresponding to the conditions of the director relaxation of Fig. 4. The figure shows that at higher De the viscous mode dominates and the effect of relative magnitude of U is small, while at lower De the elastic mode dominates and the effect of relative magnitude of U is small.

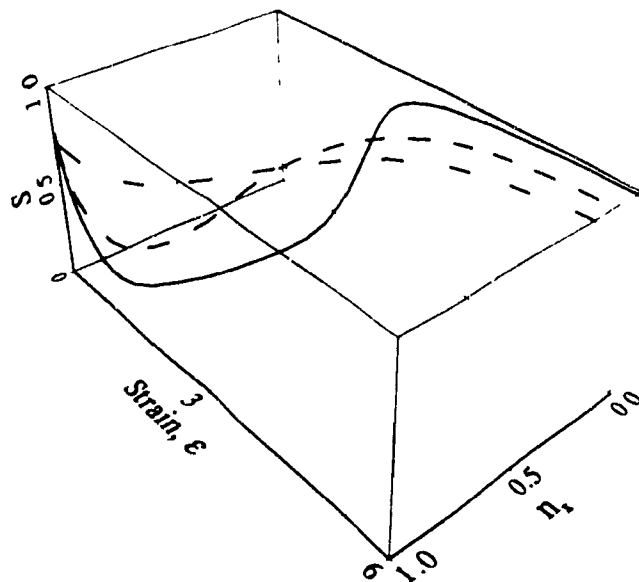
this figure n_0 is in R_1 , the alignment relaxation always shows an initial decrease in S . Comparing the steady state alignment S_{SS} for all cases, it is seen that at larger De , the viscous mode dominates and the effect of U is small, while at lower De , the elastic mode dominates and the effect of U is large.

Figure 7 (a) shows the alignment S and x-component of the director n_x as a function of strain ϵ , and Fig. 7 (b) shows the projection of Fig.7(a) on the (S, n_x) plane, with the initial orientation $(\theta_0, \phi_0)=(45, 2.56)$ close to the pole, for $U=5$, and $De=0.1$ (dash-triple dot line), 0.5 (dash-dot line), and 1 (full line). Figure 7(a) shows the coupling of the orientation and alignment relaxations, which indicates that by increasing De the increasing follows a two step process: an initial decrease in S followed by monotonic increase (decrease) in S (n_x). The nature of the (n_x, S) coupling is shown figure 7 (b), where the dotted line corresponds to $dS/dn_x=0$. For the given n_0 , the higher De the lower the value of n_x at which S starts increasing; for large De , discotic nematics undergo practically a temporary melting while the director is in R_1 ($n_x > (3)^{-1/2}$). For this particular case a more accurate model should include the fluctuations that are present near the isotropic-nematic phase transition.

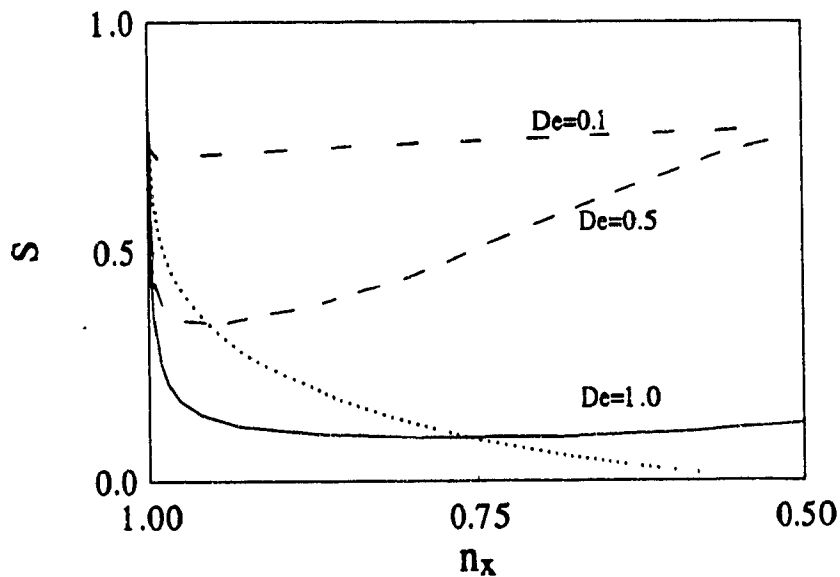
In contrast to the steady state director orientation which may exhibit a strong sensitivity to the initial orientation, the steady state scalar order parameter is independent of the initial orientation, and depends on the magnitudes of De and U , as shown by the lower equation (23 b).

2.4.3. Tensor Order Parameter Relaxation and Flow Birefringence

Figure 8 shows the relaxation of the components of the tensor order parameter Q with the initial orientation $(\theta_0, \phi_0)=(45, 2.56)$ close to the pole, for $U=5$, and $De=0.1$ (triple dot-dash line), 0.5(dash-dot line), and 1(full line). For the chosen initial orientation $n_{y0}=n_{z0}$, and from equation (6) it follows that $Q_{xy}=Q_{xz}$ and $Q_{zz} = Q_{yy}$. For the shown parameters the relaxation is virtually complete after 5 strain units. At low De the relaxation of the trace components (Q_{ii}) are dominated by the director relaxation shown in Fig. 4, since for $U=5$ the alignment is nearly constant (see Fig. 6). At higher De the relaxation of the trace components is dominated by the viscous mode, and reflect the two step process described in Fig. 7. At low De the non-diagonal terms of Q are again governed by the director relaxation, while at higher De , the viscous effect introduces an initial large decrease in S while n is in R_1 and a subsequent increase in S while n is in R_2 , with the result that the only large component is Q_{yz} , which follows a lag plus exponential growth relaxation.



(a)



(b)

Fig. 7. (a) Alignment S and x -component of the director n_x as a function of strain ϵ , and (b) projection of Fig. 7(a) on the (S, n_x) plane, with the initial orientation $(\theta_0, \phi_0) = (45, 2.56)$ close to the pole, for $U = 5$, and $De = 0.1$ (dash-triple dot line), 0.5 (dash-dot line), and 1 (full line). The dotted line corresponds to $dS/dn_x = 0$; at high De discotic nematics undergo practically a temporary melting while the director is in R_1 ($n_x > (3)^{-1/2}$).

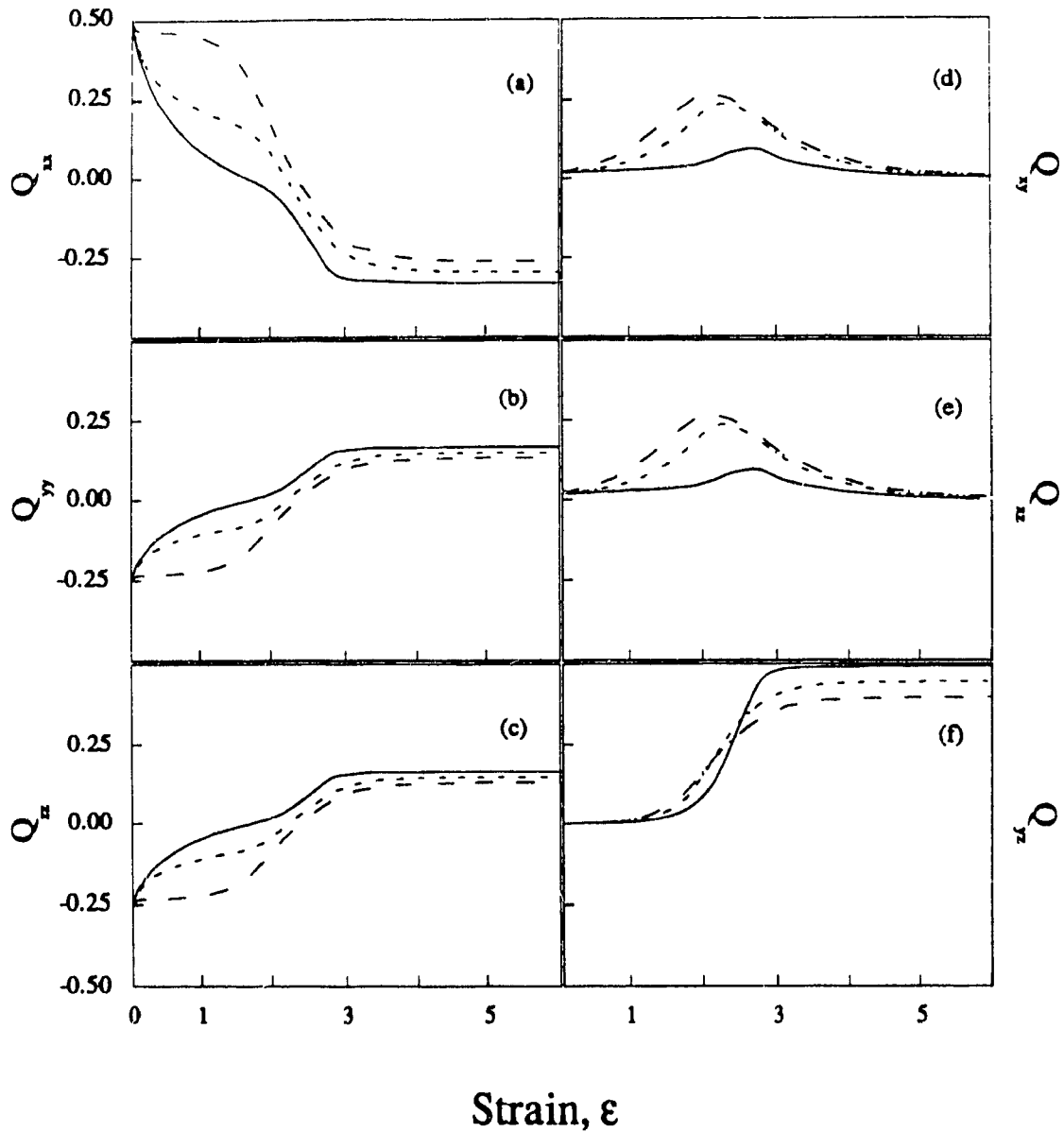


Fig. 8. Relaxation of the components of the tensor order parameter Q with the initial orientation $(\theta_0, \phi_0) = (45, 2.56)$ close to the pole, for $U=5$, and $De=0.1$ (triple dot-dash line), 0.5 (dash-dot line), and 1 (full line). For the chosen initial orientation $n_{y0} = n_{z0}$, and from equation (6) it follows that $Q_{xy} = Q_{xz}$ and $Q_{zz} = Q_{yy}$.

According to [27], the birefringence $\Delta\eta$ can be expressed by:

$$\Delta\eta = \sqrt{e_{//}} - \sqrt{e_{\perp}} \approx \frac{\Delta e_{\max} S}{2\sqrt{\bar{e}}} \quad (27)$$

where $e_{//}$ and e_{\perp} are the elements of the dielectric tensor e_{ij} parallel and normal to the director, the tensor is given by $e_{ij} = \bar{e}\delta_{ij} + \Delta e_{\max} Q_{ij}$, where the first term is the average trace of e_{ij} and Δe_{\max} is the anisotropy for $S=1$; for discotics, $\Delta\eta < 0$ since $\Delta e_{\max} < 0$. In deriving equation (27) we have assumed that $\bar{e} \gg 2 \Delta e_{\max} S/3$ for the values of S corresponding to the nematic phase. Equation (27) shows that the steady flow-induced birefringence $\Delta\eta_{SS}$ is proportional to the magnitude of the steady alignment S_{SS} .

Figure 9 shows the steady state alignment S_{SS} as a function of De , for $U=3$ (dash-dot line) and $U=5$ (full line). The figure shows a monotonic increase in the flow birefringence, at high De the viscous mode dominates and the effect of the magnitude of U is small, while at low De the elastic mode dominates and the effect of the magnitude of U on S_{SS} is large.

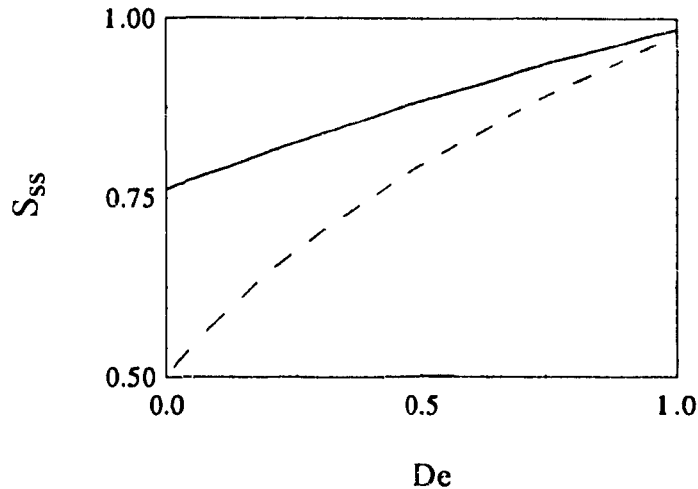


Fig. 9. Steady state alignment S_{SS} as a function of De , for $U=3$ (dash-dot line) and $U=5$ (full line). The flow birefringence is proportional to S_{SS} and increases with De .

2.5. Conclusions

In this initial investigation of the nematorheology of uniaxial discotics in uniaxial extensional flows, we have performed a useful characterization of the sensitivity of the director, scalar order parameter, and tensor order parameter relaxation with respect to the nematic potential, the alignment Deborah number, and the initial director orientation. Use of unit sphere description identified the director dynamics as a geodesic flow. This observation is used to explain the loss of predictability when the director is initially aligned along the extension direction, and allows for the use of the simple geometrical principle to identify the director orbits. The identification of the governing De parameter allows for the classification into the different elastic and viscous dominated relaxations. For large De, temporarily flow induced melting of the nematic phase may occur. This unified picture of relaxation under extension may be used to explain the characteristic patterns found in the cross-section of melt spun carbonaceous mesophases. In the extension-dominated flow process the normals to the molecular planes always align anywhere in the plane normal to the fiber axis, as shown in this paper for the stretching of a model discotic. The present analysis provides for a basis for the more general spatially inhomogeneous case, where Frank elasticity must be included.

2.6. Appendix

Substituting of equation (1) into (7), and the negative of equation (13) yield, respectively, the following equations for the dissipation Δ and the Langrangian Λ^H :

$$2D (\nu KT)^{-1} = \Delta (\nu KT)^{-1} = \alpha_1 (n_i A_{ik} n_k)^2 + \alpha_4 A_{ij} A_{ji} + (\alpha_5 + \alpha_6) (n_j A_{jk} A_{kl} n_l) + \gamma_1 N_i^2 + 2 \gamma_2 n_i A_{ij} N_j + \mu_1 \dot{S}^2 + \mu_2 \dot{S} (n_i A_{ij} n_j) \quad (\text{A.1})$$

$$\Lambda^H = -\nu KT \left\{ \frac{1}{9} (3 - U) S^2 - \frac{2}{27} U S^3 + \frac{1}{9} U S^4 \right\} \quad (\text{A.2})$$

where:

$$\alpha_1 = \sigma_1 S^2 \quad (\text{A.3a})$$

$$\alpha_4 = \sigma_2 - 2 \sigma_5 S/3 + 2 (\sigma_3 + \sigma_7/3) S^2/3 \quad (\text{A.3b})$$

$$\alpha_5 + \alpha_6 = 2 \sigma_5 S + 2 \sigma_7 S^2/3 \quad (\text{A.3c})$$

$$\gamma_1 = 2 (\tau_1 + \tau_2 S/3) S^2 \quad (\text{A.3d})$$

$$\gamma_2 = 2 (\sigma_4 + \sigma_6 S/3) S \quad (\text{A.3e})$$

$$\mu_1 = 2 (3 \tau_1 + 2 \tau_2 S)/9 \quad (\text{A.3f})$$

$$\mu_2 = 2 (9 \sigma_4 + 6 \sigma_6 S)/9 \quad (\text{A.3g})$$

$$N_i = \frac{\partial n_i}{\partial t} + (v_j \partial_j) n_i - W_{ij} n_j \quad (\text{A.3h})$$

Taking the space Euler-Lagrange derivative of D (equations (16e, 16f)), yields:

$$\frac{\tilde{\delta D}}{\delta \dot{n}_i} = vKT (\delta_{ij} - n_i n_j) (\gamma_1 N_j + \gamma_2 A_{jl} n_l + \chi n_j) \quad (\text{A.4a})$$

$$\frac{\tilde{\delta D}}{\delta \dot{S}} = vKT (\mu_1 \dot{S} + \mu_2 A_{jl} n_j n_l / 2) \quad (\text{A.4b})$$

where χ is a scalar Lagrange multiplier. Taking the total Euler-Lagrange derivative of Λ^H (equations (16c, 16d)) yields :

$$\frac{\delta \Lambda^H}{\delta n_i} = 0 \quad (\text{A.5a})$$

$$\frac{\delta \Lambda^H}{\delta S} = -vKT \left[2[(3-U)S - US^2 + 2US^3]/9 \right] \quad (\text{A.5b})$$

Subtracting equation (A.4a) from equation (A.5a), and equation (A.4b) from equation (A.5b) yields:

$$(\delta_{ij} - n_i n_j) (\gamma_1 N_j + \gamma_2 A_{jk} n_k + \chi n_j) = 0 \quad (\text{A.6})$$

$$-2[(3-U)S - US^2 + 2US^3]/9 - \mu_1 \dot{S} - \frac{1}{2} \mu_2 A_{lk} n_k n_l = 0 \quad (\text{A.7})$$

which yield equations (17a, 17b), upon the following identification

$$\lambda = -\frac{\gamma_2}{\gamma_1}; \beta_1 = -\frac{\mu_2}{2\mu_1}; \frac{\beta_2}{\tau_1} = -\frac{2[(3-U)S - US^2 + 2US^3]/9}{\mu_1} \quad (\text{A.8})$$

2.7. References

- [1] Gasparoux H., *Mol. Cryst. Liq. Cryst.* **63** (1981) 231-248.
- [2] Otani S., *Mol. Cryst. Liq. Cryst.* **63** (1981) 249-264.
- [3] Zimmer J. E., White J. L., *Disclination Structures in the Carbonaceous Mesophase*. In : Brown H. G. (ed.), *Advances in liquid Crystals*, Vol. 5, 1982, Academic Press, New York.
- [4] Chandrashekhara S., *Mol. Cryst. Liq. Cryst.* **63** (1981) 171-179.
- [5] Destrade C., Tinh N.H., Gasparoux H., Malthete J., Levelut A. M., *Mol. Cryst. Liq. Cryst.*, **71** (1981) 111-135.
- [6] Singer L. S., "The Mesophase in Carbonaceous Pitches", *Faraday Discuss. Chem. Soc.* **73** (1985) 265-272.
- [7] Volovik G. E., *JETP Lett.* **31** (1980) 273-275.
- [8] Carlsson T., *Mol. Cryst. Liq. Cryst.* **89** (1982) 57-66.
- [9] Carlsson T., *J. Physique* **44** (1983) 909-911.
- [10] Baals H. and Hess S., *Z. Naturforsch.* **43A** (1988) 662-670.
- [11] Ho A.S.K. and Rey A.D., *Rheol. Acta* **30** (1991) 77-88.
- [12] Leslie F.M., "Theory of Flow Phenomena in Liquid Crystals", in : Brown H. G. (ed.) *Advances in Liquid Crystals* vol.4, Academic Press, New York, (1981), 1-81.
- [13] de Gennes P. G., "The Physics of Liquid Crystals", Oxford University Press, London, (1975) p 153-165.
- [14] Ericksen J. L., "Liquid Crystals with variable degree of Orientation," *IMA Preprint Series No. 559* (1989).
- [15] Imura H. and Okano K., *Jpn. J. Appl. Phys.*, **11** (1972) 1440-1445.
- [16] Diogo A. C. and Martins A. F., *J. Phys.*, **43** (1982), 779-786.
- [17] Edwards B.J., Beris A.N. and Grmela M., *Mol. Cryst. Liq. Cryst.* **201** (1991) 51-86.
- [18] Farhoudi Y. and Rey A.D., *J. Rheol.*, **37** (1993) 289-314.
- [19] Marrucci G., "Rheology of Nematic Polymers", in : Ciferri A (ed) *Liquid Crystallinity in Polymers*, VCH Publishers, New York, (1991), 395-423.

- [20] Larson R.G., *Macromolecules*, **23** (1990) 3983-3992.
- [21] Honda , *Mol. Cryst. Liq. Cryst.* **94** (1983) 97-108.
- [22] Thurston R.N., *J.Physique* **42** (1981) 413-417.
- [23] Thurston R.N., *J. Appl. Phys.*, **52** (1981), 3040-3052.
- [24] Porte G. and Jadot J.P., *J. Physique* **39** (1978) 213-223
- [25] Carlsson T. , *Phys. Rev A* , **34** (1986) 3393-3404
- [26] Bird R., Armstrong R.C. and Hassager O., "Dynamics of Polymeric Liquids", Wiley, New York, 1987 .
- [27] Gramsbergen E.F., Longa L., de Jeu W.H., *Physics Reports* **135** (1986) 195-257.
- [28] Weinstock R., " Calculus of Variations". McGraw-Hill, New York, 1954, p 26-28.
- [29] Doi M. and Edwards S.F., " The Theory of Polymer Dynamics" Oxford University Press, New York (1986) p 358-362.
- [30] Hurd A.J., Fraden S., Lonberg F. and Meyer R.B., *J. Physique* (1985) 905-917.
- [31] Maugin G.A., *J. Non-Equilib. Thermodyn.*, **15** (1990) 173-192.
- [32] Farhoudi Y. and Rey A.D., *Rheol. Acta*, **32** (1993) 207-217.
- [33] Fathollahi B., Gopalakrishnan M.K., and White J.L., *Carbon* **92**, Proc. 5th Intl. Conf., A5, (1992) 36-38.
- [34] Ericksen J.L., *Koll. Zeit.*, **173** (1960) 117-122.
- [35] Duffy B.R., *J. Non. Fluid Mechanics*, **28** (1988) 77-97.
- [36] MacMillan E.H., *J. Rheol.*, **33** (1989) 1071-1105.
- [37] Finlayson B.A., "Nonlinear Analysis in Chemical Engineering", McGraw-Hill, New York, 1980, p 28-31.
- [38] Ruelle D., " Chance and Chaos", Princeton University Press, New Jersey, (1991) p47.

Chapter 3

Computer Simulation of Dynamics and Morphology of Discotic Mesophases in Extensional Flows ¹

3.1. Abstract

A previously presented model [1] is used to simulate the dynamics and microstructure of spatially invariant uniaxial discotic nematic liquid crystals in isothermal, incompressible, irrotational, extensional (shear-free or elongational) flows. Numerical and analytical solutions of the director \mathbf{n} and alignment S are presented for given uniaxial extensional, equi-biaxial extensional and planar extensional start-up flows. The unit sphere description of the director is used to discuss and analyze the sensitivity of the director trajectories and the alignment relaxation to the initial conditions (\mathbf{n}_0, S_0), to the alignment Deborah number (De), and to the type of flow. The numerical results are used to characterize the relaxation of the tensor order parameter Q and to compute the steady flow birefringence. The various flows are classified according to their orienting strength and alignment strength, and according to whether they generate geodesic (shortest path) director orbits. Equi-biaxial extensional and planar extensional flows are found to be strongly orienting and strongly aligning flows, while uniaxial extensional flow is a weakly orienting and weakly aligning flow. The number of strain units required to achieve steady state are shown to depend on whether the flow is geodesic (uniaxial extensional and equi-biaxial extensional flows) or not (planar extensional flow).

3.2. Introduction

Carbonaceous mesophases are an important class of naturally occurring discotic nematic liquid crystals [2, 3, 4]. These mesophases are formed by condensation of aromatic rings and tend to adopt a uniaxial discotic nematic phase Nd [5, 6], with the unit normals to the disc-like molecules more or less aligned along a common direction (see Fig. 2(b)), represented by the director \mathbf{n} ; in this paper we use \mathbf{n} and orientation

¹ This chapter has been accepted as an article for publication in *Liquid Crystals* (1994).

interchangeably. Carbonaceous mesophases can be spun into stiff and strong (high performance) fibers [3, 4, 7], and understanding their flow behavior is of practical utility.

Many industrial materials processing methods, such as the molding of polymers, are designed with the objectives that the alignment and orientation introduced during the deformation and forming stages are controlled [8]. The process choices are based on these two independent qualities of the flow, its orienting and aligning strength, which also form the basis for polymer flow classifications [9]. Although such classification has not been developed for discotic mesophase fluids, it certainly can provide useful guidelines on the dependence of orientation and alignment on flow type. In this respect extensional flows, such as spinning flows, seem to be the most relevant to processing discotic mesophase fluids.

Previous work [10, 11, 12, 13, 14] on the flow properties of uniaxial discotic nematics assumed that the scalar order parameter S (alignment) remains unaffected by the flow, and were based on the Leslie-Ericksen (L-E) theory [15, 16] for uniaxial nematics. The important differences in sign and magnitude of the material parameters corresponding to uniaxial rod-like and discotic nematics follow from the fact that rod-like nematics orient their longest molecular dimension along the director while disc-like nematics orient their shortest molecular dimension along the director. As is well known, the orienting properties of uniaxial nematics during shear flow are governed by the sign and magnitude of the tumbling (reactive) parameter λ : for aligning (non-aligning) rods $\lambda > 1$ ($0 < \lambda < 1$), and for aligning (non-aligning) discs $\lambda < -1$ ($-1 < \lambda < 0$); the tumbling parameter λ is given by the negative ratio of the irrotational torque coefficient (γ_2) and the rotational viscosities (γ_1), and represents the coefficient of the ratio of strain to vorticity torques acting on the director \mathbf{n} . Previous work [11, 12] focused on the orienting properties of aligning uniaxial discotic nematics in steady shear, and it was found that shear orients the director in the shear plane and at a steady angle θ , lying in the $90^\circ \leq \theta \leq 135^\circ$ sector with respect to the flow direction. In steady uniaxial extensional flows, the orienting behavior of uniaxial nematics is again determined by the sign of λ : when $\lambda > 0$ the director aligns along the stretching (extension) direction, and when $\lambda < 0$ the director aligns somewhere in the compression plane, orthogonal to the stretching direction [14].

For materials of larger molecular weights the coupling between the director and the scalar order parameter should be retained [17]. This coupling introduces additional nonlinearities through the dependence of the generalized Leslie coefficients on the scalar order parameter, as shown in various works [17, 18, 19, 20, 21, 22]. In a previous

work [1], the authors developed from variational principles a model that takes into account variable alignment in discotic nematics, and applied it to uniaxial extensional flow. It was found that the director trajectories on the unit sphere ($\mathbf{n} \cdot \mathbf{n} = 1$) follow a geodesic flow from the initial orientation to the compressional plane, and that the alignment relaxation was sensitive to the initial orientation, to the extension rate, and to the nematic potential that controls the magnitude of S in the absence of flow. The sensitivity to initial conditions, typical of geodesic flows, was shown to be the cause for the loss of predictability that occurs when the initial orientation lies along the extension axis of the flow.

Our main objective in this work is to establish the relevant qualitative features that describe the relations between extensional deformation inputs and orientation and alignment responses, in a model discotic nematic liquid crystal, and to use these results to formulate a practical flow classification of various extensional flows. In the present paper the phenomenological parameters of the particular model discotic nematic liquid crystal chosen for study are not fitted to those of any existing real material, and their choice is based on previous results [1]. The particular objectives of this paper are :

- (1) To characterize the sensitivity of the director paths to the compressional axis or compressional plane, to the initial conditions, to the extension rate, and to the flow type, by using numerical simulation;
- (2) To characterize the alignment relaxation along the director paths, to the initial conditions, to the extension rate, and to the flow type by using numerical simulation;
- (3) To determine the geometry of the director trajectories to the compression axis or compressional plane, and to classify various extensional flows as geodesic or non-geodesic flows;
- (4) To provide a general classification for extensional flows according to the magnitude of their alignment strength and orientation strength.

The organization of this paper is as follows. In section 3.3 we define the coordinate system and the state variables, present the governing equations, and briefly present the elements of the unit sphere description used to discuss and classify the numerical solutions. A brief description of the numerical method used to integrate the governing equations is presented. In section 3.4 we present, discuss, and classify the solution vector, consisting of the time dependent director and alignment fields, obtained from numerical integration and analytical solutions of the governing equations. Typical computations of the tensor order parameter relaxation and steady flow birefringence are presented. Overall classifications according to trajectory geometry of the director on the

unit sphere, alignment strength, and orientation strength are given.

3.3. Governing Equations

3.3.1. Definitions of Coordinates, Kinematics, Orientation and Alignment

In this paper we study the temporal and spatially invariant microstructural response of a model uniaxial discotic nematic, subjected at time $t=0$, to a range of extensional flows of constant extension rate $\dot{\epsilon}$. In this paper the adopted fluid flow terminology is that of Bird et. al. [23]. Due to their prevalence in applications here we emphasize the three representative extensional flows: uniaxial extensional flow, equibiaxial extensional flow, and planar extensional flow, but whenever possible allow for further generalizations by introducing representative parameters, as given in [23]. In the rest of this paper equi-biaxial extensional flow is referred to as biaxial extensional flow. Figure 1 shows the deformation of a cube of discotic nematic liquid crystal subjected at time $t=0$ to: (a) uniaxial extensional flow (UE), (b) biaxial extensional flow (BE), and (c) planar extensional flow (PE). We note that the word uniaxial in uniaxial extensional flow and biaxial in biaxial extensional flow refer to the number of extension (stretching or pulling) directions; these irrotational flows are three dimensional. Equibiaxial extensional flow is kinematically the inverse of uniaxial extensional flow. On the other hand, planar extensional flows, also known as pure shear [32, 33] or strip biaxial flows, are irrotational two dimensional flows, where the deformation characterized by an extension direction and an orthogonal contraction direction occurs on a plane. In planar extensional flow the stream lines are a family of rectangular hyperbola whose center is a stagnation (saddle) point [33].

An experimental set up to generate a uniaxial extensional flow is to pull a cylindrical sample from its two opposite ends at a rate that increases exponentially with time; in Figure 1 the sketch representing uniaxial extension (UE), using rectangular coordinates, shows the extension direction along the x -axis while the contraction directions are along the y - and z -axes. A way to generate a biaxial extensional flow is to stretch a thin sheet of material in two orthogonal directions simultaneously at equal rate, with a corresponding decrease in the sheet thickness. An approximation to this flow is found in lubrication squeeze-film flow and during the inflation of a balloon; in figure 1 the sketch representing biaxial extension (BE), using rectangular coordinates, shows the two extension directions along the y - and z -axes while the contraction direction is along the x -axis. Planar extensional flow is equivalent to stretching a flat

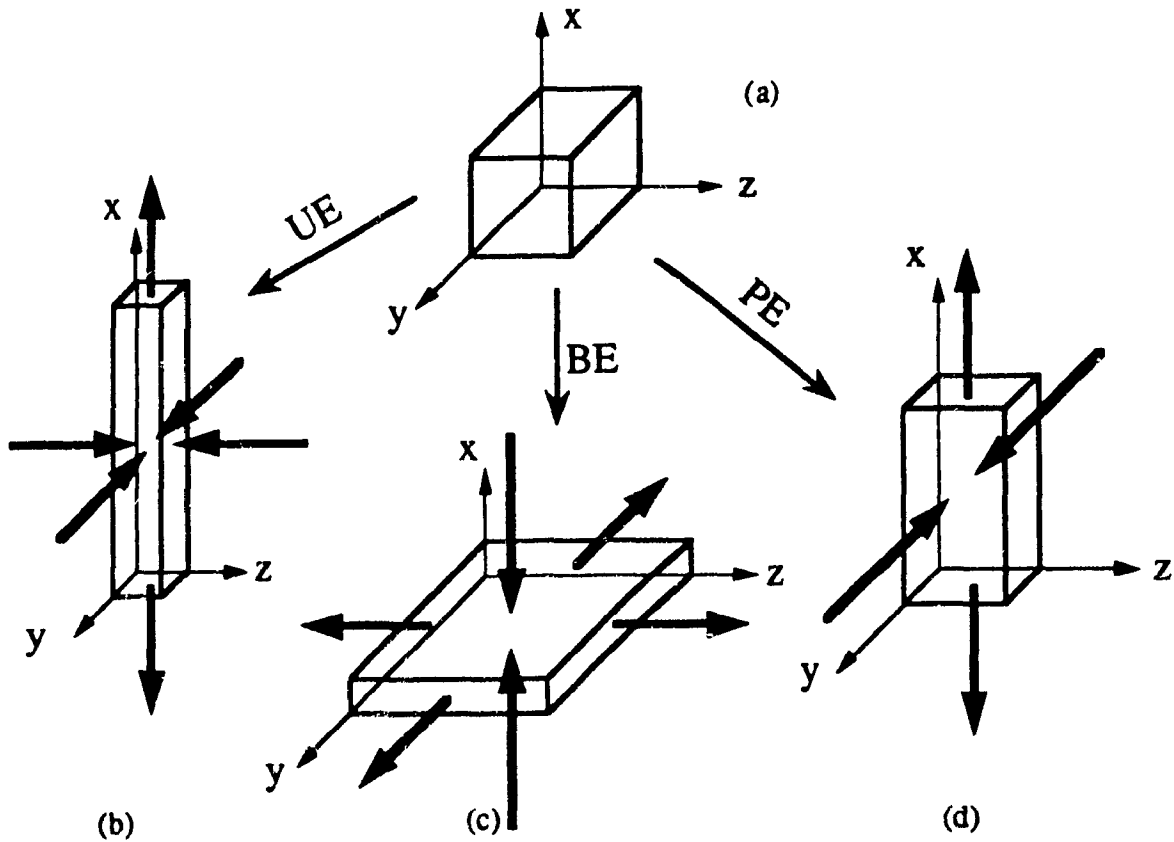


Fig. 1. Deformation of (a) unit cube of material at time $t > 0$ submitted to (b) uniaxial extensional flow (UE), (c) biaxial extensional flow (BE), and (d) planar extensional flow (PE). The velocity components for these flows are given in equation (10). In uniaxial extensional (UE) flow, the x -axis is the extension direction and the y - and z -axes are the directions of compression; this flow is an irrotational 3D flow. In biaxial extensional (BE) flow the y - and z -axes are the extension directions and the x -axis is the compression direction; this three dimensional irrotational flow is kinematically the inverse of uniaxial extension. In planar extension, the extension direction is along the x -axis, the contraction direction is along the y -axis, while no motion occurs along the z -axis; planar extensional flow is a two dimensional (planar) irrotational flow.

thin sheet of fluid in one direction , with a corresponding contraction in an orthogonal direction, but with no motion in the third direction ; in Figure 1 the sketch representing planar extension (PE) , using rectangular coordinates, shows the extension direction along the x- axis , the contraction direction along the y- axis, while along the z- axis no motion occurs. An experimental generation of an approximate planar extensional flow is the four-roll mill flow, where four long cylinders of equal radii, placed along the four corners of a square are set to rotate with equal magnitude but with directions opposite to the two nearest neighbors. The resulting essentially two dimensional irrotational flow generates a family of rectangular hyperbolic stream lines , with a stagnation point at the center of the square.

The microstructure of the model nematic considered here is characterized by the uniaxial tensor order parameter $Q_{ij}(t)$ [16]:

$$Q_{ij} = S (n_i n_j - \delta_{ij} / 3) \quad (1a)$$

where the following restrictions apply:

$$Q_{ij} = Q_{ji}; \quad Q_{ii} = 0; \quad -1/2 \leq S \leq 1; \quad n_i n_i = 1 \quad (1b)$$

and δ_{ij} is the unit tensor. The magnitude of the scalar order parameter S is a measure of the molecular alignment along the director \mathbf{n} , and its magnitude is given by $S = 3 (n_i Q_{ij} n_j) / 2$. Equation (1a) gives a proper description of the macroscopic order in a discotic nematic phase if we identify the director as the average orientation of the unit normals to the molecular discs; see Fig. 2(b); as explained in [24], with this identification, S is positive for both rod-like and disc-like uniaxial nematic liquid crystals, and no further distinction is required in this paper since rods are not considered here. Since extensional flows will not induce negative values of the scalar order parameter S we further restrict its variation to the positive unit interval, $0 \leq S \leq 1$ [24].

To enforce the unit length constraint $\mathbf{n} \cdot \mathbf{n} = 1$ and to visualize the director orbits on the unit sphere, we parametrize the director with:

$$\mathbf{n} = (n_x, n_y, n_z) = (\cos \phi, \sin \phi \cos \theta, \sin \phi \sin \theta) \quad (2)$$

where θ ($0 \leq \theta \leq 2\pi$) is the azimuthal angle and ϕ ($0 \leq \phi \leq \pi$) is the polar angle, see Fig. 2(a). The north pole of the sphere is located at $\phi = 0$, the south pole at $\phi = \pi$, and the equator at $(\theta, \phi) = ([0, 2\pi], \pm \pi/2)$.

In the unit sphere description [25, 26, 27] the director tip, in the presence of flow, defines a trajectory $O(\mathbf{n}_0)$ on the surface of the sphere :

$$O(\mathbf{n}_0) = \{ \mathbf{n} \in \Omega^2 ; \mathbf{n} = \mathbf{n}(t, \mathbf{n}_0), t \in P^+ \} \quad (3)$$

where $\mathbf{n}_0 = \mathbf{n}(t=0)$, Ω^2 denotes the surface of the unit sphere and P^+ the positive reals . To characterize some of the director orbits $O(\mathbf{n}_0)$ of interest we need to define some unique trajectories such as geodesics and meridians. A geodesic G is the shortest arc connecting two points on the sphere, and is given by [28]:

$$\sin(N_2) \cos\phi - (\cos N_2) \sin\phi \cos\theta - \frac{\sin\phi \sin\theta}{\sqrt{1/N_1^2 - 1}} = 0 \quad (4)$$

where N_1 and N_2 are constants that depend on two points belonging to G ; the geodesic or great circle, is the intersection of the sphere with the plane containing the given points and the center of the sphere. When the two points are the poles ($N_2=\pi$) the degenerate geodesics are the meridians M , which in terms of (θ, ϕ) and the director components $(n_i, i = x, y, z)$, are given by [28] :

$$\tan \theta = 1/d_1 ; d_1^2 = 1/(N_1^2 - 1) ; 0 \leq \phi \leq \pi \quad (5a,b,c)$$

$$n_y = d_1 n_z ; -1 \leq n_y \leq 1 ; -1 \leq n_z \leq 1 \quad (6a,b,c)$$

where d_1 ($-\infty < d_1 < \infty$) is a constant whose numerical value defines a particular meridian; a family of meridians is shown, by the full lines, in Fig. 2 (a).

To characterize the initial relaxation of the alignment as the director traverses the surface of the sphere, we divide the sphere into different characteristic regions, as shown in Fig. 5, by the R^+ and R^- regions. In irrotational extensional flows, the only flow effect on the orientation and alignment is due to the symmetric part of the velocity gradient tensor $(v_{i,j})$, known as the rate of strain tensor and here denoted by A , and whose ij^{th} and ji^{th} components are given by $A_{ij} = A_{ji} = (v_{i,j} + v_{j,i})/2$. An important observation, used below to classify the numerical results of alignment relaxation, is that a director whose tip lies in the R^- regions, samples extensional strains ($A:nn > 0$), while a director whose tip lies in the R^+ regions, samples compressional strains ($A:nn < 0$).

3.3.2. Governing Orientation and Alignment Equations

The macroscopic model used in this paper has been described in detail in [1]. Here we just present the governing equations for the temporal evolution of the director field $\mathbf{n}(t)$ and the alignment $S(t)$, and refer the reader to the above mentioned paper for details. The governing equations for our model uniaxial discotic nematics, subjected to a given isothermal flow, are:

$$\begin{bmatrix} \frac{dn_i}{dt} \\ \frac{dS}{dt} \end{bmatrix} = \begin{bmatrix} W_{ij} n_j + \lambda (A_{ij} n_j - (A_{ik} n_i n_k) n_i) \\ \beta_1 A_{ik} n_i n_k + \beta_2 / \tau_1 \end{bmatrix} \quad (7a, b)$$

where the components of the vorticity tensor \mathbf{W} are $W_{ij} = (v_{i,j} - v_{j,i})/2$. $\lambda(S)$ is the tumbling function, $\beta_1(S)$ the ordering function, and $\beta_2(S, U)$ is proportional to the thermodynamic driving force; these functions are given by :

$$\lambda = -\frac{\gamma_2}{\gamma_1} = - (3 \sigma_4^* + \sigma_6^* S) / (3S + \tau_2^* S^2) \quad (8a)$$

$$\beta_1 = - (9 \sigma_4^* + 6 \sigma_6^* S) / (6 + 4 \tau_2^* S) \quad (8b)$$

$$\beta_2 = (-3S + US + US^2 - 2US^3) / (3 + 2 \tau_2^* S) \quad (8c)$$

where the starred coefficients are scaled with the alignment relaxation time τ_1 that appears in equation (7b).

To select numerical values for the three phenomenological parameters σ_4^* , σ_6^* , τ_2^* , we enforce the following constraints on the signs of λ and γ_1 [10, 11, 12, 13] and on the values of λ when $S=0$ and $S=1$ [10] :

$$\lambda = -\frac{\gamma_2}{\gamma_1} < 0 ; \quad \gamma_1 \geq 0 ; \quad \lim_{S \rightarrow 0} \lambda = -\infty ; \quad \lim_{S \rightarrow 1} \lambda = -1 \quad (9a,b,c,d)$$

The adopted values that satisfy the constraints are: $\sigma_4^* = 1/10$, $\sigma_6^* = 1.7$, $\tau_2^* = -1.0$, and the resulting λ and β_1 are shown in Fig. 3; the relevant phenomena described in this paper are captured by other arbitrary triplets that satisfy equations (9), and the values adopted here were chosen only for convenience. It is worth noting that for extensional flows all steady states are simple fixed points and thus adoption of the different $\lambda(S)$ and $\beta_1(S)$ will

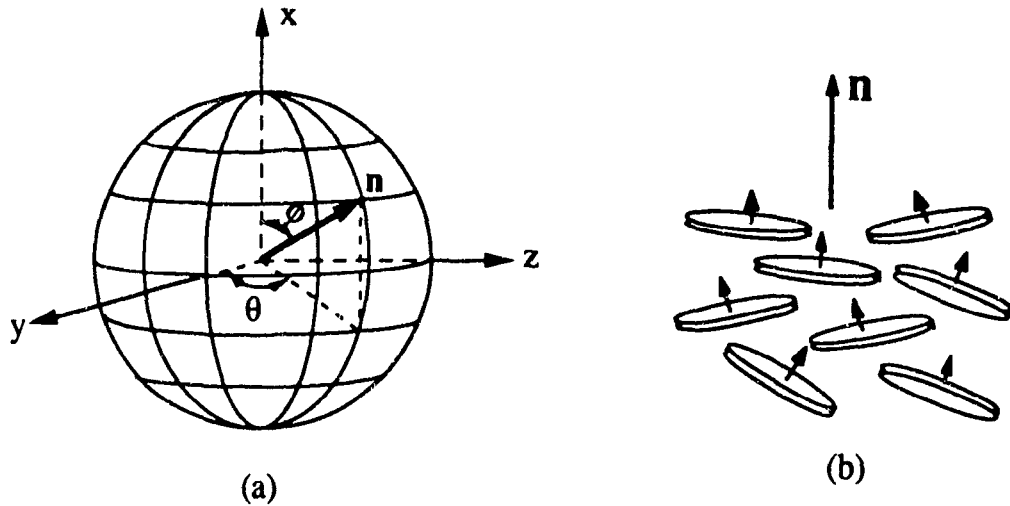


Fig. 2. Definition of (a) coordinate system, and (b) director orientation of a uniaxial discotic nematic liquid crystal. (a) Director angles and unit sphere: θ ($0 \leq \theta \leq 2\pi$) is the azimuthal angle and ϕ ($0 \leq \phi \leq \pi$) is the polar angle. The north pole of the sphere is located at $\phi = 0$, the south pole at $\phi = \pi$, and the equator at $(\theta, \phi) = ([0, 2\pi], \pm\pi/2)$, \mathbf{n} denotes the director. (b) The director in a discotic nematic phase is the average orientation of the unit normals to the disc-like molecules.

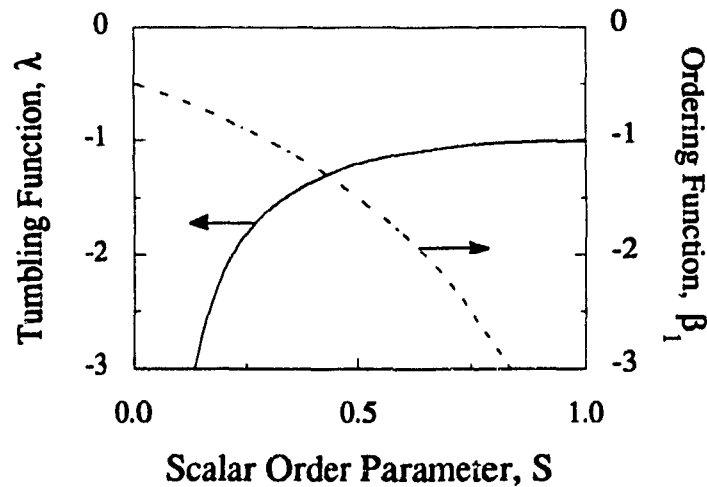


Fig. 3. Tumbling function λ and the ordering function β_1 as a function of the scalar order parameter S . The tumbling function is the ratio of the coefficient for strain and vorticity viscous torques, while the ordering function is the coefficient for the ambient strain rate $\mathbf{A}:\mathbf{nn}$ that governs the relaxation of S . For discotics (rod-like) nematics both are negative (positive).

only change the time scales but the significant phenomena will be essentially unchanged.

The simplifying assumptions and approximations made in deriving the mathematical model that describes the flow-induced alignment and orientation of an ideal discotic nematic liquid crystal, as given by equations (7, 8), can be found in [1].

The velocity field $v(x, y, z)$ corresponding to the extensional start-up flow of the nematic sample, is given by [23]:

$$v_x = a \dot{\epsilon} x H(t); \quad v_y = -a \frac{\dot{\epsilon}}{2} (1+b) y H(t); \quad v_z = -a \frac{\dot{\epsilon}}{2} (1-b) z H(t); \quad (10a,b,c,d)$$

$$H(t) = \begin{cases} 0 & t < 0 \\ 1 & t \geq 0 \end{cases}$$

where $\dot{\epsilon}$ is the given constant extension rate. The corresponding rate of deformation tensor A , is given as:

$$A = \dot{\epsilon} \begin{bmatrix} a & 0 & 0 \\ 0 & -\frac{a}{2}(1+b) & 0 \\ 0 & 0 & -\frac{a}{2}(1-b) \end{bmatrix} \quad (11)$$

where $a=+1$ or -1 , and $0 \leq b \leq 1$ captures the range of possible extensional flows. Uniaxial extensional flow (UE) is given by $a=+1$, $b=0$, biaxial extensional flow (BE) by $a=-1$, $b=0$, and planar extensional flow (PE) by $a=+1$, $b=+1$. These flows are irrotational and the vorticity tensor is zero ($\mathbf{W} = 0$). Replacing equations (10, 11) in equations (7), the following set of coupled nonlinear ordinary differential equations for extensional isothermal, incompressible flows of uniaxial discotic nematic crystals are obtained:

$$\frac{dn_x}{d\epsilon} = \frac{a}{2} \lambda [3(1-n_x^2) + (n_y^2 - n_z^2)] n_x \quad (12a)$$

$$\frac{dn_y}{d\epsilon} = -\frac{a}{2} \lambda [3n_x^2 + b(1 - n_y^2 + n_z^2)] n_y \quad (12b)$$

$$\frac{dn_z}{d\epsilon} = -\frac{a}{2} \lambda [3n_x^2 - b(1 + n_y^2 - n_z^2)] n_z \quad (12c)$$

$$\frac{dS}{d\epsilon} = \frac{a}{2} \beta_1 [3(n_x^2 - 1) - b(n_y^2 - n_z^2)] n_z + De^{-1} \beta_2 \quad (12d)$$

where $\epsilon = \dot{\epsilon}t$ is the strain (dimensionless time) , $De = \dot{\epsilon}\tau_1$ is the alignment Deborah number (dimensionless strain rate). We note that equations (12) are dimensionless, and thus, for a given set of parameters , the solution vector (S, \mathbf{n}) is only a function of the strain (dimensionless time) $\epsilon = \dot{\epsilon}t$. In the absence of Frank elasticity [16] , strain scaling is typical of liquid crystalline flow phenomena [34] . When $De \rightarrow 0$ the alignment (S) relaxation is elastic, when $De \rightarrow \infty$ it is purely viscous, and for the intermediate values it is viscoelastic. At intermediate De the director relaxation is also viscoelastic, since it is coupled to S through $\lambda(S)$.

The initial conditions used to solve equations (12) are :

$$@ \epsilon = 0 : \mathbf{n} = \mathbf{n}_0 ; S = S_{eq} ; \mathbf{n}_0 \cdot \mathbf{n}_0 = 1 \quad (13)$$

where $S_{eq}(U)$ is the equilibrium scalar order parameter of the normal ($S > 0$) uniaxial nematic phase, found by setting the numerator of equation (8c) equal to zero [29]:

$$S_{eq} = \frac{1}{4} + \frac{3}{4} \sqrt{1 - \frac{8}{3U}} \quad (14)$$

For $U < 8/3$ the stable phase is isotropic, for $8/3 \leq U \leq 3$ there is biphasic equilibrium. In this paper we use two representative nematic potentials $U = 3$ and $U = 5$, and the corresponding initial conditions are: $S_{eq}(U=3) = 0.5$ and $S_{eq}(U=5) = 0.76$. All angles are reported in degrees.

Equations (12) are integrated using an implicit corrector-predictor first order Euler integration method with an adaptable time step [30]. Application of the implicit corrector-predictor method transforms the set of coupled nonlinear ordinary differential equations (12) into a set of coupled nonlinear algebraic equations . For each time step the algebraic equations are solved using the Newton-Raphson iteration scheme [30] ; the predictor step generates a first guess for the iteration loop and the corrector step is the iteration loop itself. The adopted convergence criteria is that the length of the difference vector between the calculated solution vectors corresponding to two successive iterations is less than 10^{-6} . The transient solution vector obtained from the numerical solutions ($\mathbf{n}(\epsilon), S(\epsilon)$), is used to calculate the tensor order parameter $Q(\epsilon)$, and the converged steady state solutions (\mathbf{n}_{ss}, S_{ss}) are used to compute the steady flow birefringence. To facilitate the discussion and perform an analysis of the numerical solutions, some of the computed results are presented in reference to the unit sphere description of the director field.

3.4. Analytical Results

3.4.1. Director Dynamics

Integration of the set of equations (12) yields, with \mathbf{A} given by equation (11), the following expression for the director relaxation $\mathbf{n}(\epsilon)$ for any extensional start-up flow :

$$n_i(\epsilon) = \frac{E_{ij} n_{j0}}{|\mathbf{E} \cdot \mathbf{n}_0|}; \quad n_i(0) = n_{i0}; \quad (15a,b,c,d)$$

$$E_{ij}(\epsilon) = \exp \left\{ \tilde{A}_{ij} \int_0^\epsilon \lambda d\epsilon' \right\}; \quad \tilde{A}_{ij} = A_{ij} / \dot{\epsilon}$$

and in the component form:

$$n_x = \frac{E_{xx} n_{x0}}{|\mathbf{E} \cdot \mathbf{n}_0|}; \quad n_y = \frac{E_{yy} n_{y0}}{|\mathbf{E} \cdot \mathbf{n}_0|}; \quad n_z = \frac{E_{zz} n_{z0}}{|\mathbf{E} \cdot \mathbf{n}_0|} \quad (16a,b,c)$$

$$E_{xx} = \exp \left(a \int_0^\epsilon \lambda d\epsilon' \right) \quad (16d)$$

$$E_{yy} = \exp \left(-\frac{1}{2} a(1+b) \int_0^\epsilon \lambda d\epsilon' \right) \quad (16e)$$

$$E_{zz} = \exp \left(-\frac{1}{2} a(1-b) \int_0^\epsilon \lambda d\epsilon' \right) \quad (16f)$$

$$E_{ij} = 0 \text{ for } i \neq j \quad (16g)$$

where n_{j0} is the j th component of the initial director orientation ($\mathbf{n}(0)$). Figure 4 shows representative computed director trajectories for uniaxial extensional, biaxial extensional and planar extensional flows projected onto the y - z plane, here the x -axis is normal to the plane of the paper, and the direction of the director paths are indicated by the direction of arrows. The figure shows that for uniaxial extensional and biaxial extensional flows the director follows identical paths but in reverse directions. In terms of the adopted polar (θ) and azimuthal (ϕ) angles, the director trajectories, given by equations (16), are as follows:

$$\text{Uniaxial Extensional Flow: } \tan(\theta) = 1/d_1; 0 \leq \phi \leq \pi; -\infty < d_1 < \infty \quad (17a)$$

$$\text{Biaxial Extensional Flow: } \tan(\theta) = 1/d_1; 0 \leq \phi \leq \pi; -\infty < d_1 < \infty \quad (17b)$$

$$\text{Planar Extensional Flow: } \tan(\theta) \sin(\theta) = 1/d_2 \cot(\phi); 0 \leq \phi \leq \pi; -\infty < d_2 < \infty \quad (17c)$$

where $d_1 = n_y/n_z$, and $d_2 = n_x n_y/n_z^2$. for time $t \geq 0$. Comparing equations (5, 6) and (16) it follows that for uniaxial extensional and biaxial extensional flows, the director trajectories belong to the meridians of the unit sphere, and the director dynamics belong to the class of geodesic flows [1]. Equation(17c) and Fig 4 shows that planar extensional flow is not a geodesic flow, except when $d_2 \rightarrow \infty$ (n_0 lying along the x-y plane or the y-z plane); in practice due to the presence of the fluctuations this exceptional case will not occur. The director trajectories should exhibit the characteristic sensitive dependence on initial conditions which is typical of geodesic flows [31] or of arbitrary flows on a sphere with multiple fixed points. The sensitive dependence on initial conditions for each extensional flow type are:

$$\text{Uniaxial Extensional Flow: } n_{x0} = \pm 1 \quad (18a)$$

$$\text{Biaxial Extensional Flow: } n_{x0} = 0 \quad (18b)$$

$$\text{Planar extensional Flow: } n_{y0} = 0 \quad (18c)$$

When the initial director orientation for each flow type is along those defined in equations (18) predictability is lost; for example in planar extensional flow, if $n_{y0} = 0$ the director may evolve with equal likelihood towards the positive y-axis or towards the negative y-axis. Table I summarizes the relations between flow types ($a = \pm 1, 0 \leq b \leq 1$), the compression direction or compression plane, and the stable steady state director orientations. The entries in Table I show that for all cases the director always aligns along the compression direction or the compression plane of the flow. It is worth noting that when $a = -1$, the stable steady state director orientation is insensitive to the magnitude of b , since for these flows the strongest compression direction always lies along the x-axis. On the other hand when $a = +1$, the strongest compression plane changes from the y-z plane when $b = 0$, to the y-axis when $b \neq 0$. These observations can be used to classify the orienting strength of each extensional flow, since as shown above, the sensitive

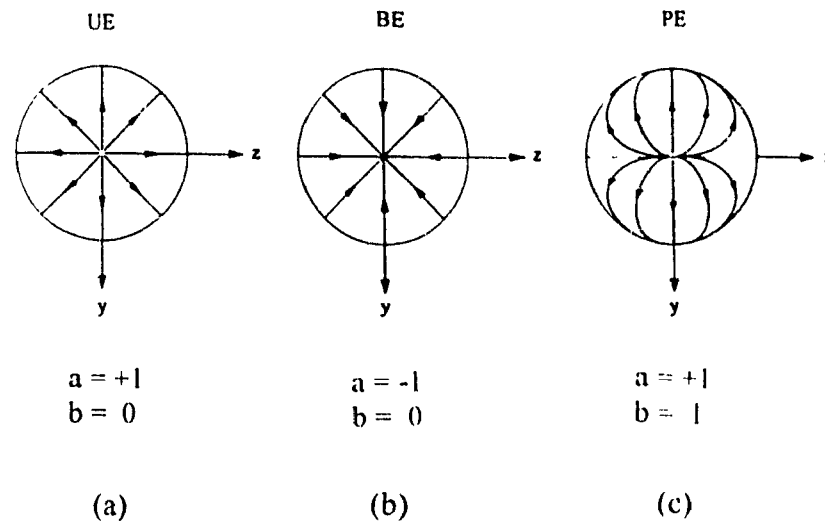


Fig. 4. Schematics of the director trajectories on the y - z plane for (a) uniaxial extensional flow (UE), (b) biaxial extensional flow (BE), and (c) planar extensional flow (PE). For uniaxial (biaxial) extensional flow the sources are the poles (equator) and the sink is the equator (poles). For planar extensional flow the sources are the poles and the sinks are $n_y = \pm 1$.

Table I
Steady States and Sensitive Initial Conditions of the Director

Flow Type		Strongest Compression Direction	Director Steady States			Sensitive Dependence to Initial Conditions
			n_{xss}	n_{yss}	n_{zss}	
$a = +1$	$b = 0$	y - z plane	0	$\frac{\pm n_{y0}}{\sqrt{1 - n_{x0}^2}}$	$\frac{\pm n_{z0}}{\sqrt{1 - n_{x0}^2}}$	$n_{x0} = \pm 1$
$a = +1$	$0 < b \leq 1$	y -axis	0	± 1	0	$n_{y0} = 0$
$a = -1$	$0 \leq b \leq 1$	x -axis	± 1	0	0	$n_{x0} = 0$

dependence to initial conditions for biaxial extensional and planar extensional flows lead to no uncertainty (since $\mathbf{n} = -\mathbf{n}$) while for uniaxial extensional flow the magnitude of largest uncertainty is the whole equator ($n_x = 0$). Thus, on a relative scale, biaxial extensional and planar extensional flows are strongly orienting flows while uniaxial extensional flow is a weakly orienting flow.

Another important practical property of each flow is the presence or absence of geodesic flow, because this will determine the number of strain units required to achieve the steady director orientation; geodesic flows will, in general, require less strains because a geodesic path is the shortest. For example Fig. 4(c) shows that for planar extensional flows the paths are generally longer and thus the number of applied strains to achieve steady state must be larger than for the uniaxial extensional and biaxial extensional flows.

3.4.2. Alignment Dynamics

The alignment relaxation $S(\epsilon)$ depends on \mathbf{n}_0 through the ambient strain rate $\mathbf{A}:\mathbf{nn}$. Figure 5 shows different representative regions for $\mathbf{A}:\mathbf{nn}$: in the R^- regions the ambient strain rate is positive ($\mathbf{A}:\mathbf{nn} > 0$), and in the R^+ regions the ambient strain rate is negative ($\mathbf{A}:\mathbf{nn} < 0$). The initial alignment relaxation characteristics are given by:

$$\begin{aligned} \mathbf{n}_0 \text{ in } R^- : \left(\frac{dS}{d\epsilon} \right)_{\epsilon=0^+} < 0; \quad \mathbf{n}_0 \text{ in } R^+ : \left(\frac{dS}{d\epsilon} \right)_{\epsilon=0^+} > 0; \\ \mathbf{n}_0 \text{ in } \partial R^- = \partial R^+ : \left(\frac{dS}{d\epsilon} \right)_{\epsilon=0^+} = 0 \end{aligned} \quad (19a,b,c)$$

It follows from equations (19) that for any De , a sufficient condition for increasing S is that \mathbf{n}_0 is in R^+ . For large De , discotic nematics, initially in R^- , undergo a temporary melting while the director is in region R^- [1].

In case of polymer flows [9] a flow type may be characterized as weakly aligning or strongly aligning depending on the degree of alignment change in the flowing units. In the present case, our model predicts that the alignment strength is directly proportional to $|(\tilde{\mathbf{A}}:\mathbf{nn})_{SS}|$. Figure 6 shows the dimensionless steady state alignment strength $|(\tilde{\mathbf{A}}:\mathbf{nn})_{SS}|$ for all the possible extensional flows ($a = \pm 1, 0 \leq b \leq 1$). The figure clearly shows that when $a = -1$ the alignment strength is insensitive to the magnitude of b , but for $a = +1$, it is highly sensitive to the value b . The figure also shows the location of the three representative extensional flows. Table II shows the relations between the flow aligning

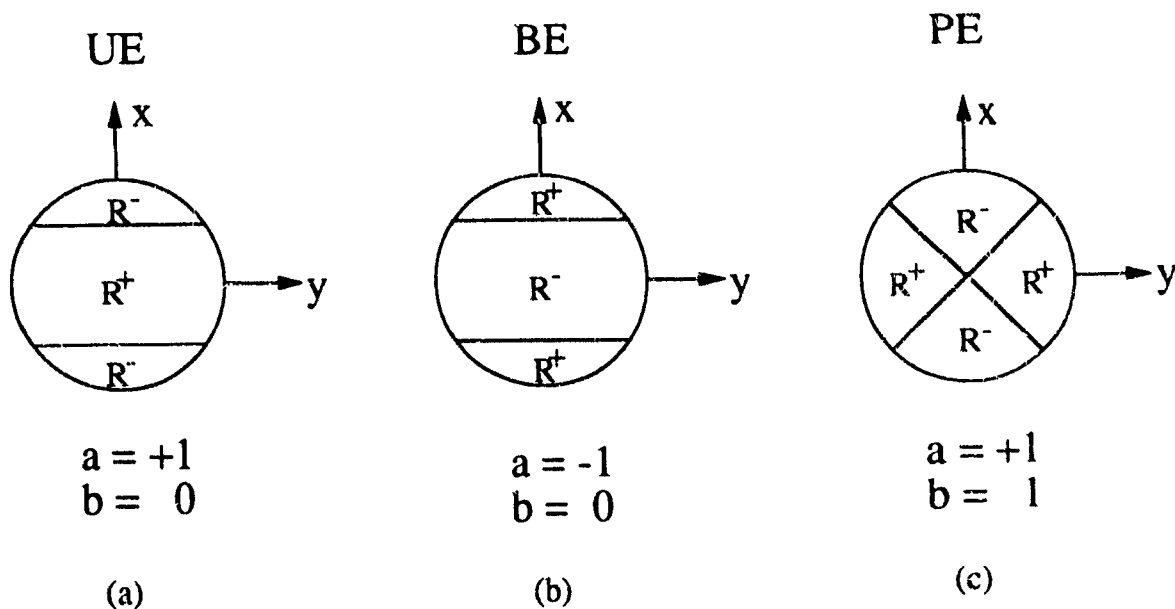


Fig. 5. Sensitivity of the initial alignment S relaxation to the initial director orientation. The different characteristic regions for the ambient strain rate $A:nn$ for (a) uniaxial extensional flow (UE), (b) biaxial extensional flow (BE), and (c) planar extensional flow (PE). In the R^- regions the alignment rate is positive ($A:nn > 0$), and in the R^+ regions the alignment rate is negative ($A:nn < 0$).

Table II
Alignment Strength of Extensional Flows

Flow Type		Alignment Strength $ (\tilde{A} : nn)_{ss} $
$a = +1$	$b = 0$	$\frac{1}{2}$
$a = +1$	$0 < b \leq 1$	$\frac{1}{2}(1 + b)$
$a = -1$	$0 \leq b \leq 1$	1

strength and the flow parameters a and b , for general extensional flows. Comparing the various entries in Table II, it follows that the highest flow alignment strength scales with the strongest compressional strains ($a = -1, 0 \leq b \leq 1$; and $a = 1, b = 1$) as in biaxial extensional and planar extensional flows, while the lowest flow alignment strength scales with the weakest compressional strains ($a = +1, b = 0$) as in uniaxial extensional flow.

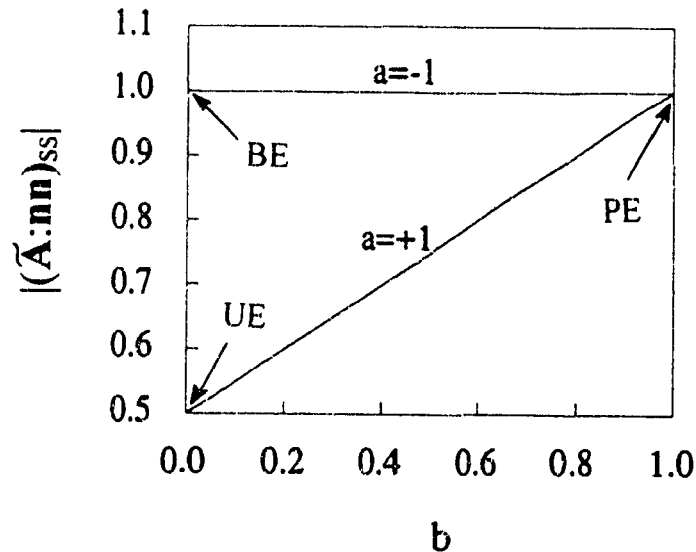


Fig. 6. Alignment strength (absolute value of steady state dimensionless ambient strain rate) $|(\tilde{A}:nn)_{SS}|$ as a function of the flow parameter b , for all types of extensional flows. The biaxial extensional and planar extensional flows are more strongly aligning than uniaxial extensional flow.

3.5. Numerical Results

3.5.1. Orientation Relaxation

Figure 7(a) shows the director orientation relaxation, in terms of the azimuthal director angle θ and the polar director angle ϕ as a function of strain (dimensionless time) $\varepsilon = \dot{\varepsilon} t$, for uniaxial extensional flow (solid line), biaxial extensional flow (dot-dash line), and planar extensional flow (triple dot-dash line), for $De=0.5$, $U=5$, and with the initial director orientation $(\theta_0, \phi_0)=(45, 45)$. Figure 7(b) shows the corresponding computed scientific visualization of the director relaxation, represented by the normals to the shown discs. Figure 7(a) shows that for uniaxial extensional flow the steady director orientation is $(\theta_{SS}, \phi_{SS}) = (45, 90)$, for biaxial extensional flow it is $(\theta_{SS}, \phi_{SS}) = (45, 0)$, and

for planar extensional flow it is $(\theta_{ss}, \phi_{ss}) = (0, 90)$, in agreement with the predictions summarized in Table I. The visualization in Fig. 7(b) shows that the director exhibits different combinations of twisting and tilting as the strain increases but that the final steady state orientation is always along the strongest compression direction(s) for each flow. It can be shown that for all extensional flows, the director relaxation is faster at higher De and at lower U , since for these conditions the adapted $\lambda(S)$ samples larger absolute values.

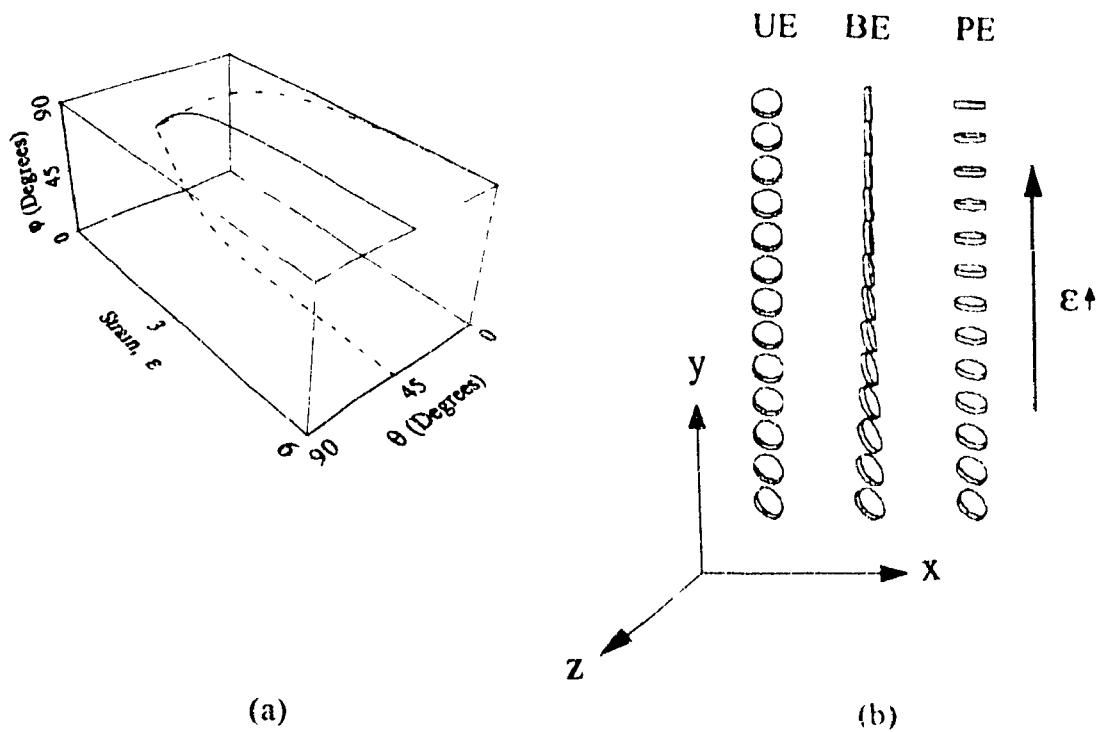


Fig. 7. (a) Azimuthal director angle θ and polar director angle ϕ as a function of strain (dimensionless time) $\epsilon = \dot{\epsilon} t$, for uniaxial extensional flow (solid line), biaxial extensional flow (dot-dash line), and planar extensional flow (triple dot-dash line) for $De=0.5$, $U=5$, and initial director orientation $(\theta_0, \phi_0) = (45, 45)$. The figure shows the orientation relaxation of the director for three different types of extensional flows. (b) Corresponding computed scientific visualization of the director relaxation, represented by the normals to the shown discs. For the same initial orientation, the steady state director orientation is different and the final steady state depends on the type of extensional flow.

Figure 8 shows the x and z components of the director as a function of strain (dimensionless time) $\epsilon = \dot{\epsilon} t$, for uniaxial extensional flow (solid line) and planar extensional flow (dot-dash line), for $De=0.5$, $U=5$, and with the initial director orientation ($n_{x0}=0.9990$, $n_{y0}=0.0004$, $n_{z0}=0.0447$) or $(\theta_0, \phi_0) = (89.4, 2.56)$. The figure shows that the number of strain (dimensionless time) units required to achieve steady state director orientation for planar extensional flow is considerably larger than those for uniaxial extensional flow. For the selected \mathbf{n}_0 , the director follows, in both cases, a trajectory close to the x - z plane till the equator is reached; this is the reason for the comparable n_x dynamics in both the cases. The main difference in required strains arises from the fact that for planar extensional flow only the y -axis is the compression direction, and thus n_z must now decay to zero.

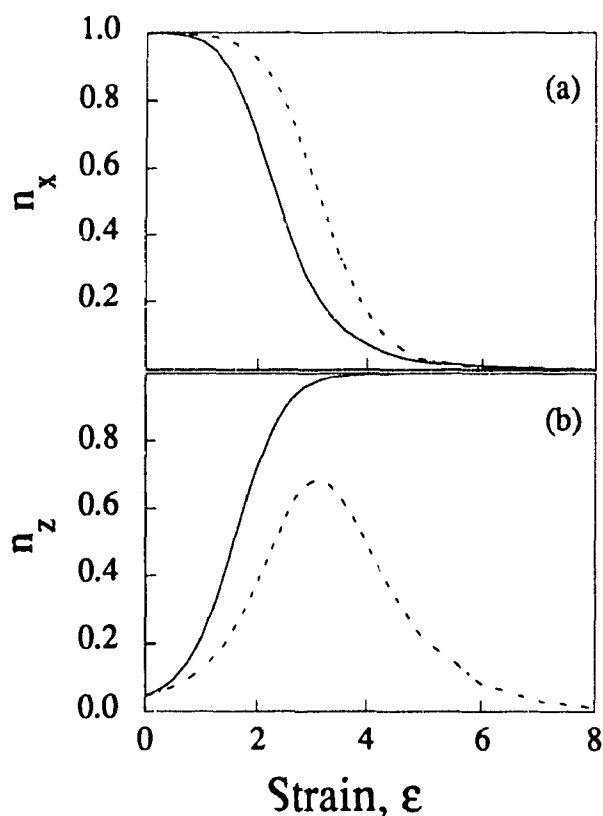


Fig. 8. Director components as a function of strain (dimensionless time) $\epsilon = \dot{\epsilon} t$, for uniaxial extensional flow (solid line) and planar extensional flow (dot-dash line) for $De=0.5$, $U=5$, and initial director orientation ($n_{x0}=0.9990$, $n_{y0}=0.0004$, $n_{z0}=0.0447$) or $(\theta_0, \phi_0)=(89.4, 2.56)$. The number of strains (dimensionless time) units required to achieve steady state orientation for planar extensional flow is considerably larger than for uniaxial extensional flow

3.5.2. Alignment Viscoelastic Relaxation

Figure 9 shows the alignment relaxation $S(\epsilon)$ for uniaxial extensional flow (solid line), biaxial extensional flow (dash-dot line), and planar extensional flow (triple dot-dash line) corresponding to the initial director orientation of Fig. (7), and for (a) $U=5$, $De=0.5$; (b) $U=5$, $De=0.1$; (c) $U=3$, $De=0.5$; and (d) $U=3$, $De=0.1$. The relaxation coordinate $\epsilon = \dot{\epsilon} t$ is the strain (dimensionless time). The figure shows that biaxial extensional and planar extensional flows have similar relaxations and both lead to higher steady state values of the alignment S than in case of uniaxial extensional flow, as predicted in

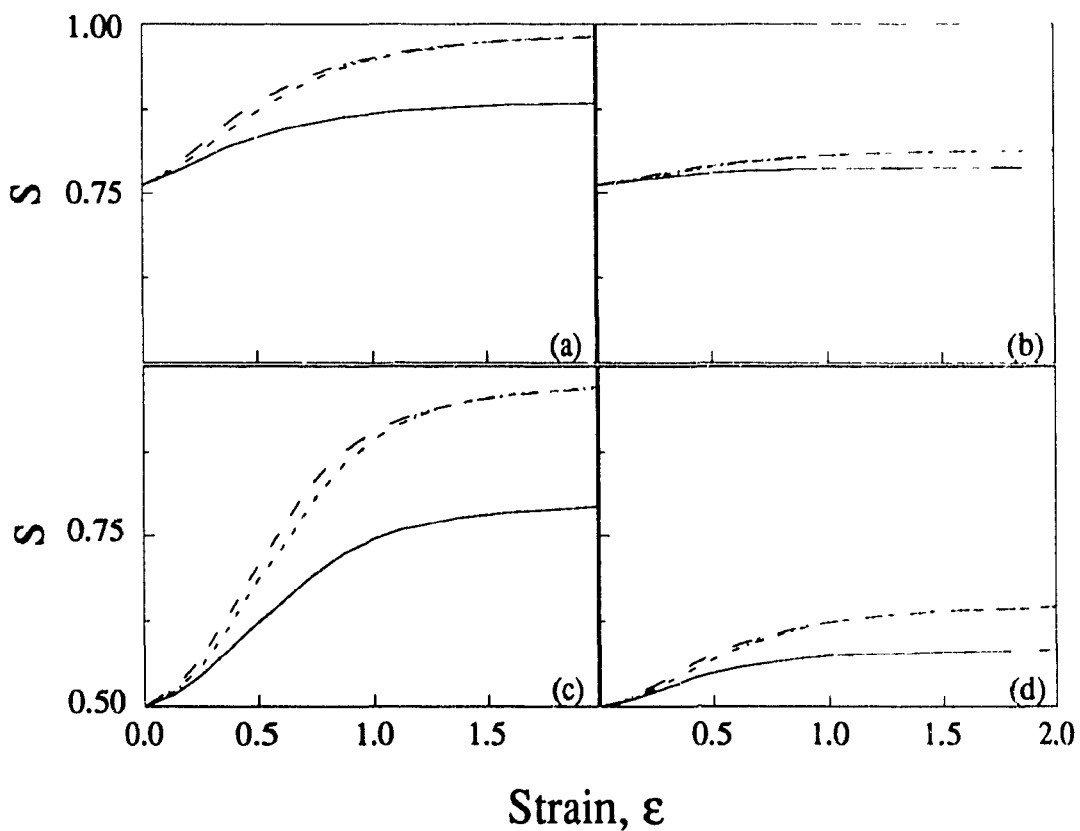


Fig. 9. The alignment relaxation $S(\epsilon = \dot{\epsilon} t)$ for uniaxial extensional flow (solid line), biaxial extensional flow (dash-dot line), and planar extensional flow (triple dot-dash line) corresponding to the initial director orientation of Fig (6), for (a) $U=5$, $De=0.5$; (b) $U=5$, $De=0.1$, (c) $U=3$, $De=0.5$; and (d) $U=3$, $De=0.1$. Here $\epsilon = \dot{\epsilon} t$ denotes strain or dimensionless time. The figure shows that the relaxation is more sensitive to the alignment strength of the flow at higher De (viscous mode) and at lower U (elastic mode).

Table II. The figure shows that at higher De , the dynamics of S are slower than at lower De , for both low and high values of U , and that this trend is independent of the flow type. In addition at higher De , the viscous mode dominates the viscoelastic relaxation at all the times, and the effect of the relative magnitude of U is smaller, while at lower De , the elastic mode dominates and the effect of U is larger. It also follows from the figure that at higher De , the dynamics and steady state value of S is more sensitive to the value of U in the case of uniaxial extensional flow than in case of biaxial extensional and planar extensional flows, because at a given De , the flow alignment strength $|\langle \tilde{\mathbf{A}}:\mathbf{nn} \rangle_{ss}|$ in the former is lower than in the last two cases. At lower De , the flow-type sensitivity is weaker since in this regime the elastic mode dominates.

3.5.3. Tensor Order Parameter Relaxation and Flow Birefringence

Figure 10 shows the relaxation of the components of the tensor order parameter \mathbf{Q} as a function of strain (dimensionless time) $\epsilon = \dot{\epsilon}t$ with initial director orientation $(\theta_0, \phi_0) = (45, 45)$, for $U=3$ and $De=0.5$, and for (a) uniaxial extensional flow (solid line), (b) biaxial extensional flow (dash-dot line), and (c) planar extensional flow (triple dash-dot line). For the shown parameters the relaxation is virtually complete after 5 strain (dimensionless time) units. The trace elements of \mathbf{Q} scale with the alignment strength of the flow and the relative orientation between \mathbf{n}_{ss} and compression directions of \mathbf{A} . A summary of the main features of the steady state values of trace of \mathbf{Q} is as follows:

Q_{yy} : The biaxial extensional flow exhibits the lowest value since n_y is normal to the compression axis (x -axis) while planar extensional flow attains the highest magnitude since n_y is along the compression axis (y -axis) and the alignment strength is high.

Q_{xx} : Since n_x is normal to the extension direction for uniaxial extensional and planar extensional flows, thus Q_{xx} is small, while for biaxial extensional flow, the net combination due to the fact that n_x is along the compressional axis and that the high alignment strength gives a relative large Q_{xx} .

Q_{zz} : Here the compression directions for biaxial extensional and planar extensional flows are orthogonal to n_z and thus for these flows Q_{zz} is small. For uniaxial extensional flow, although n_z lies in the compressional plane the weakly aligning character of the flow yields a relatively low Q_{zz} .

The steady state values of the off-diagonal components ($Q_{ij}, i \neq j$) are equally explained by taking into account the alignment strength of the flow and the compression directions of the flow. For example Q_{yz} vanishes for biaxial extensional and planar extensional

flows since n_z is parallel to the compression direction of these flows, while for uniaxial extensional flow Q_{yz} is relatively large since n_y and n_z are both in the compression plane of the flow.

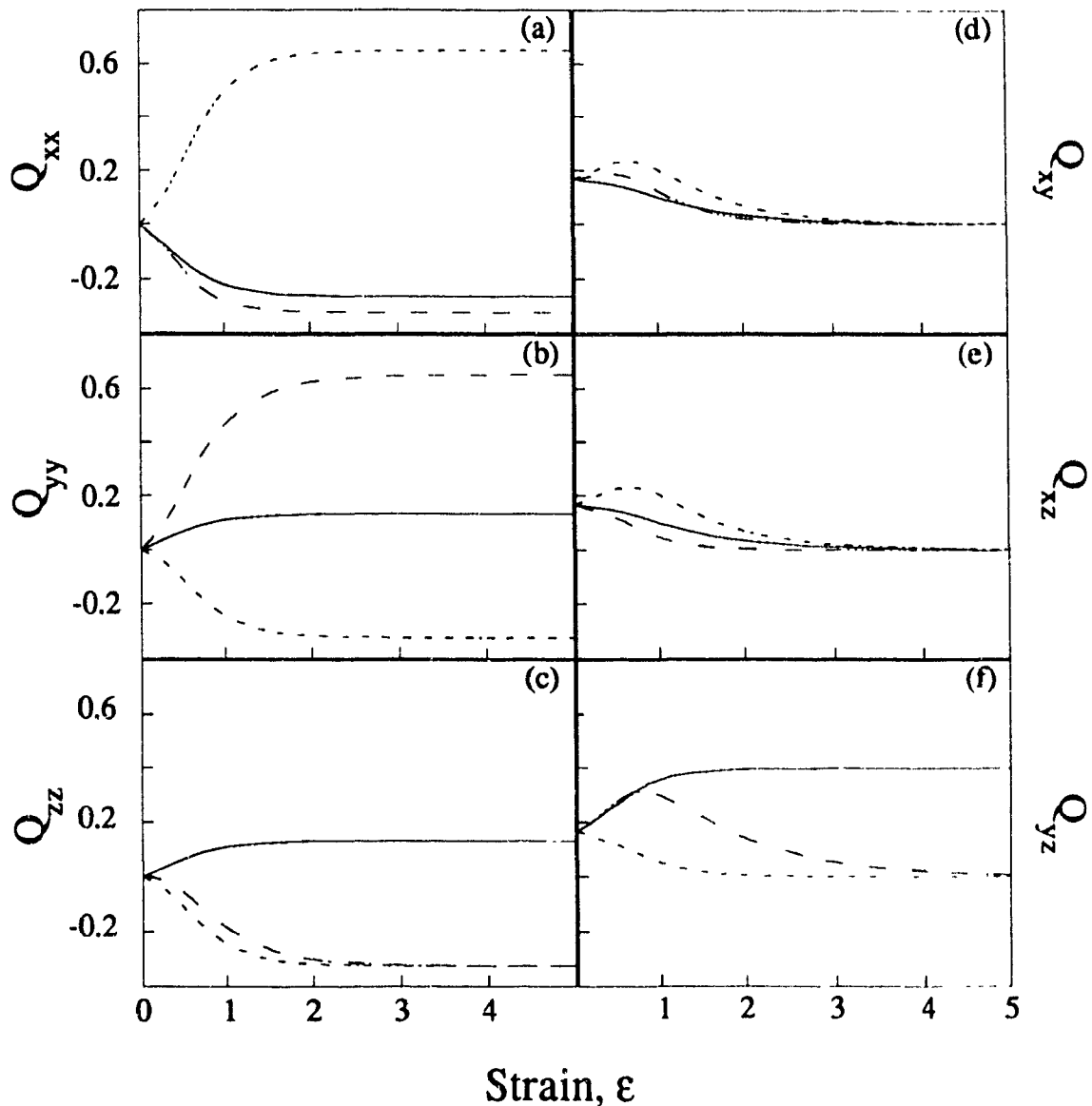


Fig. 10. The relaxation of the components of the tensor order parameter Q ($\epsilon = \dot{\epsilon} t$) with initial director orientation $(\theta_0, \phi_0) = (45, 45)$, for $U=3$ and $De=0.5$, and for (a) uniaxial extensional flow (solid line), (b) biaxial extensional flow (dash-dot line), and (c) Planar extensional flow (triple dash-dot line). The magnitude of the different components scale with the alignment strength of each flow, and with the relative orientations between the different elements of Q and the compression directions of each flow.

According to [24], the birefringence $\Delta\eta$ can be expressed by:

$$\Delta\eta = \sqrt{e_{//}} - \sqrt{e_{\perp}} \approx \frac{\Delta e_{\max} S}{2\sqrt{\bar{e}}} \quad (20)$$

where $e_{//}$ and e_{\perp} are the elements of the dielectric tensor e_{ij} parallel and normal to the director respectively, the tensor e_{ij} is given by $e_{ij} = \bar{e}\delta_{ij} + \Delta e_{\max} Q_{ij}$, where the first term is the average trace of e_{ij} and Δe_{\max} is the anisotropy for $S=1$; for discotics, $\Delta\eta < 0$ since $\Delta e_{\max} < 0$. In deriving equation (20) we have assumed that $\bar{e} \gg 2 \Delta e_{\max} S/3$ for the values of S corresponding to the nematic phase. Equation (20) shows that the steady flow-induced birefringence $\Delta\eta_{SS}$ is proportional to the magnitude of the steady alignment S_{SS} .

Figure 11 shows the steady state alignment S_{SS} as a function of De for uniaxial extensional flow (solid line), for biaxial extensional and planar extensional flows (dash-dot line) for (a) $U=5$, and (b) $U=3$. As shown in Table II, the alignment strength of biaxial extensional and planar extensional flows is identical and thus the shown curve for these two flows superpose. The figure shows a monotonic increase in the flow birefringence. At high De the viscous mode dominates and the effect of the magnitude of U is smaller, while at low De the elastic mode dominates and the effect of the magnitude of U on S_{SS} is larger irrespective of the flow type. The figure shows, in agreement with Table II, that the birefringence for uniaxial extensional flow is smaller than for other flow types since it is a weakly aligning flow. The alignment strength of each flow type explains the relative sensitivity of the birefringence to De for the various flows. At higher U the effect due to the different alignment strengths is smaller than at lower U . At lower U , the viscous mode dominates and the effect due to the different degrees of alignment strengths increases rapidly with increasing De .

3.6. Conclusions

In this initial investigation of the nematic rheology of uniaxial discotics in extensional flows, we have performed a useful characterization of the sensitivity of the director, scalar order parameter, and tensor order parameter relaxation with respect to the flow type, the alignment Deborah number, and the initial director orientation. Use of the unit sphere description identified the director dynamics of uniaxial extensional and biaxial extensional flows as geodesic flows, and as non-geodesic (except for one special case) for planar extensional flow. The three flows exhibit sensitive dependence to initial

conditions, but due to the double arrow nature of the director vector ($\mathbf{n} = -\mathbf{n}$) biaxial extensional and planar extensional flows are strongly orienting flows since they have one stable fixed point. On the other hand, uniaxial extensional flow is a weakly orienting flow, since the stable steady states are a degenerate circle, and when \mathbf{n}_0 is on the poles of the unit sphere, predictability is lost. Significant differences between flow types arise in the number of strain units required to achieve steady state orientations, according to whether the flow is geodesic (uniaxial extensional or biaxial extensional flows) or non-geodesic (planar extensional flow). The alignment strength ($|\langle \tilde{\mathbf{A}} : \mathbf{nn} \rangle_{SS}|$) of the flows scale with the magnitude of the ambient strain rate ($\mathbf{A} : \mathbf{nn}$). It is found that uniaxial extensional flow is a weakly aligning flow but biaxial extensional and planar extensional flows are strongly aligning flows. A summary of the aligning and orienting properties, and of the geometry of the director orbits of the main extensional flows, is given in Table III.

Table III
Classification of Extensional Flows

Flow Type	Orientation Strength (Director)	Alignment Strength (Scalar Order Parameter)	Geodesic Flow
Uniaxial	Weaker	Weaker	Yes
Biaxial	Stronger	Stronger	Yes
Pure Shear	Stronger	Stronger	No

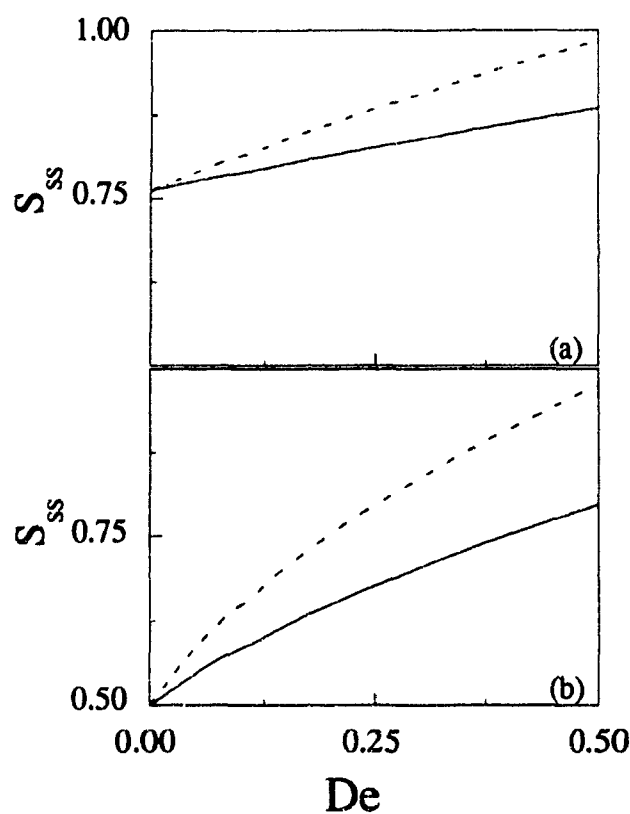


Fig. 11. The steady state alignment S_{SS} as a function of De for uniaxial extensional flow (solid line), and for both biaxial extensional and planar extensional flows (dash-dot line), for (a) $U=5$, and (b) $U=3$. The flow birefringence is proportional to S_{SS} and increases with De . The birefringence for biaxial extensional and planar extensional flows is identical and is greater than for uniaxial extensional flow for all U and De .

3.7. References

- [1] Singh A. P., Rey A. D. and , *J. Phys. II (France)*, **4** (1994) 645-665.
- [2] Gasparoux H., *Mol. Cryst. Liq. Cryst.* **63** (1981) 231-248.
- [3] Otani S., *Mol. Cryst. Liq. Cryst.* **63** (1981) 249-264.
- [4] Zimmer J. E., White J. L., Disclination Structures in the Carbonaceous Mesophase. In : Brown H. G. (ed.), *Advances in liquid Crystals*, Vol. 5 , 1982, Academic Press, New York.

- [5] Chandrashekar S., *Mol. Cryst. Liq. Cryst.* **63** (1981) 171-179.
- [6] Destrade C., Tinh N.H., Gasparoux H., Malthete J., Levelut A. M., *Mol. Cryst. Liq. Cryst.*, **71** (1981) 111-135.
- [7] Singer L. S., "The Mesophase in Carbonaceous Pitches", *Faraday Discuss. Chem. Soc.* **73** (1985) 265-272.
- [8] Tadmor Z., Gogos R. G., "Principles of Polymer Processing", 1979, John Wiley and Sons., New York.
- [9] Larson R. G., "Constitutive Equations for Polymer Melts and Solutions", 1988, Butterworths, Boston.
- [10] Volovik G. E., *JETP Lett.* **31** (1980) 273-275.
- [11] Carlsson T., *Mol. Cryst. Liq. Cryst.* **89** (1982) 57-66.
- [12] Carlsson T., *J. Physique* **44** (1983) 909-911.
- [13] Baals H. and Hess S., *Z. Naturforsch.* **43A** (1988) 662-670.
- [14] Ho A.S.K. and Rey A.D., *Rheol. Acta* **30** (1991) 77-88.
- [15] Leslie F.M., "Theory of Flow Phenomena in Liquid Crystals", in : Brown H. G. (ed.) *Advances in Liquid Crystals vol.4*, Academic Press, New York, (1981), 1-81.
- [16] de Gennes P. G., "The Physics of Liquid Crystals", Oxford University Press, London, (1975) p 153-165.
- [17] Ericksen J. L., "Liquid Crystals with variable degree of Orientation," IMA Preprint Series No. **559** (1989).
- [18] Imura H. and Okano K., *Jpn. J. Appl. Phys.*, **11** (1972) 1440-1445.
- [19] Diogo A. C. and Martins A. F., *J. Phys.*, **43** (1982), 779-786.
- [20] Edwards B.J., Beris A.N. and Grmela M., *Mol. Cryst. Liq. Cryst.* **201** (1991) 51-86.
- [21] Farhoudi Y. and Rey A.D., *J. Rheol.*, **37** (1993) 289-314.
- [22] Marrucci G., "Rheology of Nematic Polymers", in : Ciferri A (ed) *Liquid Crystallinity in Polymers*, VCH Publishers, New York, (1991), 395-423.
- [23] Bird R., Armstrong R.C. and Hassager O., "Dynamics of Polymeric Liquids", Wiley, New York, 1987 .
- [24] Gramsbergen E.F., Longa L., de Jeu W.H., *Physics Reports* **135** (1986) 195-257.
- [25] Thurston R.N., *J. Physique* **42** (1981) 413-417.
- [26] Thurston R.N., *J. Appl. Phys.*, **52** (1981) 3040-3052.
- [27] Carlsson T., *Phys. Rev. A*, **34** (1986) 3393-3404.
- [28] Weinstock R., "Calculus of Variations", McGraw-Hill, New York, 1954, p 26-28.
- [29] Doi M. and Edwards S.F., "The Theory of Polymer Dynamics", Oxford

- University Press, New York (1986) p 358-362.
- [30] Finlayson B.A., "Nonlinear Analysis in Chemical Engineering", McGraw-Hill, New York, 1980, p 28-31.
 - [31] Ruelle D., " Chance and Chaos", Princeton University Press, New Jersey, (1991) p47.
 - [32] Barnes H.A., Hutton J.F., Walters K. " An Introduction to Rheology", Elsevier, Amsterdam (1989) pg. 75.
 - [33] Petrie C.J.S., " Elongational Flows ", Pitman, London (1979) .
 - [34] Han W.H., and Rey A.D., Phys . Rev. E , **49**, 597-613 (1994).

Chapter 4

Theory and Simulation of Extensional Flow-Induced Biaxiality in Discotic Mesophases ¹

4.1. Abstract

Flow-induced biaxiality is simulated for a uniaxial discotic nematic liquid crystal subjected to a constant uniaxial, isothermal, incompressible, irrotational, extensional, three dimensional flow. Numerical and analytical solutions of the director triad (\mathbf{n} , \mathbf{m} , \mathbf{l}), and uniaxial (S) and biaxial (P) alignments are given. The unit sphere description of the director triad is used to discuss and analyze the sensitivity of the director triad trajectories and the coupled alignment (uniaxial and biaxial) relaxations to the initial orientation, nematic potential (U), and to the alignment Deborah number (dimensionless extension rate). The evolution of the director triad is given by the rotation of a moving diad (\mathbf{n} , \mathbf{l}) around a fixed director (\mathbf{m}). When the poles of the orientation unit sphere are along the extension axis, and the equator lies in the compression plane of the flow, it is found that the director diad (\mathbf{n} , \mathbf{l}) dynamics follow geodesic flow and the trajectories belong to the same meridians (great circles through the poles). The space of stable steady state orientation of the uniaxial director \mathbf{n} and the biaxial director \mathbf{m} is the whole compression plane (the equator of the unit sphere), while that of the biaxial director \mathbf{l} is the extension direction (poles). A high degree extension flow-induced biaxiality is found when the uniaxial director is away from the extension axis and when S is relatively low. The scalar order parameter couplings are captured by analyzing the trajectories in the alignment triangle. Computed scientific visualizations of biaxial molecular orientation distributions are used to correlate the director triad dynamics and the alignment's dynamics. The tensor order parameter is used to calculate the main flow-birefringences.

¹ This chapter has been submitted as an article for publication in *Journal de Physique II (France)*, (August 17, 1994).

4.2. Introduction

Carbonaceous mesophases are an important class of low cost precursors in the manufacture of high performance carbon fibers [1, 2, 3]. This mesophase precursor is a uniaxial discotic nematic liquid crystalline material. These mesophases are formed by the condensation of the aromatic molecules present in the coal or petroleum pitches [1, 2, 4] and tend to adopt a uniaxial discotic nematic phase Nd [5, 6], with unit normals to the disc-like molecules more or less aligned along a common direction (see upper Fig. 1), represented by the uniaxial director \mathbf{n} ; in what follows we use \mathbf{n} and uniaxial orientation interchangeably. The degree of alignment of the unit normals along \mathbf{n} is given by the scalar order parameter S [7]; in what follows we use S and uniaxial alignment interchangeably. Since spinning of discotic carbonaceous mesophases involves stretching and extension, a fundamental understanding of extensional flow-induced orientation and alignment is highly desirable. In this paper we use the extensional flow classification terminology of [8].

For flow of mesophase materials of relatively large molecular weights, the coupling between the director and the scalar order parameter should be retained [9]. This dynamic coupling introduces additional nonlinearities through the dependence of the generalized Leslie coefficients on the scalar order parameter, as shown in various works [9, 10, 11, 12, 13]. In previous works [14, 15], the authors used variational principles to develop an approximate macroscopic model that allows for variable uniaxial orientation and alignment in discotic nematics, and applied it to various extensional flows. For uniaxial extensional flow, it was found that the uniaxial director trajectories on the unit sphere ($\mathbf{n} \cdot \mathbf{n} = 1$) follow, from the initial orientation to the compressional plane (normal plane to the extension direction), a geodesic meridian flow and that the uniaxial alignment relaxation was sensitive to the initial orientation, to the extension rate, and to the nematic potential that controls the magnitude of S in the absence of flow. The sensitivity to initial conditions, typical of geodesic flows, was shown to be the cause for the loss of predictability that occurs when the initial uniaxial director orientation lies along the extension axis of the flow. In addition, strong extension was found to produce large decreases in the uniaxial scalar order parameter when the uniaxial director was aligned near the extension axis. The previous works [14, 15] precluded flow-induced biaxiality because they are based on a uniaxial macroscopic model.

Field-induced biaxiality in nematic liquid crystals has been shown to occur under various conditions. Uniaxial nematic liquid crystals of negative dielectric anisotropy display biaxial ordering when subjected to an electric field normal to the uniaxial director

axis [16]. Uniaxial nematics of negative magnetic susceptibility also display biaxial ordering when subjecting the material to a magnetic field oriented parallel to the initial director orientation [17]. Extensional flows are known [14, 15] to have orienting qualities similar to those of electromagnetic fields, and this forms the basis for the industrial manufacturing of organic fibers. The basic flow orienting phenomena of nematics in uniaxial extensional flows depends on the molecular geometry. In extensional flows the reactive parameter λ [7] plays the analogous role as the diamagnetic susceptibility in the magnetic field-induced reorientations. For rod-like nematics $\lambda > 0$ and extension aligns the director along the stretching direction, while for discotic nematics $\lambda < 0$ and extension aligns the director anywhere in the compression plane. Given the stated field-orienting properties of the uniaxial discotic nematics and the analogy with magnetic reorientation phenomena, we expect that a uniaxial extensional flow will also induce biaxial ordering. The biaxial state is described by orthogonal director triad $(\mathbf{n}, \mathbf{m}, \mathbf{l})$ and two scalar order parameters (S, P) [18, 19]. Although no experimental measurements of the state of alignment of uniaxial discotic during extensional flows exist, significant flow-induced changes of the uniaxial scalar order parameter of rod-like mainchain nematic polymers are believed to dominate their rheology [20]. Thus we expect that flow-induced biaxiality may be accessible and significant for discotic mesophases subjected to uniaxial extensional flows.

The main objective of this work is to establish the relevant qualitative features that describe the relations between uniaxial extensional deformations inputs and orientation (uniaxial and biaxial) and alignment (uniaxial and biaxial) responses in an idealized, uniaxial discotic nematic liquid crystalline phase. The particular objectives of this paper are:

- (1) To characterize the sensitivity of director triad $(\mathbf{n}, \mathbf{m}, \mathbf{l})$ trajectories and their stable steady states to the initial conditions, and to the extension rate, using analysis and numerical simulation;
- (2) To characterize the sensitivity of uniaxial (S) and biaxial (P) alignment relaxations, along the corresponding director paths, to the initial conditions and to the extension rate, using numerical simulation.

In this paper we use the unit sphere description [14, 15] of nematics only to facilitate the discussion and classification of the numerical results that pertain to the above mentioned objectives.

The organization of this paper is as follows. In section 4.3 we define the coordinate system and the state variables, define the uniaxial extensional flow, briefly present the elements of the unit sphere description used to discuss and classify the

analytical and numerical solutions, and present the governing equations. In this section we also present analytical orientation (uniaxial and biaxial) and alignment (uniaxial and biaxial) results, and the principles used to select the phenomenological parameters of the model. A brief description of the numerical method used to integrate the governing equations is also presented. In section 4.4 we present, discuss, and classify the solution vector, consisting of the time dependent director and alignment fields, obtained from numerical integration and analytical solutions of the governing equations. Typical computations of the tensor order parameter relaxation and flow birefringence are presented.

4.3. Theory and Governing Equations

4.3.1. Definition of Coordinates, Kinematics, Orientation and Alignment

In this paper we study the temporal, spatially uniform microstructural response of a model uniaxial discotic nematic subjected at time $t = 0$ to a constant uniaxial extension rate $\dot{\epsilon}$. The microstructure of the nematic is characterized by the tensor order parameter $Q_{ij}(t)$ [19]:

$$Q_{ij} = S \left(n_i n_j - \frac{1}{3} \delta_{ij} \right) + \frac{1}{3} P (m_i m_j - l_i l_j); \quad (1a)$$

where the following restrictions apply:

$$\begin{aligned} Q_{ij} = Q_{ji}; \quad Q_{ii} = 0; \quad -\frac{1}{2} \leq S \leq 1; \quad -\frac{3}{2} \leq P \leq \frac{3}{2}; \\ n_i n_i = m_i m_i = l_i l_i = 1; \end{aligned} \quad (1b,c,d,e,f)$$

where $i, j = x, y, z$. The uniaxial director \mathbf{n} corresponds to the maximum eigenvalue $\frac{2}{3}S$, the biaxial director \mathbf{m} corresponds to the second largest eigenvalue $-\frac{1}{3}(S - P)$, and the biaxial director $\mathbf{l} = \mathbf{n} \times \mathbf{m}$ corresponds to the smallest eigenvalue $-\frac{1}{3}(S + P)$. The orientation is defined by the orthogonal director triad $(\mathbf{n}, \mathbf{m}, \mathbf{l})$. The magnitude of the uniaxial scalar order parameter S is a measure of the molecular alignment along the uniaxial director \mathbf{n} , and is given by $S = 3 (n_i Q_{ij} n_j)/2$. The magnitude of the biaxial scalar order parameter P is a measure of the molecular alignment along the biaxial director \mathbf{m} in a plane perpendicular to uniaxial director \mathbf{n} , and is given as

$P = 3 (m_i Q_{ij} m_j - l_i Q_{ij} l_j) / 2$. On the principal axes, the tensor order parameter $Q_{ij}(t)$ is given by :

$$Q_{ij} = \begin{bmatrix} -\frac{1}{3}(S - P) & 0 & 0 \\ 0 & -\frac{1}{3}(S + P) & 0 \\ 0 & 0 & \frac{2}{3}S \end{bmatrix}. \quad (2)$$

We next adopt this well known description to discotic nematic liquid crystals. Figure 1 shows a schematic side view (top) and top view (bottom) of a typical flow-induced biaxial ordering in a discotic nematic liquid crystal. The top figure shows that the uniaxial director \mathbf{n} describes the average orientation of the normals to the circular discs. The bottom figure shows a projection on a plane perpendicular to the uniaxial director, here given by the \mathbf{m} - \mathbf{l} plane. The bottom figure shows that \mathbf{m} is the average orientation of the projection of the normals to the circular discs onto the \mathbf{m} - \mathbf{l} plane. As explained in [17, 19], with the above given identification, both S and P are positive for both rod-like and disc-like uniaxial nematic liquid crystals, and no further distinction is required in this paper since rods are not considered here. Here S and P are the scalar order parameters in the direction of the directors \mathbf{n} and \mathbf{m} respectively.

Having established the ordering and orientation measures, we briefly discuss their restrictions and magnitudes in typical states. The correspondence between phase and alignment is : isotropic ($S = 0, P = 0$), uniaxial nematic ($S \neq 0, P = 0$), and biaxial nematic ($S \neq 0, P \neq 0$). Since the eigenvalues μ_i ($i = 1, 2, 3$) of the tensor order parameter \mathbf{Q} are restricted by :

$$-\frac{1}{3} \leq \mu_i \leq \frac{2}{3}; \quad (3)$$

hence it follows that biaxial order parameter P obeys the following restrictions :

$$S - 1 \leq P \leq 1 - S \quad (4)$$

Equations (1d, 1e, 4) define the alignment triangle containing all the possible ordering states of discotic nematic liquid crystals. Figure 2 shows a schematic of the alignment triangle, whose sides are given by $P = 1 - S$ ($P \geq 0$), $P = S - 1$ ($P \leq 0$), and $S = -0.5$. The seven limiting alignment states are shown by an arrow originating from each

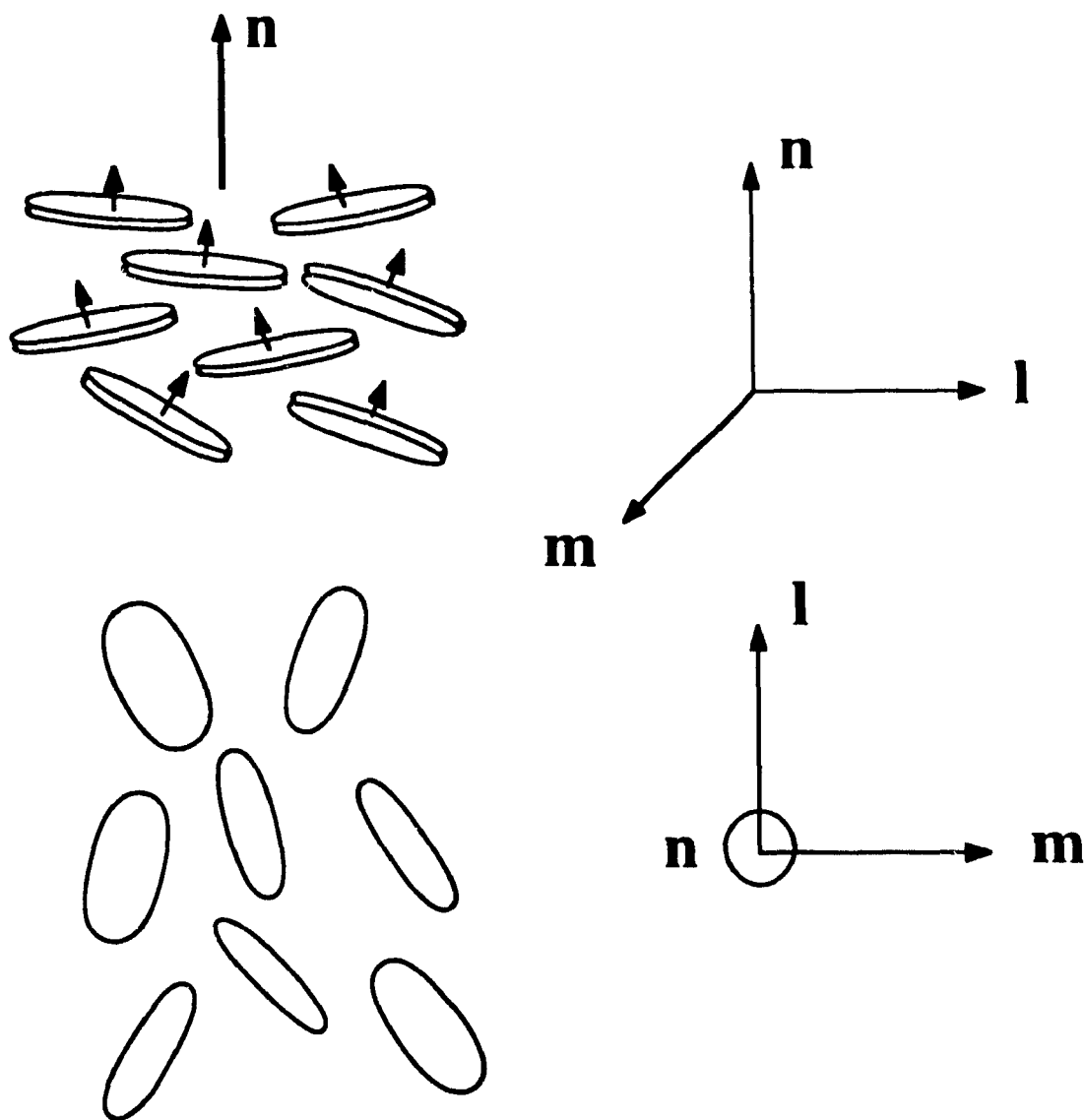


Fig. 1. Definition of director orientations of a discotic nematic liquid crystal undergoing flow induced biaxiality. The uniaxial director \mathbf{n} in a discotic nematic phase is the average orientation of the unit normals to the disc-like molecules. The biaxial directors \mathbf{m} , \mathbf{l} lie in a plane perpendicular to uniaxial director \mathbf{n} , and form a right hand triad. The biaxial director \mathbf{m} is the average orientation of the projection of the unit normals to the disc-like molecules in a plane orthogonal to uniaxial director \mathbf{n} . The biaxial director \mathbf{l} is given as $\mathbf{n} \times \mathbf{m}$. The lower 2-D figure is the projection, of the upper 3-D schematic, in \mathbf{m} - \mathbf{l} plane. In this paper we consider the extension dynamics of a discotic nematic that is uniaxial prior to the imposition of flow.

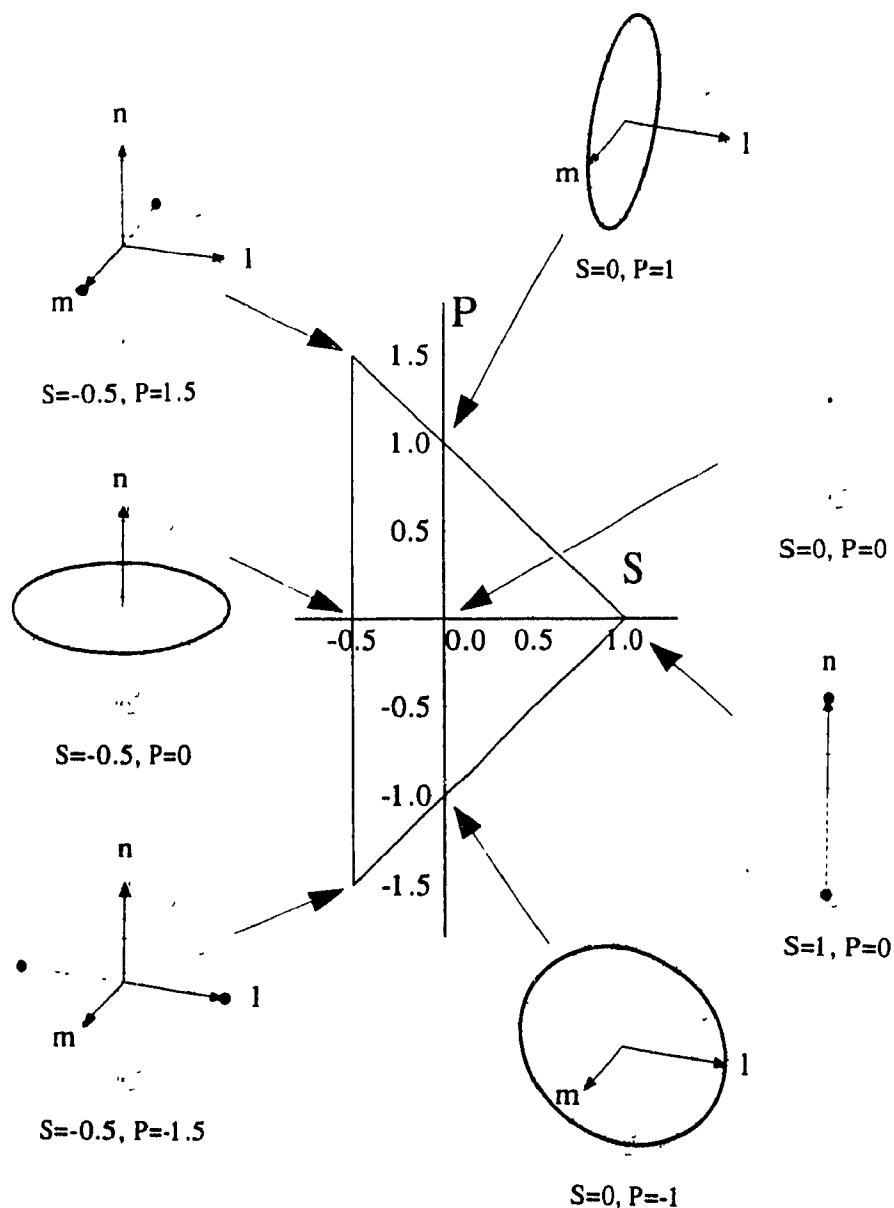


Fig. 2. The alignment (uniaxial and biaxial) P-S triangle. The unit sphere description of the director triad $(\mathbf{n}, \mathbf{m}, \mathbf{l})$ is used to explain the alignment characteristics at different limiting points on the alignment phase plane. The dark rings or dots represent the direction in which the unit normals to the disc-like molecules point. Seven limiting alignment states are shown by an arrow originating from each corresponding unit sphere. Wherever $S = 0$, the uniaxial director \mathbf{n} is undefined, and wherever $P = 0$, the biaxial directors \mathbf{m}, \mathbf{l} are undefined. The figure shows that when $P \rightarrow -P$, then $\mathbf{m} \rightarrow \mathbf{l}$.

corresponding unit sphere description [14] of the molecular orientation state. Wherever $S = 0$, the uniaxial director \mathbf{n} is undefined, and wherever $P = 0$, the biaxial directors \mathbf{m} , \mathbf{l} are undefined. The dark dot or the dark ring on the unit sphere indicates the orientation of the normals to the discs. For example, for ($S = 0$, $P = 1$), the uniaxial director \mathbf{n} is undefined, and the unit normals to the disc-like molecules lie along the meridian passing through the biaxial director \mathbf{m} . The figure also shows that when $P \rightarrow -P$, then $\mathbf{m} \rightarrow \mathbf{l}$. The rings in the figure corresponding to ($S = 0$, $P = 1$), ($S = -0.5$, $P = 0$), and ($S = 0$, $P = -1$) correspond to planar orientation. The dark dots in the figures of ($S = -0.5$, $P = 1.5$), ($S = 1$, $P = 0$), and ($S = -0.5$, $P = -1.5$) correspond to various perfect alignments. Since uniaxial extensional flow will not induced negative values of S and P , in the present study the state of alignment lies within the triangle defined by $S = 0$, $P = 0$, and $P = 1 - S$, whose vertices are the isotropic plane, the perfect uniaxial nematic phase, and the planar oriented phase. In what follows we refer to this restricted alignment space as the alignment triangle.

To enforce the unit length constraint on the orthogonal director triad ($\mathbf{n} \cdot \mathbf{n} = \mathbf{m} \cdot \mathbf{m} = \mathbf{l} \cdot \mathbf{l} = 1$) and to visualize and analyze the director triad orbits on the unit sphere, we parametrize director triad as follows :

$$[\mathbf{n}, \mathbf{m}, \mathbf{l}] : \left[\begin{array}{l} \mathbf{n} = (n_x, n_y, n_z) = (\cos \phi, \sin \phi \cos \theta, \sin \phi \sin \theta) \\ \mathbf{m} = (m_x, m_y, m_z) = (\cos \psi, \sin \psi \cos \alpha, \sin \psi \sin \alpha) \\ \mathbf{l} = \mathbf{n} \times \mathbf{m} \end{array} \right] \quad (5a)$$

where

$$\psi = \tan^{-1} \left(\frac{\cot(-\phi)}{\cos(\theta - \phi)} \right). \quad (5b)$$

The parametrization is shown in figure 3(a), where θ ($0 \leq \theta \leq 2\pi$) is the uniaxial azimuthal angle and ϕ ($0 \leq \phi \leq \pi$) is the uniaxial polar angle defining the uniaxial director \mathbf{n} . The biaxial director \mathbf{m} is completely defined by the biaxial polar angle ψ ($0 \leq \psi \leq \pi$) and biaxial azimuthal angle α ($0 \leq \alpha \leq 2\pi$). In terms of the uniaxial angles, the north pole of the sphere is located at $\phi = 0$, the south pole at $\phi = \pi$, and the equator at $(\theta, \phi) = ([0, 2\pi], \pm \pi/2)$. In this paper x is along the extension direction of the imposed flow.

The unit sphere description of the director triad is used just to facilitate the analysis and discussion of the analytical and numerical results of director triad relaxation and alignment relaxation. In the unit sphere description [14, 15, 21, 22, 23, 24] each director tip, in the presence of flow, defines a trajectory. As shown below, in uniaxial extensional flow, $\mathbf{m}(t) \equiv \mathbf{m}(0)$ and the trajectory of \mathbf{m} is just a point on the equator of the unit sphere. To characterize the moving director diad ($\mathbf{n}(t)$, $\mathbf{l}(t)$) orbits we define geodesics and meridians. A geodesic is the shortest arc connecting two points on the surface of the sphere, and is given, in terms of the uniaxial director angles, by [25]:

$$\sin N_2 \cos \phi - \cos N_2 \sin \phi \cos \theta - \frac{\sin \phi \sin \theta}{\sqrt{N_1^2 - 1}} = 0 ; \quad (6)$$

where N_1 and N_2 are constants that depend on the two points; the geodesic or great circle, is the intersection of the sphere with the plane containing the given points and the center of the sphere. When the two points are the poles ($N_2 = \pi$) the degenerate geodesics are the meridians M , which in terms of (θ, ϕ) and the director components $(\hat{\mathbf{a}}_i, i = x, y, z)$, $\hat{\mathbf{a}} = \mathbf{n}, \mathbf{l}$), are given by [25] :

$$\tan \theta = \frac{1}{b}; \quad b^2 = \frac{1}{(N_1^2 - 1)}; \quad 0 \leq \phi \leq \pi ; \quad (7a,b,c)$$

$$\hat{a}_y = b \hat{a}_z; \quad -1 \leq \hat{a}_y \leq 1; \quad -1 \leq \hat{a}_z \leq 1; \quad (8a,b,c)$$

where b ($-\infty < b < \infty$) is a constant whose numerical value defines a particular meridian. A family of meridians is shown by the solid lines passing through the poles in figure 3 (a).

Figure 3(b) shows the deformations of a unit cube of discotic nematic subjected at time $t = 0$ to a uniaxial extensional flow; as shown below, the applied extension direction along the x -axis (polar axis), is parallel to the steady state biaxial director $\mathbf{l}_{ss} = (l_{xss}, 0, 0) = (\pm 1, 0, 0)$. The uniform compression along the $(y-z)$ plane contains the equator of the unit sphere, and as shown below represents the degenerate circle of stable steady uniaxial and biaxial director orientations : $\mathbf{n}_{ss} = (0, n_{yss}, n_{zss}) = (0, \cos \theta_{ss}, \sin \theta_{ss})$; and $\mathbf{m}_{ss} = (0, m_{yss}, m_{zss}) = (0, \cos \alpha_{ss}, \sin \alpha_{ss})$ respectively; where the subscript 'ss' denotes steady state.

To characterize the relaxation of the uniaxial and biaxial alignments as the directors traverse the surface of the sphere, we divide the sphere into three characteristic

regions, denoted by R^- and R^+ , and shown in the schematic of figure 4. The two equivalent R^- regions are given by $|\hat{a}_x| > 1/\sqrt{3}$, and the R^+ region is given by $|\hat{a}_x| < 1/\sqrt{3}$, where $\hat{\mathbf{a}}$ is a unit vector. In an irrotational uniaxial extensional flow, the only flow effect on the orientation and alignment is due to the symmetric part of the velocity gradient tensor ($v_{i,j}$), usually known as the rate of strain tensor or rate of deformation tensor and denoted by \mathbf{A} , and whose ij and ji components are given by $A_{ij} = A_{ji} = (v_{i,j} + v_{j,i})/2$. An important observation, used below to classify the numerical results of alignment relaxations, is that a director whose tip lies in the R^- region samples extensional strains ($\mathbf{A} : \hat{\mathbf{a}} \hat{\mathbf{a}} > 0$, $\hat{\mathbf{a}} = \mathbf{n}, \mathbf{l}$), while a director whose tip lies in the R^+ region samples compressional strains ($\mathbf{A} : \hat{\mathbf{a}} \hat{\mathbf{a}} < 0$, $\hat{\mathbf{a}} = \mathbf{n}, \mathbf{l}$).

4.3.2. Governing Equations for Uniaxial Extensional Start-up Flow

The macroscopic model used in this paper is described in detail in [14, 15]. Here we just present the governing equations for the temporal evolution of the tensor order parameter and refer the reader to the above mentioned references for further details. The dimensional governing equations for the microstructure response of the model discotic nematics, subjected to isothermal, incompressible, irrotational extensional flow are approximated by :

$$\begin{aligned} & \left(1 - \frac{U}{3}\right) Q_{ij} - U \left(Q_{ik} Q_{kj} - \frac{1}{3} Q_{ik} Q_{kl} \delta_{ij} \right) + U (Q_{ik} Q_{kl}) Q_{ij} \\ & + \sigma_4 A_{ij} + \tau_4 \dot{Q}_{ij} + \sigma_6 \left(Q_{ik} A_{kj} + A_{ik} Q_{kj} - \frac{2}{3} Q_{ik} A_{kl} \delta_{ij} \right) \\ & + \tau_6 \left(Q_{ik} \dot{Q}_{kj} + \dot{Q}_{ik} Q_{kj} - \frac{2}{3} Q_{ik} \dot{Q}_{kl} \delta_{ij} \right) = 0_{ij} \end{aligned} \quad (9)$$

where ($i, j = x, y, z$); U is the nematic potential, A_{ij} is the rate of deformation tensor, \dot{Q}_{ij} is the time rate of change of the ij component of the symmetric traceless tensor order parameter Q_{ij} , and $\sigma_6, \sigma_4, \tau_6, \tau_4$ are the dimensional phenomenological parameters. The simplifying assumptions and approximations made in deriving the model that describe the flow-induced tensor order parameter of an ideal discotic nematic liquid crystal, as given by equation (9) can be found in [14, 26]. The numerically integrated set of dimensionless governing equations in component form and the dimensionless variables are given in Appendix A. The corresponding eigenvector-eigenvalue versions, governing the evolution of the director triad and alignment's extension dynamics, are given by :

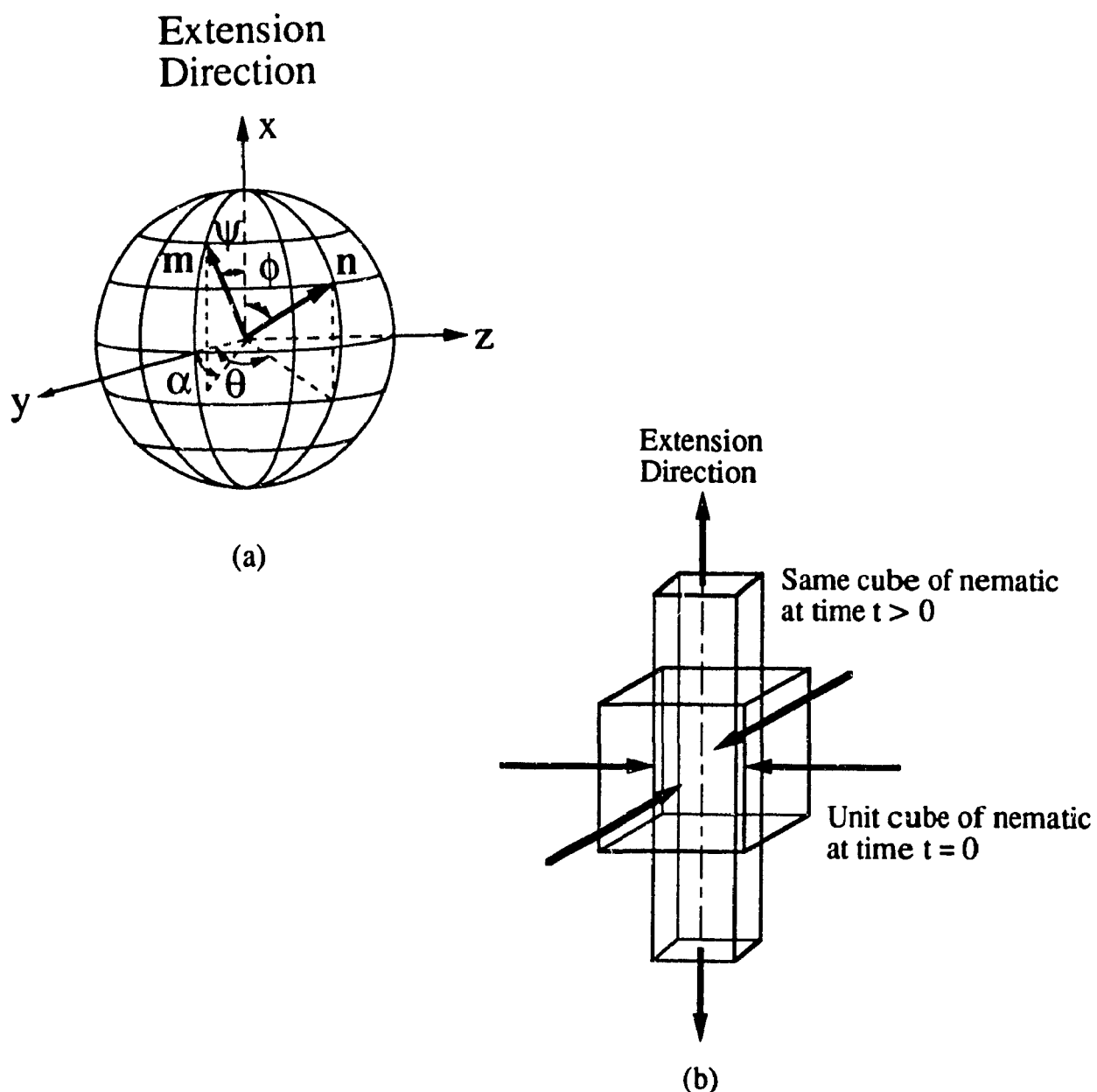


Fig. 3. Definition of (a) coordinate system, (b) uniaxial extensional flow deformation. (a) Director angle and unit sphere : θ ($0 \leq \theta \leq 2\pi$) is the azimuthal angle and ϕ ($0 \leq \phi \leq \pi$) is the polar angle which define completely the orientation of the uniaxial director n . The biaxial director m is completely defined by the polar angle ψ ($0 \leq \psi \leq \pi$) and azimuthal angle α ($0 \leq \alpha \leq 2\pi$). The north pole of the sphere is located at $\phi = 0$, the south pole at $\phi = \pi$, and the equator at $(\theta, \phi) = ([0, 2\pi], \pm \pi/2)$. (b) Deformation of a unit cube, subjected at time $t = 0$ to a uniaxial extensional flow. The x-axis is along the extension direction, and the y-z plane contains the uniform compression; the flow is an irrotational 3-D flow.

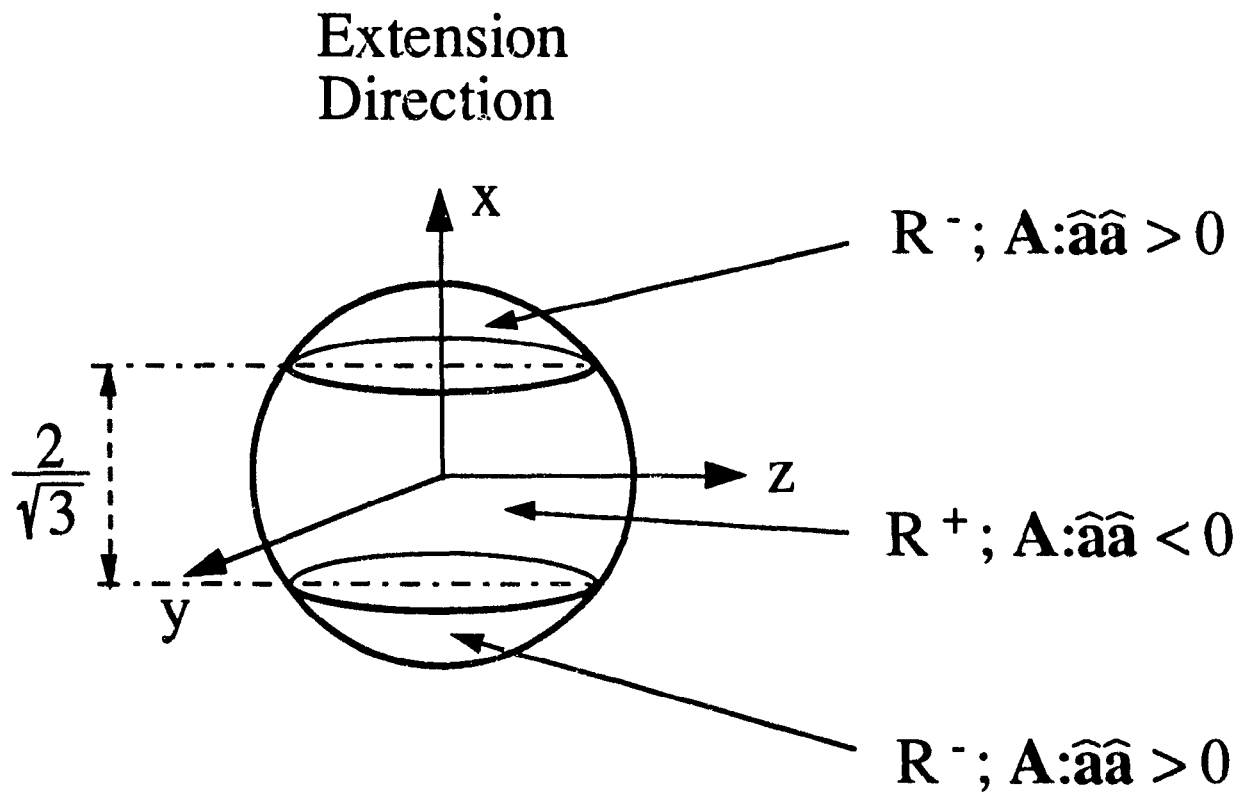


Fig. 4. Sensitivity of initial uniaxial alignment S and initial biaxial alignment P relaxation to the initial director orientation. The three characteristic regions for the ambient strain rate $\mathbf{A}:\hat{\mathbf{a}}\hat{\mathbf{a}}$ (where $\hat{\mathbf{a}} = \mathbf{n}, \mathbf{l}$). In the region R^- the ambient strain is positive ($\mathbf{A}:\hat{\mathbf{a}}\hat{\mathbf{a}} > 0$); in the region R^+ the ambient strain rate is negative ($\mathbf{A}:\hat{\mathbf{a}}\hat{\mathbf{a}} < 0$); and on the boundary of the two regions $\partial R^+ = \partial R^-$ the ambient rate is zero ($\mathbf{A}:\hat{\mathbf{a}}\hat{\mathbf{a}} = 0$).

$$\frac{d\mathbf{n}}{d\varepsilon} = \lambda_n^n (\tilde{\mathbf{A}} \cdot \mathbf{n} - (\tilde{\mathbf{A}} : \mathbf{nn}) \mathbf{n}) + \lambda_{\text{mix}}^n (\tilde{\mathbf{A}} : \mathbf{mn}) \mathbf{m} \quad (10)$$

$$\frac{d\mathbf{m}}{d\varepsilon} = 0 \quad (11)$$

$$\frac{d\mathbf{l}}{d\varepsilon} = \lambda_l^l (\tilde{\mathbf{A}} \cdot \mathbf{l} - (\tilde{\mathbf{A}} : \mathbf{ll}) \mathbf{l}) + \lambda_{\text{mix}}^l (\tilde{\mathbf{A}} : \mathbf{ml}) \mathbf{m} \quad (12)$$

$$\frac{d\mathbf{S}}{d\varepsilon} = \beta_{1,S}^n \tilde{\mathbf{A}} : \mathbf{nn} + \beta_{1,S}^m \tilde{\mathbf{A}} : \mathbf{mm} + \text{De}^{-1} \beta_{2,S} \quad (13)$$

$$\frac{d\mathbf{P}}{d\varepsilon} = \beta_{1,P}^n \tilde{\mathbf{A}} : \mathbf{nn} + \beta_{1,P}^m \tilde{\mathbf{A}} : \mathbf{mm} + \text{De}^{-1} \beta_{2,P} \quad (14)$$

where $\tilde{\mathbf{A}} = \mathbf{A} / \dot{\varepsilon}$ is the dimensionless rate of strain tensor, $\text{De} = \dot{\varepsilon} \tau_4$, is the alignment Deborah number (dimensionless strain rate), and $\varepsilon = \dot{\varepsilon} t$ is the strain (dimensionless time). Equations (10 - 14) are only used to obtain analytical results and to develop a selection procedure for the parameters of the model; all numerical results of this paper were obtained by numerical integration of equations (A.1 - A.5). Equation (11) shows that $\mathbf{m} \equiv \text{constant}$ for uniaxial extensional flow, as we prove below (see Fig. 5); this analytical result is not used in the numerical integration of equations (A.1 - A.5). The director diad (\mathbf{n}, \mathbf{l}) evolution equations (10, 12) contain uncoupled and mixed flow terms. The parametric functions introducing these terms are the four reactive parameters $(\lambda_j^i; i = \mathbf{n}, \mathbf{l}; j = \mathbf{n}, \mathbf{l}, \text{mix})$, where the subscript mix denotes the cross coupling reactive parameters. In this paper the following terminology is used for the set of reactive parameters: uniaxial reactive parameter λ_n^n , mixed-uniaxial reactive parameter λ_{mix}^n , biaxial reactive parameter λ_l^l , and mixed-biaxial reactive parameter λ_{mix}^l . The alignments relaxation equations (13, 14) contain only uncoupled flow terms and the parametric functions introducing these terms are the four ordering functions $(\beta_{1,j}^i; i = \mathbf{n}, \mathbf{m}; j = \text{S}, \text{P})$, and the two elastic functions $(\beta_{2,j}; j = \text{S}, \text{P})$. The following terminology is used for the set of ordering functions: \mathbf{n} -S ordering function $\beta_{1,S}^n$, \mathbf{m} -S ordering function $\beta_{1,S}^m$, \mathbf{n} -P ordering function $\beta_{1,P}^n$, and \mathbf{m} -P ordering function $\beta_{1,P}^m$. The elastic functions are called uniaxial elastic function $\beta_{2,S}$ and biaxial elastic function $\beta_{2,P}$ and contain the thermodynamic contribution. The expressions for the set of reactive parameters $(\lambda_n^n, \lambda_{\text{mix}}^n, \lambda_l^l, \lambda_{\text{mix}}^l)$, the ordering function set $(\beta_{1,S}^n, \beta_{1,S}^m, \beta_{1,P}^n, \beta_{1,P}^m)$, and the elastic functions $(\beta_{2,S}, \beta_{2,P})$ are given in Appendix B. When $\text{De} \rightarrow 0$ the alignments dynamics are purely elastic, when $\text{De} \rightarrow \infty$ purely viscous, and for the intermediate De

values viscoelastic. At intermediate De the moving director diad (\mathbf{n}, \mathbf{l}) is also viscoelastic, as it is coupled to alignments (S, P) through the set of reactive parameters $(\lambda_{\mathbf{n}}^{\mathbf{n}}, \lambda_{\text{mix}}^{\mathbf{n}}, \lambda_{\mathbf{l}}^{\mathbf{l}}, \lambda_{\text{mix}}^{\mathbf{l}})$.

The velocity field $\mathbf{v}(x, y, z)$ corresponding to the uniform uniaxial, irrotational, 3-D extensional start-up flow of the discotic nematic crystals, is given by [8] :

$$\begin{aligned} v_x &= \dot{\epsilon} x H(t); & v_y &= -\frac{\dot{\epsilon}}{2} y H(t); & v_z &= -\frac{\dot{\epsilon}}{2} z H(t); \\ H(t) &= \begin{cases} 0 & t < 0 \\ 1 & t \geq 0 \end{cases}; \end{aligned} \quad (15a,b,c,d)$$

where $\dot{\epsilon}$ is the constant uniaxial extension rate. The non-zero components of the corresponding rate of deformation tensor \mathbf{A} are : $A_{11} = \dot{\epsilon}$; $A_{22} = A_{33} = -\dot{\epsilon}/2$; this flow is irrotational and the vorticity tensor is zero, $\mathbf{W} = \mathbf{0}$.

The initial conditions used to solve equations (A.1 - A.5), in eigenvalue-eigenvector form, are :

$$\begin{aligned} @ t = 0 : \quad \mathbf{n} &= \mathbf{n}_0; & \mathbf{m}_0 &= (0, m_{y0}, m_{z0}); & \mathbf{l}_0 &= \mathbf{n}_0 \times \mathbf{m}_0; \\ \mathbf{n}_0 \cdot \mathbf{n}_0 &= \mathbf{m}_0 \cdot \mathbf{m}_0 = \mathbf{l}_0 \cdot \mathbf{l}_0 = 1; \\ S_0 &= S_{\text{eq}}; & P_0 &= 0; \end{aligned} \quad (16)$$

where $S_{\text{eq}}(U)$ is the equilibrium scalar order parameter of the normal ($S > 0$) uniaxial nematic phase , given by [27]:

$$S_{\text{eq}} = \frac{1}{4} + \frac{3}{4} \sqrt{\left(1 - \frac{8}{3U}\right)} \quad (17)$$

For $U < 8/3$ the stable phase is isotropic, for $8/3 \leq U \leq 3$ there is biphasic equilibrium, and for higher values of uniaxial nematic potential U the phase is uniaxial nematic. High values of U correspond to stronger uniaxial alignment. In this paper we use two representative nematic potential $U = 3$ and $U = 5$, and the corresponding initial condition values for uniaxial scalar order parameter are : $S_{\text{eq}}(U=3) = 0.5$ and $S_{\text{eq}}(U=5) = 0.76$. In this paper, all angles are reported in degrees.

Equations (A.1 - A.5) are integrated using an implicit corrector-predictor first order Euler integration method with an adaptable time step [28]. Application of the implicit corrector-predictor method transforms the set of coupled nonlinear ordinary

differential equations (A.1 - A.5) into a set of coupled nonlinear algebraic equations . For each time step the algebraic equations are solved using the Newton-Raphson iteration scheme [28]; the predictor step generates a first guess for the iteration loop and the corrector step is the iteration loop itself. The adopted convergence criteria is that the length of the difference vector between the calculated solution vectors corresponding to two successive iterations is less than 10^{-6} . The transient solution vector obtained from the numerical solutions consists of the five independent components of the tensor order parameter ($\mathbf{Q}(\epsilon)$) as a function of the strain (dimensionless time) $\epsilon = \dot{\epsilon}t$. In addition to the uniaxial nematic potential U , the other dimensionless parameter investigated in this paper is alignment Deborah number De . The numerically obtained tensor order parameter $\mathbf{Q}(\epsilon)$ is subsequently transformed into principal form to find its eigenvectors or director triad ($\mathbf{n}, \mathbf{m}, \mathbf{l}$) and its eigenvalues, given by equation (2).

4.3.3. Analytical Results

4.3.3.1. Director Triad Dynamics

Assuming that the biaxial director \mathbf{m} always lies on the equator, or the plane of uniform compression, then it can be written as $\mathbf{m} = (0, m_y, m_z)$. Using this restriction ($m_x = 0$) and the symmetry of the flow type ($A_{yy} = A_{zz}$) the mixed terms, $\mathbf{A} : \mathbf{m}\mathbf{n}$ and $\mathbf{A} : \mathbf{m}\mathbf{l}$, in the director diad (\mathbf{n}, \mathbf{l}) relaxation equations (10, 12) take the following form :

$$\mathbf{A} : \mathbf{m}\mathbf{n} = A_{yy} (m_y n_y + m_z n_z) ; \quad (18)$$

and

$$\mathbf{A} : \mathbf{m}\mathbf{l} = A_{yy} (m_y l_y + m_z l_z) . \quad (19)$$

The orthogonality of the directors ($\mathbf{m} \perp \mathbf{n}$ and $\mathbf{m} \perp \mathbf{l}$) now gives :

$$m_y n_y + m_z n_z = 0 ; \quad m_y l_y + m_z l_z = 0 \quad (20a,b)$$

Use of equations (20) in equations (18, 19) shows that the mixed terms $\mathbf{A} : \mathbf{m}\mathbf{n}$ and $\mathbf{A} : \mathbf{m}\mathbf{l}$ appearing in the director diad relaxation equations (10, 12) are zero. Hence the uniaxial director relaxation $\mathbf{n}(\epsilon)$ and biaxial director relaxation $\mathbf{l}(\epsilon)$ are affected only by the uniaxial reactive parameter λ_n^u and the biaxial reactive parameter λ_l^b ,

respectively. Integration of equations (10) and (12) yields the following expressions for the moving director diad (\mathbf{n}, \mathbf{l}) relaxation in the uniaxial start-up extensional flow:

$$\hat{a}_i(\epsilon) = \frac{E_{ij} \hat{a}_{j0}}{|\mathbf{E} \cdot \hat{\mathbf{a}}_0|}; \quad \hat{a}_i(0) = a_{i0};$$

$$E_{ij}(\epsilon) = \exp \left\{ \tilde{A}_{ij} \int_0^\epsilon \lambda_{\hat{\mathbf{a}}}^{\hat{\mathbf{a}}} d\epsilon' \right\}; \quad \tilde{A}_{ij} = \frac{A_{ij}}{\dot{\epsilon}};$$
(21a,b,c,d)

and in the component form:

$$\hat{a}_x = \frac{E_{xx} \hat{a}_{x0}}{|\mathbf{E} \cdot \hat{\mathbf{a}}_0|}; \quad \hat{a}_y = \frac{E_{yy} \hat{a}_{y0}}{|\mathbf{E} \cdot \hat{\mathbf{a}}_0|}; \quad \hat{a}_z = \frac{E_{zz} \hat{a}_{z0}}{|\mathbf{E} \cdot \hat{\mathbf{a}}_0|};$$

$$E_{xx} = \exp \left(\int_0^\epsilon \lambda_{\hat{\mathbf{a}}}^{\hat{\mathbf{a}}} d\epsilon' \right); \quad E_{yy} = E_{zz} = \exp \left(-\frac{1}{2} \int_0^\epsilon \lambda_{\hat{\mathbf{a}}}^{\hat{\mathbf{a}}} d\epsilon' \right);$$
(22a,b,c)

$$E_{ij} = 0 \quad \text{for } i \neq j;$$

where $\hat{\mathbf{a}} = \mathbf{n}, \mathbf{l}$; and a_{j0} is the j th component of the initial director orientation ($\hat{\mathbf{a}}(0) = \mathbf{n}(0), \mathbf{l}(0)$). The direction of the director trajectory and steady state is governed by the sign of the corresponding director reactive parameter. The uniaxial reactive parameter $\lambda_{\hat{\mathbf{n}}}^{\hat{\mathbf{n}}}$ is negative for discotic nematics [14] (see figure 7). For the present case ($m_x = 0$), it can be shown that the biaxial reactive parameter $\lambda_{\hat{\mathbf{l}}}^{\hat{\mathbf{l}}}$ is related to the uniaxial reactive parameter by the following relation:

$$\lambda_{\hat{\mathbf{l}}}^{\hat{\mathbf{l}}} = -\lambda_{\hat{\mathbf{n}}}^{\hat{\mathbf{n}}};$$
(24)

which, since $\lambda_{\hat{\mathbf{n}}}^{\hat{\mathbf{n}}} < 0$ [14], implies that $\lambda_{\hat{\mathbf{l}}}^{\hat{\mathbf{l}}} > 0$ for discotic nematics (this relation follows from equations (B.1, B.3)). The equations (22, 23, 24) show that the y and z components of the uniaxial director \mathbf{n} will increase, whereas the corresponding components of the biaxial director \mathbf{l} will decrease; hence \mathbf{n} rotates towards the equator, and \mathbf{l} towards the closest pole. From equations (22, 23) it also follows that y and z components of the moving director diad (\mathbf{n}, \mathbf{l}) are related by: $n_y = b n_z$ ($b = n_{y0}/n_{z0}$), and $l_y = b l_z$ ($b = l_{y0}/l_{z0}$). Using the last result and equations (7, 8), we conclude that the uniaxial director \mathbf{n} and biaxial director \mathbf{l} orbits belong to the meridians, and the

director diad (\mathbf{n}, \mathbf{l}) dynamics belong to the class of geodesic flows. Comparison of equations (22, 23, 24) with equations (7, 8) also shows that the director diad (\mathbf{n}, \mathbf{l}) belong to the same meridian of the unit sphere. From the meridian flow of the director diad (\mathbf{n}, \mathbf{l}) it follows that the biaxial director \mathbf{m} should lie somewhere on the equator of the unit sphere. The computed numerical simulations for the director triad relaxation, shown below, confirm the above analysis.

The selection criteria for the biaxial director \mathbf{m} can be explained by the following argument. Biaxiality will be present in a plane normal to the extension direction, that is, in the (y-z) plane. Since \mathbf{m} is normal to \mathbf{n} and must lie on the equator, hence $\mathbf{m}(0)$ is normal to $\mathbf{P} \cdot \mathbf{n}(0)$, where $\mathbf{P} = (\delta - \mathbf{n}\mathbf{n})$ is the projection operator. In addition, since \mathbf{n} follows a geodesic meridian flow ($n_y = b n_z$, $b = n_{y0}/n_{z0}$), thus it follows that :

$$\hat{\mathbf{n}}_{\perp} = \frac{\mathbf{P} \cdot \mathbf{n}(0)}{|\mathbf{P} \cdot \mathbf{n}(0)|} = \frac{1}{\sqrt{1+b^2}} (\hat{\mathbf{j}} + b \hat{\mathbf{k}}) ; \quad (25)$$

and from $\mathbf{m} \perp \hat{\mathbf{n}}_{\perp}$ we finally get the following components for \mathbf{m} :

$$m_x = 0 ; \quad m_y = \pm \frac{1}{\sqrt{1+b^2}} ; \quad m_z = -b m_y \quad (26a,b,c)$$

Equations (26) show that for a given $b = n_{y0}/n_{z0}$, there is indeterminacy in the selection of the biaxial director \mathbf{m} , since there are two equivalent directions perpendicular to \mathbf{n}_0 and farthest away from the extension direction for each initial uniaxial orientation \mathbf{n}_0 . As $\mathbf{l} = \mathbf{n} \times \mathbf{m}$, there are also two possible equivalent biaxial director \mathbf{l} trajectories for each uniaxial director \mathbf{n} trajectory.

Equations (22,23,24, 26) show that the stable state director triad is given by :

$$[\mathbf{n}_{ss}, \mathbf{m}_{ss}, \mathbf{l}_{ss}] : \left[\begin{array}{l} \mathbf{n}_{ss} = (0, n_{y_{ss}}, n_{z_{ss}}) = \left(0, \frac{b}{\sqrt{1+b^2}}, \frac{1}{\sqrt{1+b^2}} \right) \\ \mathbf{m}_{ss} = (0, m_{y_{ss}}, m_{z_{ss}}) = \left(0, \pm \frac{1}{\sqrt{1+b^2}}, \pm \frac{b}{\sqrt{1+b^2}} \right) \\ \mathbf{l}_{ss} = (1, l_{y_{ss}}, l_{z_{ss}}) = (\pm 1, 0, 0) \end{array} \right] \quad (27a,b,c)$$

where $b = n_{y0}/n_{z0}$.

Figure 5(a) shows the computed director triad $(\mathbf{n}, \mathbf{m}, \mathbf{l})$ trajectories on the surface of the unit sphere, and figure 5(b) shows the corresponding computed director triad

trajectories on the ϕ - θ plane, for an initial uniaxial director orientation of $(\theta_0, \phi_0) = (45, 2.56)$. The figure shows that for the given uniaxial director \mathbf{n} trajectory there are two different biaxial director \mathbf{m}, \mathbf{l} trajectories, where the arrows indicate the direction of the director paths. The uniaxial director trajectory and the two corresponding equivalent biaxial director trajectories lie on the same meridian. The computed director triad steady states agree with equation (27) - \mathbf{l}_{ss} lies along the poles, \mathbf{n}_{ss} lies on the equator, and \mathbf{m}_{ss} lies on the equator and is normal to \mathbf{n}_{ss} .

The uniaxial director \mathbf{n} and biaxial director \mathbf{l} orbits follow geodesic flow due to the inherent symmetry in the uniaxial extensional flow. This result is also predicted by the TIF equations of [29], which are applicable to uniaxial nematics of constant order parameter, since as mentioned above, for irrotational flows the geometry of the director orbits are insensitive to variations in the magnitude of the alignment. The director trajectories should exhibit the characteristic sensitive dependence on initial conditions which is typical of geodesic flows [30]. When the initial uniaxial orientation is $n_x = \pm 1$, along the poles, predictability is lost. Close to the poles there is high sensitivity to initial uniaxial orientation \mathbf{n}_0 . Figure 6 shows the director triad trajectories on the surface of the unit sphere when the initial uniaxial orientation is close to the north pole, for $(\theta_0, \phi_0) = (45, 2.56)$ (solid line, corresponding director triad trajectories are denoted with subscript 'A') and $(\theta_0, \phi_0) = (315, 2.56)$ (dot-dash line, corresponding director triad trajectories are denoted with subscript 'B'). The arrows indicate the direction of the director paths. The figure illustrates that there is a high sensitivity of the director triad trajectories and steady states, when the initial uniaxial orientation is close to the poles. The whole compression plane or equator contains the space of stable uniaxial \mathbf{n}_{ss} and biaxial \mathbf{m}_{ss} orientations, while the poles or the extension directions are the stable states for the biaxial director \mathbf{l} .

4.3.3.2. Uniaxial Alignment Dynamics

The uniaxial alignment relaxation $S(\epsilon)$ and biaxial alignment relaxation $P(\epsilon)$ depend on $\hat{\mathbf{a}}_0$ ($\hat{\mathbf{a}} = \mathbf{n}, \mathbf{l}$) through the ambient strain rate $\mathbf{A} : \hat{\mathbf{a}}\hat{\mathbf{a}}$. Figure 4 shows different representative regions for $\mathbf{A} : \hat{\mathbf{a}}\hat{\mathbf{a}}$. In the R^- regions the ambient strain rate is positive ($\mathbf{A} : \hat{\mathbf{a}}\hat{\mathbf{a}} > 0$), and in the R^+ regions the ambient strain rate is negative ($\mathbf{A} : \hat{\mathbf{a}}\hat{\mathbf{a}} < 0$). The uniaxial alignment relaxation equation (13) can be written, using the right handed orthogonality of the director triad ($\delta = \mathbf{n} \cdot \mathbf{n} + \mathbf{m} \cdot \mathbf{m} + \mathbf{l} \cdot \mathbf{l}$), as :

$$\frac{dS}{d\epsilon} = (\beta_{1,S}^n - \beta_{1,S}^m) \tilde{\mathbf{A}} : \mathbf{nn} - \beta_{1,S}^m \tilde{\mathbf{A}} : \mathbf{ll} + De^{-1} \beta_{2,S} \quad (28)$$

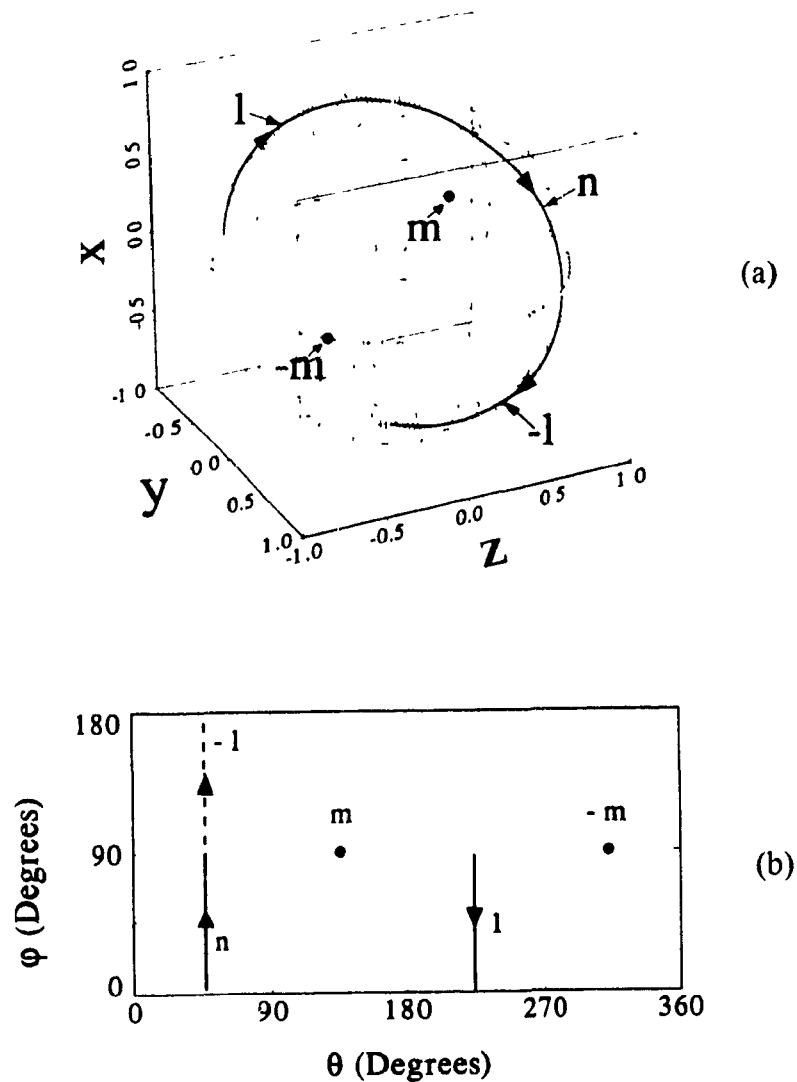


Fig. 5. (a) Computed director triad (n, m, l) trajectories on the surface of the unit sphere with representative meridians and equator. (b) Corresponding computed director trajectories on the ϕ - θ plane for initial uniaxial director orientation $(\theta_0, \phi_0) = (45, 2.56)$. There is indeterminacy in the m, l trajectories; for each uniaxial director n trajectory there are two different biaxial director m, l trajectories. The arrows indicate the direction of the director paths. The steady states for the uniaxial director n and the biaxial director m lie on the equator, the plane of uniform compression, whereas for the biaxial director l the poles (extension direction) of the unit sphere are the stable states. The uniaxial director n and biaxial director l follow geodesic meridian flow, whereas the constant biaxial director m remains at all the times on the equator.

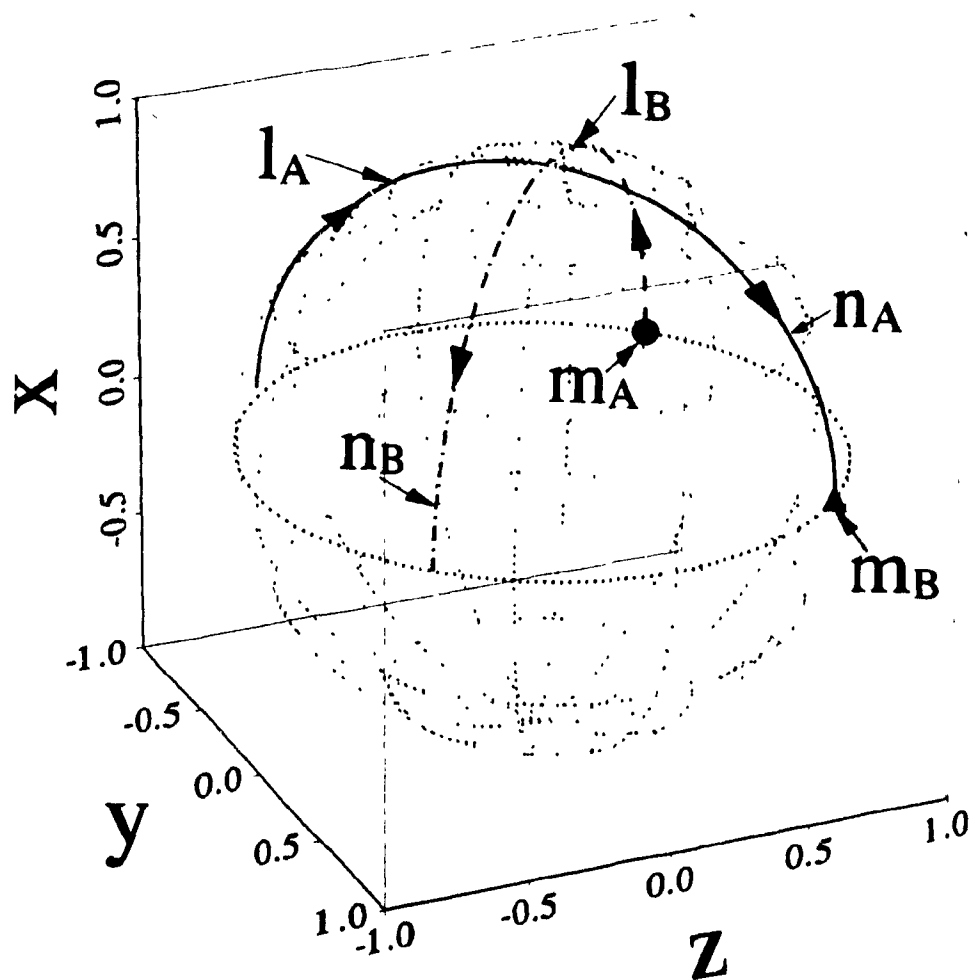


Fig. 6. Sensitivity of the director orbits to the initial director orientation. For the uniaxial director \mathbf{n} and the biaxial director \mathbf{m} , the whole equator represents stable director orientations. Predictability is lost when the initial uniaxial director orientation lies along either of the poles; close to the poles there is a high sensitivity of the final steady state orientation to the initial uniaxial director orientation \mathbf{n}_0 . The two stable orientations for the biaxial director \mathbf{l} are the poles of the unit sphere.

where $(\beta_{1,S}^n - \beta_{1,S}^m)$ and $\beta_{1,S}^m$ both are negative (see figure 7); hence the initial uniaxial alignment relaxation characteristics are given by:

$$\begin{aligned} \mathbf{n}_o \text{ in } R^- : \left(\frac{dS}{d\varepsilon} \right)_{\varepsilon=0^+} < 0; \quad \mathbf{n}_o \text{ in } R^+ : \left(\frac{dS}{d\varepsilon} \right)_{\varepsilon=0^+} > 0; \\ \mathbf{n}_o \text{ in } \partial R^- = \partial R^+ : \left(\frac{dS}{d\varepsilon} \right)_{\varepsilon=0^+} = 0; \end{aligned} \quad (29a,b,c)$$

It follows from the equations (29) that for any De , a sufficient condition for increasing uniaxial alignment S is that \mathbf{n}_0 is in R^+ . For large De , discotic nematics, initially in R^- undergo a temporary melting the uniaxial director is in the region R^- [14].

4.3.4. Selection of Phenomenological Parameters

In this section we show and use the concepts used to construct a selection procedure for the three dimensionless phenomenological parameters $(\sigma_4^*, \sigma_6^*, \tau_6^*)$ of the present model. The non-dimensionalization of the three parameters is given in equation (A.41). To select the numerical values of the three dimensionless parameters $\sigma_4^*, \sigma_6^*, \tau_6^*$ we enforce the following constraints on the signs of $\lambda_n^n, \gamma_{2,n}^n, \gamma_{1,n}^n$ [14, 15, 31, 32, 33, 34] and on the values of λ_n^n when $S = 0, S = 1$ [31]:

$$\lambda_n^n = - \frac{\gamma_{2,n}^n}{\gamma_{1,n}^n} < 0; \quad \gamma_{2,n}^n \geq 0; \quad \gamma_{1,n}^n \geq 0; \quad (30a,b,c)$$

$$\lim_{\substack{S \rightarrow 0 \\ P=0}} \lambda_n^n = -\infty; \quad \lim_{\substack{S \rightarrow 1 \\ P=0}} \lambda_n^n = -1; \quad (30d,e)$$

$$\lim_{\substack{P \rightarrow 0 \\ S=0}} \lambda_n^n = -\infty; \quad \lim_{\substack{P \rightarrow 1 \\ S=0}} \lambda_n^n = -1. \quad (30f,g)$$

where $\gamma_{1,n}^n$ is the rotational viscosity for \mathbf{n} , and $\gamma_{2,n}^n$ is the irrotational viscosity for \mathbf{n} , whose meaning is identical to that of uniaxial nematics [7].

In addition to the above mentioned well known constraints, additional restrictions imposed on the phenomenological parameters, appear for the physically meaningful alignment of the director triad at steady state (\mathbf{n}_{SS} and \mathbf{m}_{SS} lie perpendicular to the extension direction). This physically meaningful steady state director triad orientation is automatically selected by using equation (24).

The adopted values that satisfy the above mentioned constraints are : $\sigma_4^* = 0.55$, $\sigma_6^* = 0.30$, $\tau_6^* = -1.05$. The resulting uniaxial reactive parameter λ_n^n ($\lambda_l^1 = -\lambda_n^n$) and the set of ordering functions $\beta_{1,s}^n$, $\beta_{1,s}^m$, $\beta_{1,p}^n$, $\beta_{1,p}^m$, given by equations (B.1, B.5, B.6, B.7, B.8) respectively, are shown in figure 7. The values of the phenomenological parameters used in this paper are not fitted to any of the original existing discotic mesophases, but capture the essential phenomena of the problem. Other parameter values will only change the time scales for the various relaxations.

The appropriateness of the signs of the various ordering functions shown in figure 7, for discotic nematics, can be justified by expected physical phenomena [14, 15]. When extension is applied normal to the uniaxial director \mathbf{n} of a discotic nematic, there is an increase in the alignment of the molecular normals along \mathbf{n} . Hence when the uniaxial director \mathbf{n} lies on the equator (region R^+), the start-up uniaxial extensional flow should tend to increase the alignment along \mathbf{n} . Moreover when \mathbf{n} lies in region R^+ , the flow contributions in equation (13) are both negative ($\mathbf{A} : \mathbf{nn} < 0$, and $\mathbf{A} : \mathbf{mm} < 0$). Hence, for $S(\epsilon)$ to increase, equation (13) shows that the two ordering functions must be negative : $\beta_{1,s}^n < 0$, and $\beta_{1,s}^m < 0$.

When \mathbf{n} lies on the pole the effect of biaxiality is zero, since both biaxial directors (\mathbf{m}, \mathbf{l}) lie on the compression (y - z) plane. As \mathbf{n} moves towards the equator the biaxiality increases because of the preference of the projections of the molecular normals to align themselves along \mathbf{m} in a plane perpendicular to \mathbf{n} . Thus when \mathbf{n} lies on the equator (\mathbf{l} lies on the pole, and \mathbf{m} lies on the equator) the application of the flow should increase biaxiality, and when \mathbf{n} lies along the poles flow will not induce any biaxiality. Consideration of equation (14) with \mathbf{n} on the equator indicates that the expected increase of P is captured only if the two ordering functions are negative : $\beta_{1,p}^n < 0$, and $\beta_{1,p}^m < 0$.

4.4. Numerical Results

4.4.1. Uniaxial and Biaxial Orientation Relaxation

Figure 8 shows the polar uniaxial angle ϕ as a function of strain (dimensionless time) $\epsilon = \dot{\epsilon}t$, for $De=0.6$ (a), 0.4 (b), 0.1 (c); $U=3$ (dash-dot line), $U=5$ (full line), and for the initial uniaxial director orientation $(\theta_0, \phi_0)=(45, 2.56)$. The figure shows that the uniaxial director \mathbf{n} relaxation is viscoelastic, and that it is faster at higher De and lower U , since for these conditions the uniaxial reactive parameter λ_n^n samples higher absolute values. The biaxial director \mathbf{m} is fixed at the equator (see figure 5), and the biaxial director \mathbf{l} follows the viscoelastic relaxation of the uniaxial director \mathbf{n} , since $\mathbf{l} \perp \mathbf{n}$.

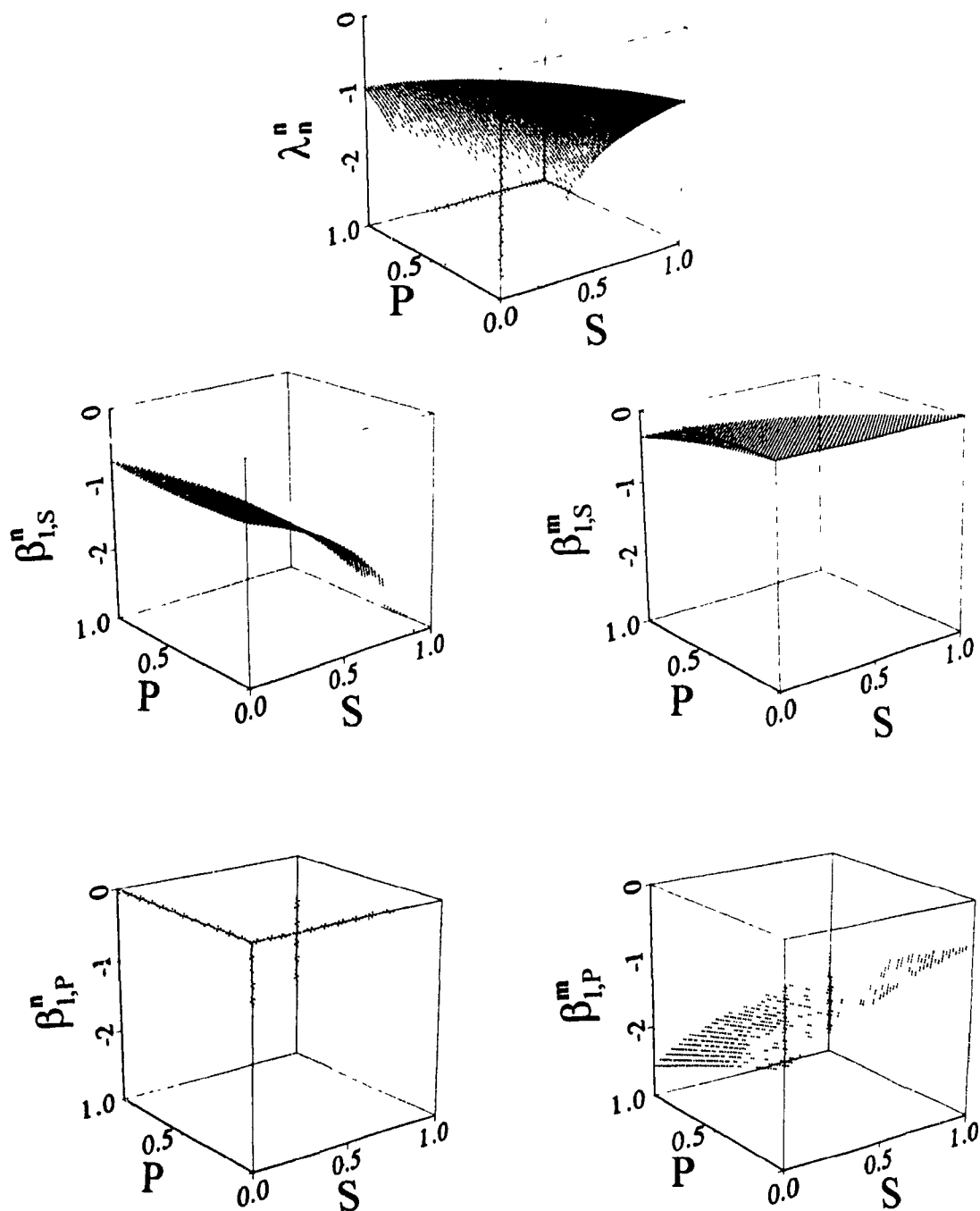


Fig. 7. Parametric functions of the model. The uniaxial reactive parameter λ_n^n and the set of ordering functions $\beta_{1,S}^n$, $\beta_{1,S}^m$, $\beta_{1,P}^n$, and $\beta_{1,P}^m$ as a function of the uniaxial scalar order parameter S and biaxial scalar order parameter P for the chosen set of dimensionless phenomenological parameters (σ_4^* , σ_6^* , and τ_6^*). For discotic nematic liquid crystals these all are negative (see text).

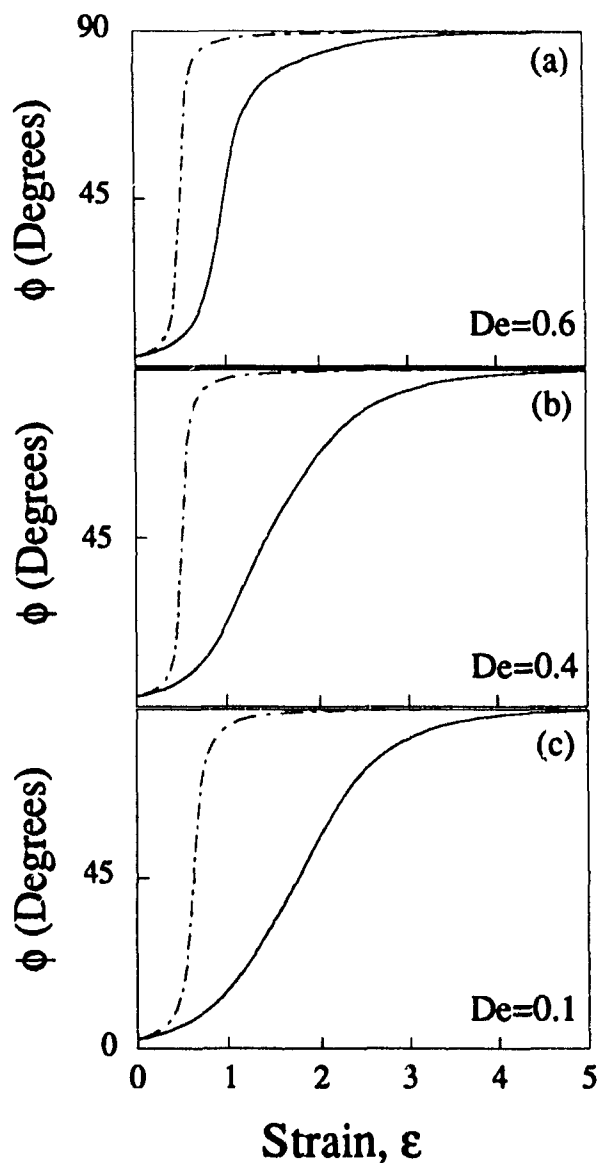


Fig. 8. Polar uniaxial angle ϕ as a function of strain (dimensionless time) $\epsilon = \dot{\epsilon}t$, for $De=0.6$ (a), 0.4 (b), 0.1 (c); $U=3$ (dash-dot line), $U=5$ (full line), and initial uniaxial director orientation $(\theta_0, \phi_0)=(45, 2.56)$. The uniaxial director relaxation is viscoelastic, and it is faster at higher De and at lower U . The biaxial director \mathbf{m} is fixed on the equator, and the biaxial director \mathbf{l} follows the viscoelastic relaxation of the uniaxial director \mathbf{n} .

4.4.2. Uniaxial and Biaxial Alignment Relaxation

Figure 9 shows the uniaxial alignment relaxation $S(\epsilon)$, and the biaxial alignment relaxation $P(\epsilon)$, for $De=0.6$ (full line), $De=0.4$ (dash-dot line), and $De=0.1$ (triple dot dash line) corresponding to the initial uniaxial director orientation of figure 8, for (a, c) $U=5$, (b, d) $U=3$. The figure shows that the uniaxial and biaxial alignment relaxations are viscoelastic. For a high nematic potential ($U=5$) the viscous mode dominates for higher De ($De=0.6$), while the elastic mode dominates the viscoelastic relaxation for lower De ($De=0.1$). For a low nematic potential ($U=3$) the viscous mode dominates at higher De ($De=0.6$); at lower De ($De=0.1$) the viscous mode dominates the initial response but the elastic mode dominates the viscoelastic relaxation at the later stage. Since in this figure

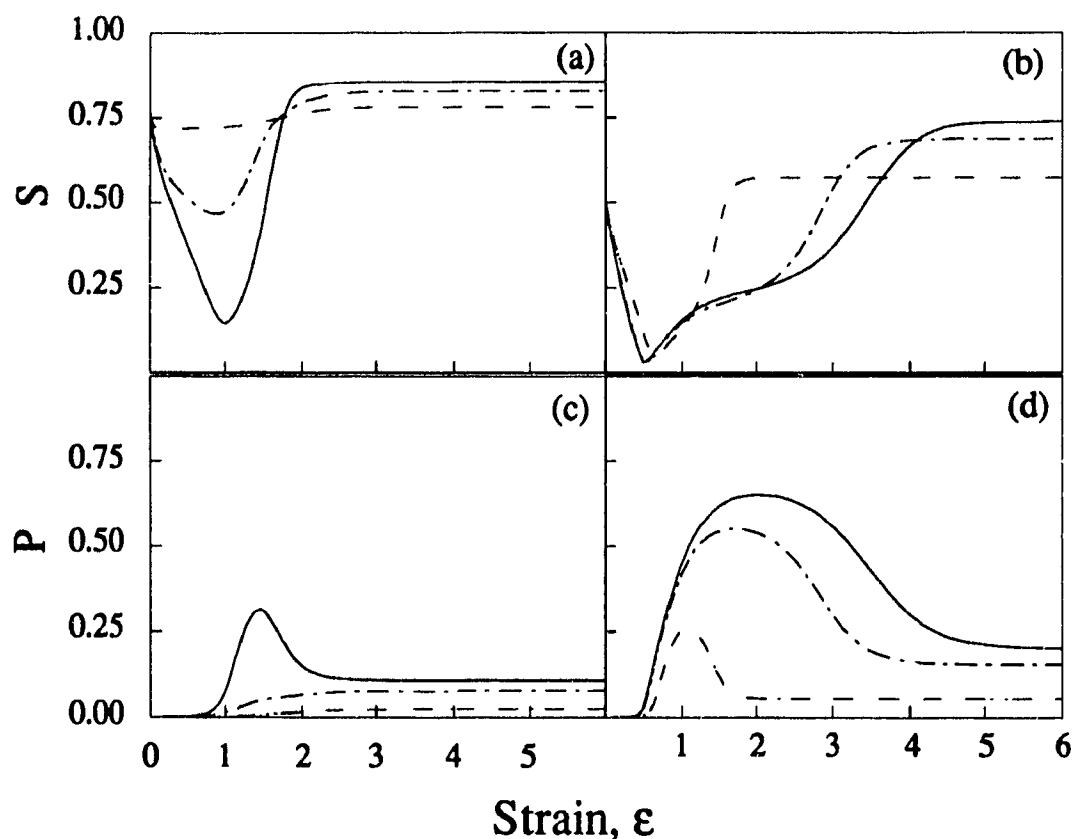


Fig. 9. Uniaxial alignment relaxation $S(\epsilon)$ and biaxial alignment relaxation $P(\epsilon)$, for $De=0.6$ (full line), $De=0.4$ (dash-dot line), and $De=0.1$ (triple dot dash line) corresponding to initial uniaxial director orientation of figure 8, for (a, c) $U=5$, (b, d) $U=3$. The figure shows that at higher De the viscous mode dominates and the effect of relative magnitude of U is small, while at lower De the elastic mode dominates and the effect of relative magnitude of U is large. The Deborah number De is the dimensionless strain rate ($De = \dot{\epsilon} \tau_d$).

the initial orientation of the uniaxial director n_0 is in R^- , there is an initial decrease in the uniaxial alignment relaxation (figure 9 a, b), and there is an initial lag in the biaxial alignment relaxation (figure 9 c, d). A comparison of the computed steady state alignment shows that at higher De , the viscous mode dominates and the effect of the relative magnitude of the nematic potential U is small, while at lower De , the elastic mode dominates and the effect of U is large.

Figure 10 shows the alignment's evolution in the alignment triangle (P-S triangle) for $De=0.6$ (full line), $De=0.4$ (dash-dot line), and $De=0.1$ (triple dot dash line) corresponding to initial the uniaxial director orientation of figure 8, for (a) $U=5$ and (b) $U=3$. The empty circles show the initial alignments condition ($S=S_{eq}$, $P=0$), and the direction of arrows represents the relaxation with increasing strain ϵ ($\epsilon = \dot{\epsilon} t$). The figure shows an initial decrease in the magnitude of the uniaxial scalar order parameter S , from the equilibrium value S_{eq} , because the uniaxial orientation prior to flow was in region R^- .

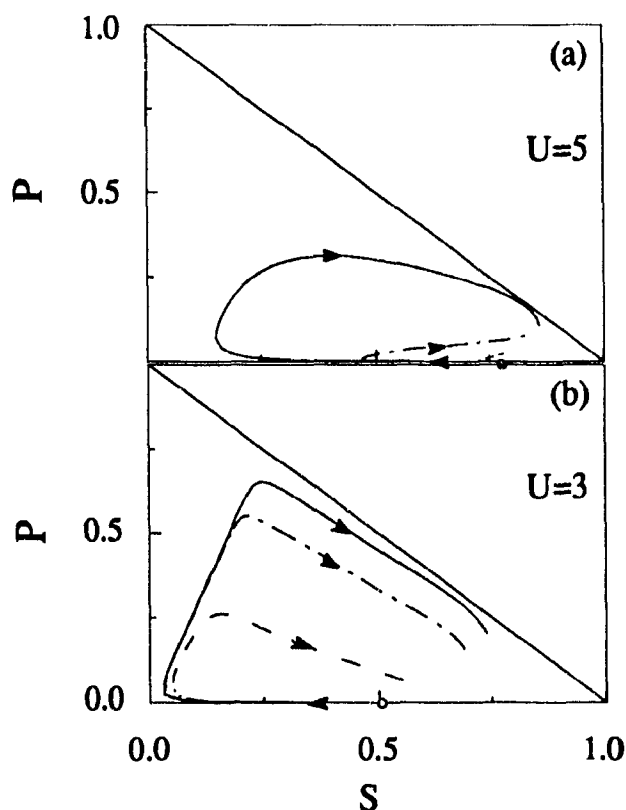


Fig. 10. Alignment trajectories in the alignment triangle (P-S triangle) for $De=0.6$ (full line), $De=0.4$ (dash-dot line), and $De=0.1$ (triple dot dash line), corresponding to initial uniaxial director orientation of figure 8, for (a) $U=5$ and (b) $U=3$. The circles show the initial alignment condition ($S=S_{eq}$, $P=0$), and the direction of arrows represent the relaxation with increasing strain ϵ ($\epsilon = \dot{\epsilon} t$).

Figure 10 shows that the alignment trajectory is well approximated by a three stage process. In the initial stage, S decreases and P remains close to zero, since the uniaxial orientation \mathbf{n} is close to the poles, and the flow will not induce biaxiality. In the intermediate stage, S is relatively low, \mathbf{n} is oriented away from the pole and both of these effects contribute to the increase of P . In the third stage, \mathbf{n} is close to the equator and the potential for flow-induced biaxiality is maximum but, the high uniaxial alignment S dominates and causes a decrease in P .

Figure 11 shows a trajectory in the alignment triangle and the corresponding computed scientific visualizations representing the density ($f(\omega_1, \omega_2)$) of the unit normals to the discs in $\mathbf{m-l}$ plane (\mathbf{n} is out of the plane of paper), for $U=3$, $De=0.6$, and for the initial uniaxial director orientation of figure 8. The density $f(\omega_1, \omega_2)$ is approximated by :

$$f(\omega_1, \omega_2) \approx \frac{1}{4\pi} + \frac{5}{8\pi} \left((2 \cos^2 \omega_1 - \sin^2 \omega_1) S + (\sin^2 \omega_1 \cos 2\omega_2) P \right); \quad (31)$$

where (ω_1, ω_2) are the polar and azimuthal angles respectively of the unit normal to a disc-like molecule. Equation (31) was obtained by using the standard single molecule distribution function $f(\mathbf{u}) \approx \frac{1}{4\pi} + \mathbf{u}\mathbf{u} : \mathbf{Q}$, where \mathbf{u} is the unit normal to the disc-like molecule. In the figure we mapped the magnitude of $f(\omega_1, \omega_2)$ onto a gray scale; darker (lighter) regions correspond to higher (lower) value of $f(\omega_1, \omega_2)$. The four insets correspond to the following alignment states: bottom right ($S = 0.5, P = 0$), bottom left ($S = 0.03, P = 0.03$), top left ($S = 0.25, P = 0.65$), and top right ($S = 0.74, P = 0.2$). A darker area represents the higher density of unit normals to the disc-like molecules. The bottom right visualization, representing the initial uniaxial state, shows that the $\mathbf{m-l}$ plane is isotropic as $P = 0$; since $S \neq 0$ the density of the unit normals is high near the center (\mathbf{n} is pointing out of the plane of paper at the center) but it decreases as we move away from the center. The bottom right visualization, representing a nearly isotropic state, shows a higher distribution of unit normals along \mathbf{m} than \mathbf{l} ; as S is nearly zero there is almost a constant density of the unit normals. The top left visualization, representing a stronger biaxial state, shows a stronger anisotropy of the distribution than in the previous bottom left case, as P is now higher. The top right visualization, representing the stable state, shows a weaker anisotropy of the distribution of the unit normals along \mathbf{m} than previous visualizations, since an increase in S has lowered P ; also as the magnitude of S is now significant there is a higher density of unit normals near the center than away from

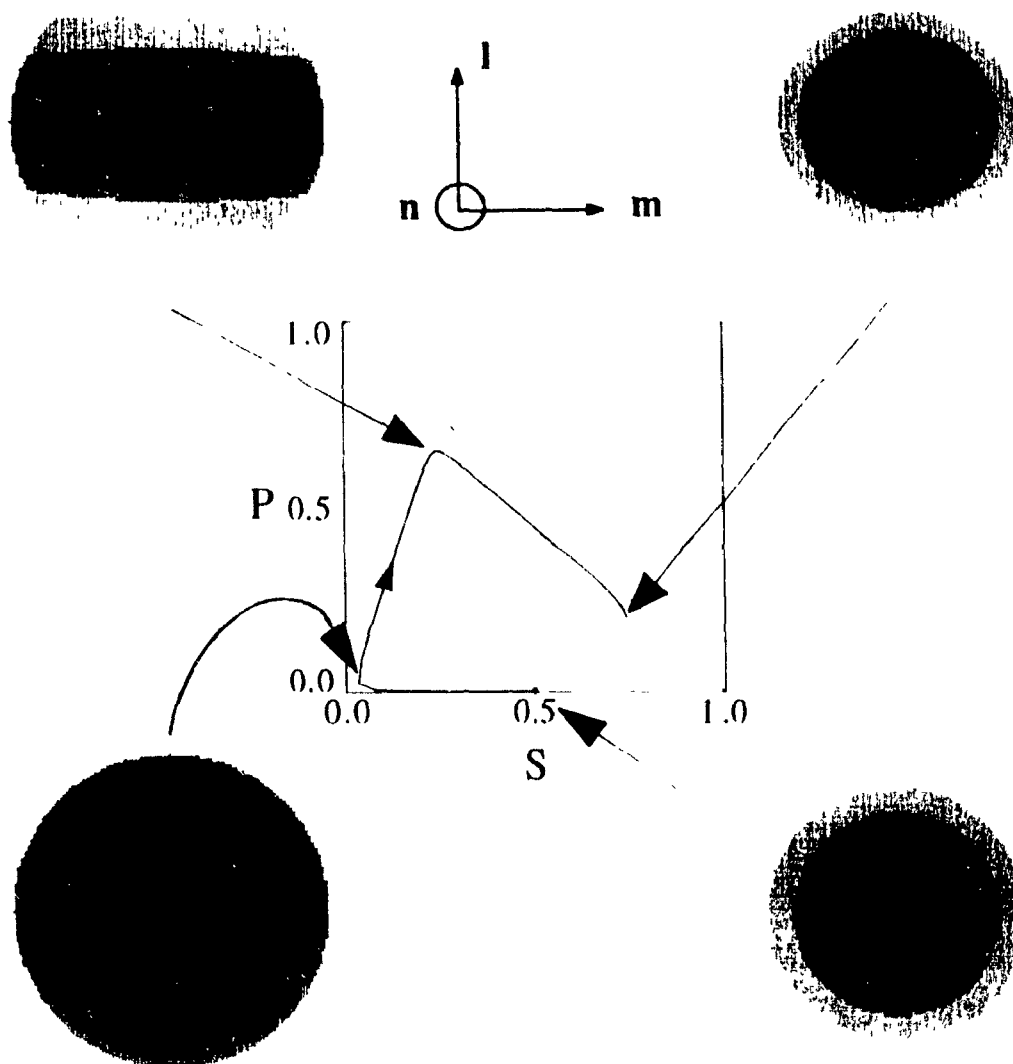


Fig. 11 Computed scientific visualizations representing the density of the unit normals to the molecular discs in m - l plane (n is out of the plane of paper,) for $U=3$, $De=0.6$ corresponding to the initial uniaxial director orientation of figure 8. The four insets correspond to the following alignment states: bottom right ($S=0.5$, $P=0$), bottom left ($S=0.03$, $P=0.03$), top left ($S=0.25$, $P=0.65$), top right ($S=0.74$, $P=0.2$). A darker area represents the higher density of unit normals to the disc-like molecules. For cases where $P \neq 0$, the figure shows a considerable higher distribution of unit normals along m than along l . See text.

the center. Comparison of the top right and the bottom right visualizations shows that the intensity of the gray level decreases more rapidly in the former than in the latter, as S has a higher value in the former.

Figure 12 shows the biaxial alignment relaxation $P(\epsilon = \dot{\epsilon}t)$ for $De=0.6$, $U=3$, and for \mathbf{n}_0 near the pole, $(\theta_0, \phi_0) = (45, 2.56)$, (full line), and \mathbf{n}_0 on the equator, $(\theta_0, \phi_0) = (45, 90)$, (dot dash line). The figure shows an initial lag in the biaxial relaxation when the initial uniaxial director orientation is near the poles (region R^-). The source of this is the competition between two effects : (i) when the initial uniaxial director orientation is near the poles (region R^-) there is always a decrease in the initial uniaxial alignment response, which does not impede an increase in biaxiality; (ii) when the uniaxial director is near the poles, the biaxial director \mathbf{l} (m) lies near (on) the equator and there is no significant competition of the unit normals to align along any one of the two biaxial directors, and hence there is no significant inducement for biaxiality. When the initial uniaxial director orientation is near the poles (region R^-) the combination of the two effects results in a lag in the initial biaxial alignment relaxation. When the initial uniaxial director orientation is in the region R^+ , the biaxial director \mathbf{l} is in the region R^- , and there is preference of the molecular normals to lie along the director which lies in the compressional plane (biaxial director \mathbf{m}), and hence the biaxial alignment relaxation shows a monotonic increase. The steady state biaxiality P is the same for both initial

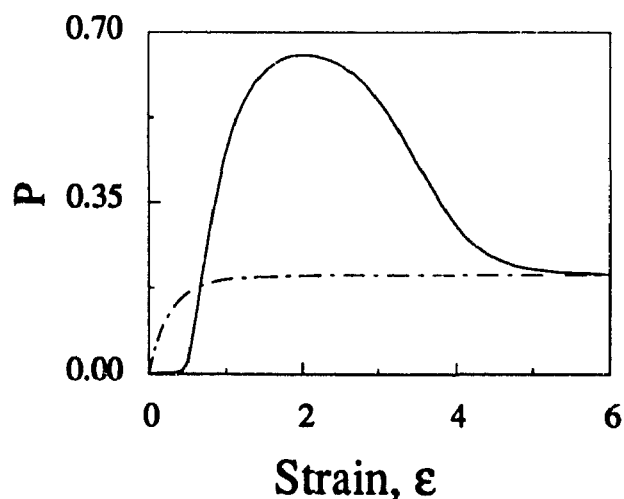


Fig. 12. Biaxial relaxation $P(\epsilon = \dot{\epsilon}t)$ for $De=0.6$, $U=3$, and for \mathbf{n}_0 near the pole, $(\theta_0, \phi_0)=(45, 2.56)$, (full line), and \mathbf{n}_0 on the equator, $(\theta_0, \phi_0)=(45, 90)$, (dot dash line). The figure shows an initial lag in the biaxial relaxation when initial uniaxial director orientation is along poles.

orientations. However, the relaxation time is considerably longer when the initial uniaxial director orientation is along the poles (region R^-) than when the initial uniaxial orientation is along the equator (region R^+).

Figure 13 shows the relaxation of the components of the tensor order parameter Q ($\epsilon = \dot{\epsilon}t$), with the initial orientation $(\theta_0, \phi_0) = (45, 2.56)$ close to the north pole, for $U = 5$, and $De = 0.6$ (full line), 0.4 (dash-dot line), and 0.1 (triple dot-dash line). For the chosen initial orientation $n_{y0} = n_{z0}$, and from equation (1a) it follows that $Q_{xy} = Q_{xz}$ and $Q_{zz} = Q_{yy}$. For the shown parameters the relaxation is virtually complete after 4 strains units. At lower De the relaxation of the components of the tensor order parameter is controlled by the orientation relaxation, as for $U = 5$ and lower De the uniaxial alignment is nearly constant and there is not much increase in the biaxial alignment (see figure 9). At higher De the relaxation of the trace components of the tensor order parameters is governed by the alignment because there is larger changes in the uniaxial and biaxial alignments as viscous mode dominates the viscoelastic relaxation. At lower De the non-diagonal components of the tensor order parameter Q are governed by the orientation relaxation, while at higher De , the viscous effects introduces an initial large decrease in uniaxial alignment and a lag in biaxial alignment. The latter case follows since the initial uniaxial orientation n_0 is in region R^- , and a subsequent increase in both uniaxial and biaxial alignment (see figure 9), with the result that the only large component is Q_{yz} , which follows a lag plus exponential growth relaxation.

At steady state, the magnitude of the differences of diagonal components of tensor order parameter are proportional to the steady flow birefringences [35]. Using equations (A.1 - A.5) these differences are given by :

$$|(Q_{xx} - Q_{yy})_{ss}| = \left| \frac{b^2 S_{ss} + \frac{1}{3}(2 + b^2) P_{ss}}{1 + b^2} \right| \quad (32a)$$

$$|(Q_{yy} - Q_{zz})_{ss}| = \left| \frac{1 - b^2}{1 + b^2} \left(S_{ss} - \frac{1}{3} P_{ss} \right) \right| \quad (32b)$$

$$|(Q_{zz} - Q_{xx})_{ss}| = \left| \frac{S_{ss} + \frac{1}{3}(2b^2 + 1) P_{ss}}{1 + b^2} \right| \quad (32c)$$

where S_{SS} and P_{SS} are the steady state alignments. Figure 14 shows the absolute of the difference of the steady state diagonal components $|(Q_{xx} - Q_{yy})_{SS}|$ (a), $|(Q_{yy} - Q_{zz})_{SS}|$ (b), and $|(Q_{zz} - Q_{xx})_{SS}|$ (c), of the tensor order parameter as a function of De , for $U=3$. The initial uniaxial director orientations are : $(\theta_0, \phi_0) = (45, 2.56)$ or $b = 1$ (full line), $(\theta_0, \phi_0) = (90, 2.56)$ or $b = 0$ (dash-dot line), and $(\theta_0, \phi_0) = (0, 2.56)$ or $b = \infty$ (triple dot-dash line). In all cases there is a monotonic increase with increasing De . The value of the y-z birefringence is identical for $b = 0$ and $b = \infty$, hence the shown curves for these cases superpose. Comparison of figures 14(a) and 14(c) show that : the x-y and the z-x birefringences are the same for $b = 1$; the x-y birefringence for $b = 0$ is equal to the z-x birefringence for $b = \infty$ and vice versa. The figure that y-z birefringence is a weaker function of De , whereas the x-y and the z-x birefringences are stronger functions of De .

4.5. Conclusions

In this initial investigation of the nematic rheology of discotic nematics subjected to uniaxial extensional flows, we have performed a useful characterization of the sensitivity of the director triad $(\mathbf{n}, \mathbf{m}, \mathbf{l})$ trajectories, uniaxial and biaxial alignments (S, P) , and tensor order parameter relaxations with respect to the strength of the uniaxial nematic potential, the alignment Deborah number (dimensionless strain rate), and the initial director orientation. The use of unit sphere description identified the dynamics of the uniaxial director \mathbf{n} and biaxial director \mathbf{l} as geodesic meridian flows, whereas the constant orientation of the biaxial director \mathbf{m} always lies on the equator. The stable steady state director triad is collinear with the axes of the strain rate ellipsoid. The uniaxial alignment undergoes an initial decrease whereas the biaxial alignment shows an initial lag when the initial uniaxial orientation is close to the extension axis. Relatively large transient decreases of the uniaxial alignment and relatively large transient increases of the biaxial alignment are predicted to occur whenever the initial uniaxial director is along the extension direction. This comprehensive and unified view of microstructure relaxation under extension may be used in the future to explain the characteristic patterns found in the cross-section of melt spun fibers from carbonaceous mesophases [3, 36, 37].

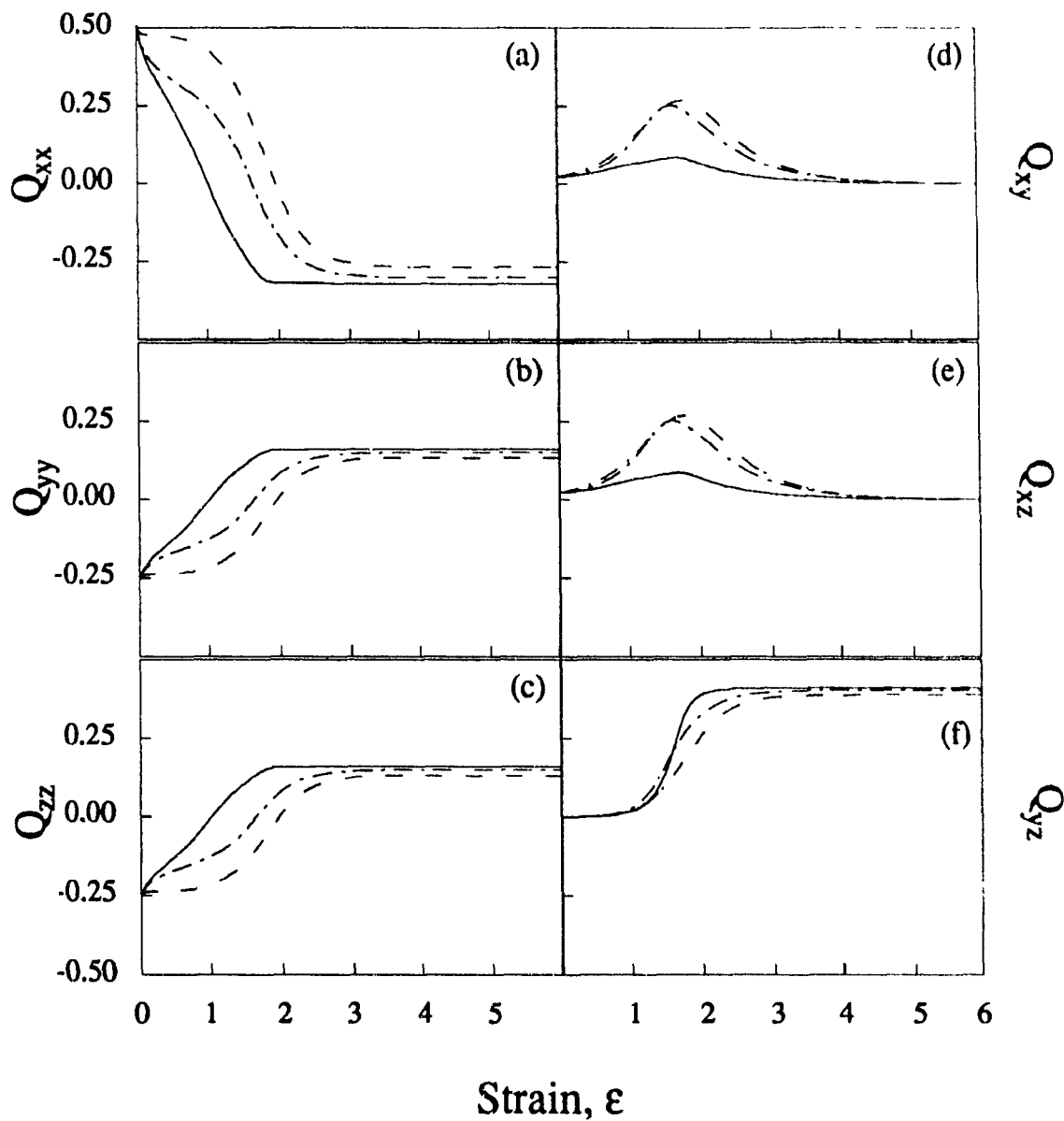


Fig. 13. Relaxation of the components of the tensor order parameter $Q(\epsilon)$ with the initial orientation $(\theta_0, \phi_0) = (45, 2.56)$ close to the pole, for $U=5$, and $De = 0.6$ (full line), 0.4 (dash-dot line), and 0.1 (triple dot-dash line). The relaxation coordinate $\epsilon = \dot{\epsilon}t$ is the strain or dimensionless time. For the chosen initial orientation $n_{y0} = n_{z0}$, and from equation (1a) it then follows that $Q_{xy} = Q_{xz}$ and $Q_{zz} = Q_{yy}$. See text for discussion.

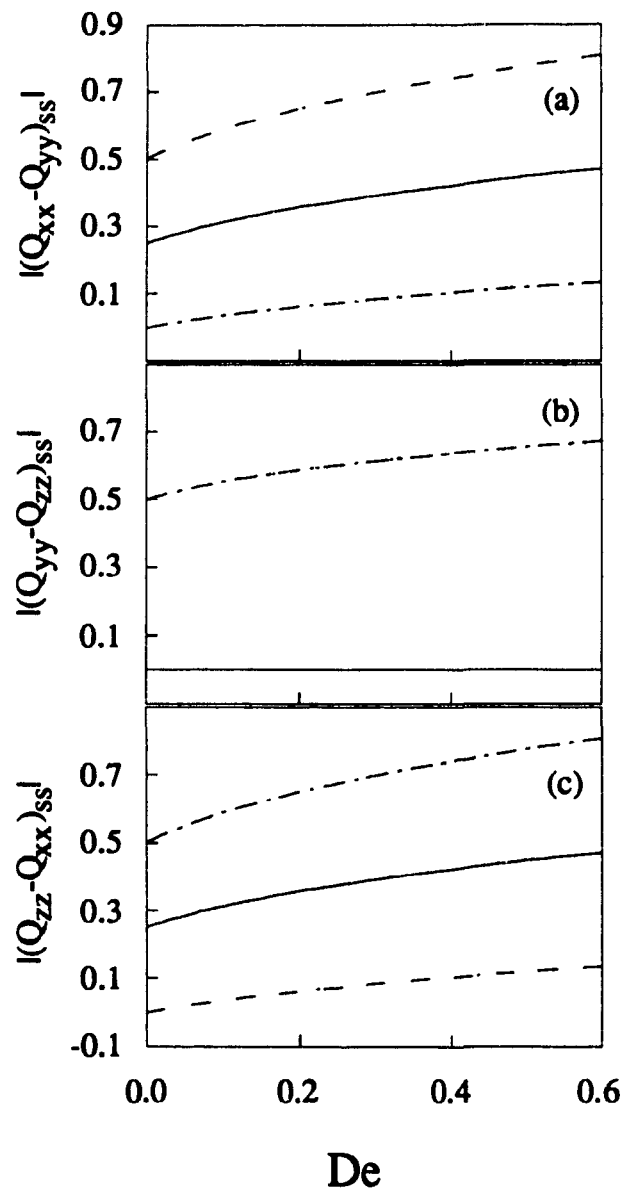


Fig. 13. Magnitude of the difference of the steady state diagonal components $|Q_{xx} - Q_{yy}|_{ss}$ (a), $|Q_{yy} - Q_{zz}|_{ss}$ (b), and $|Q_{zz} - Q_{xx}|_{ss}$ (c) of the tensor order parameter as a function of the dimensionless strain rate De , for $U=3$. The initial uniaxial director orientations are : $(\theta_0, \phi_0) = (45, 2.56)$ or $b = 1$ (full line), $(\theta_0, \phi_0) = (90, 2.56)$ or $b=0$ (dash-dot line), and $(\theta_0, \phi_0) = (0, 2.56)$ or $b = \infty$ (triple dot-dash line). These differences are proportional to the steady flow birefringences [34]. Except for one case (figure 14 (b), $b = 1$), the birefringences increase with the increasing De .

4.6. Appendix A

The dimensionless coupled, nonlinear ordinary first order differential equations governing the microstructure of a discotic nematic, subjected to uniaxial extensional flow, are:

$$\eta_1 \frac{dQ_{xx}}{d\varepsilon} + \eta_2 \frac{dQ_{xy}}{d\varepsilon} + \eta_3 \frac{dQ_{xz}}{d\varepsilon} + \eta_4 \frac{dQ_{yy}}{d\varepsilon} + \eta_5 \frac{dQ_{yz}}{d\varepsilon} + \kappa_1 De^{-1} + \zeta_1 = 0 \quad (\text{A.1})$$

$$\eta_6 \frac{dQ_{xx}}{d\varepsilon} + \eta_7 \frac{dQ_{xy}}{d\varepsilon} + \eta_8 \frac{dQ_{xz}}{d\varepsilon} + \eta_9 \frac{dQ_{yy}}{d\varepsilon} + \eta_{10} \frac{dQ_{yz}}{d\varepsilon} + \kappa_2 De^{-1} + \zeta_2 = 0 \quad (\text{A.2})$$

$$\eta_{11} \frac{dQ_{xx}}{d\varepsilon} + \eta_{12} \frac{dQ_{xy}}{d\varepsilon} + \eta_{13} \frac{dQ_{xz}}{d\varepsilon} + \eta_{14} \frac{dQ_{yy}}{d\varepsilon} + \eta_{15} \frac{dQ_{yz}}{d\varepsilon} + \kappa_3 De^{-1} + \zeta_3 = 0 \quad (\text{A.3})$$

$$\eta_{16} \frac{dQ_{xx}}{d\varepsilon} + \eta_{17} \frac{dQ_{xy}}{d\varepsilon} + \eta_{18} \frac{dQ_{xz}}{d\varepsilon} + \eta_{19} \frac{dQ_{yy}}{d\varepsilon} + \eta_{20} \frac{dQ_{yz}}{d\varepsilon} + \kappa_4 De^{-1} + \zeta_4 = 0 \quad (\text{A.4})$$

$$\eta_{21} \frac{dQ_{xx}}{d\varepsilon} + \eta_{22} \frac{dQ_{xy}}{d\varepsilon} + \eta_{23} \frac{dQ_{xz}}{d\varepsilon} + \eta_{24} \frac{dQ_{yy}}{d\varepsilon} + \eta_{25} \frac{dQ_{yz}}{d\varepsilon} + \kappa_5 De^{-1} + \zeta_5 = 0 \quad (\text{A.5})$$

where $De = \dot{\varepsilon} \tau_4$, is the alignment Deborah number (dimensionless strain rate) and $\varepsilon = \dot{\varepsilon} t$ is the strain. The coefficients η_i ($i = 1, 2, \dots, 25$) and κ_i ($i = 1, 2, \dots, 11$) are given by :

$$\eta_1 = 1 + \frac{2}{3} \tau_6^* (Q_{xx} - Q_{yy}) \quad (\text{A.6})$$

$$\eta_2 = \frac{2}{3} \tau_6^* Q_{xy} \quad (\text{A.7})$$

$$\eta_3 = \frac{2}{3} \tau_6^* Q_{xz} \quad (\text{A.8})$$

$$\eta_4 = -\frac{2}{3} \tau_6^* (Q_{xx} + 2 Q_{yy}) \quad (\text{A.9})$$

$$\eta_5 = -\frac{4}{3} \tau_6^* Q_{yz} \quad (\text{A.10})$$

$$\eta_6 = \tau_6^* Q_{xy} \quad (\text{A.11})$$

$$\eta_7 = 1 + \tau_6^* (Q_{xx} + Q_{yy}) \quad (\text{A.12})$$

$$\eta_8 = \tau_6^* Q_{yz} \quad (\text{A.13})$$

$$\eta_9 = \tau_6^* Q_{xy} \quad (\text{A.14})$$

$$\eta_{10} = \tau_6^* Q_{xz} \quad (\text{A.15})$$

$$\eta_{11} = 0 \quad (\text{A.16})$$

$$\eta_{12} = \tau_6^* Q_{yz} \quad (\text{A.17})$$

$$\eta_{13} = 1 - \tau_6^* Q_{yy} \quad (\text{A.18})$$

$$\eta_{14} = -\tau_6^* Q_{xz} \quad (\text{A.19})$$

$$\eta_{15} = \tau_6^* Q_{xy} \quad (\text{A.20})$$

$$\eta_{16} = -\frac{2}{3} \tau_6^* (2 Q_{xx} + Q_{yy}) \quad (\text{A.21})$$

$$\eta_{17} = \frac{2}{3} \tau_6^* Q_{xy} \quad (\text{A.22})$$

$$\eta_{18} = -\frac{4}{3} \tau_6^* Q_{xz} \quad (\text{A.23})$$

$$\eta_{19} = 1 - \frac{2}{3} \tau_6^* (Q_{xx} - Q_{yy}) \quad (\text{A.24})$$

$$\eta_{20} = \frac{2}{3} \tau_6^* Q_{yz} \quad (\text{A.25})$$

$$\eta_{21} = -\tau_6^* Q_{yz} \quad (\text{A.26})$$

$$\eta_{22} = \tau_6^* Q_{xz} \quad (\text{A.27})$$

$$\eta_{23} = \tau_6^* Q_{xy} \quad (\text{A.28})$$

$$\eta_{24} = 0 \quad (\text{A.29})$$

$$\eta_{25} = 1 - \tau_6^* Q_{xx} \quad (\text{A.30})$$

$$\begin{aligned} \kappa_1 = & \left(1 - \frac{U}{3}\right) Q_{xx} - 2U(Q_{xx}^2 + Q_{yy}^2 + Q_{xx} Q_{yy} + Q_{xy}^2 + Q_{xz}^2 + Q_{yz}^2) Q_{xx} \\ & - \frac{U}{3}(Q_{xx}^2 - 2Q_{yy}^2 - 2Q_{xx} Q_{yy} + Q_{xy}^2 + Q_{xz}^2 - 2Q_{yz}^2) \end{aligned} \quad (\text{A.31})$$

$$\begin{aligned} \kappa_2 = & \left(1 - \frac{U}{3}\right) Q_{xy} - 2U(Q_{xx}^2 + Q_{yy}^2 + Q_{xx} Q_{yy} + Q_{xy}^2 + Q_{xz}^2 + Q_{yz}^2) Q_{xy} \\ & - U(Q_{xx} Q_{xy} + Q_{xy} Q_{yy} + Q_{yz} Q_{xz}) \end{aligned} \quad (\text{A.32})$$

$$\begin{aligned} \kappa_3 = & \left(1 - \frac{U}{3}\right) Q_{xz} - 2U(Q_{xx}^2 + Q_{yy}^2 + Q_{xx} Q_{yy} + Q_{xy}^2 + Q_{xz}^2 + Q_{yz}^2) Q_{xz} \\ & - U(Q_{yz} Q_{xy} - Q_{yy} Q_{xz}) \end{aligned} \quad (\text{A.33})$$

$$\begin{aligned} \kappa_4 = & \left(1 - \frac{U}{3}\right) Q_{yy} - 2U(Q_{xx}^2 + Q_{yy}^2 + Q_{xx} Q_{yy} + Q_{xy}^2 + Q_{xz}^2 + Q_{yz}^2) Q_{yy} \\ & - \frac{U}{3}(-2Q_{xx}^2 + Q_{yy}^2 - 2Q_{xx} Q_{yy} + Q_{xy}^2 - 2Q_{xz}^2 + Q_{yz}^2) \end{aligned} \quad (\text{A.34})$$

$$\begin{aligned} \kappa_5 = & \left(1 - \frac{U}{3}\right) Q_{yz} - 2U(Q_{xx}^2 + Q_{yy}^2 + Q_{xx} Q_{yy} + Q_{xy}^2 + Q_{xz}^2 + Q_{yz}^2) Q_{yz} \\ & - U(Q_{xz} Q_{xy} - Q_{xx} Q_{yz}) \end{aligned} \quad (\text{A.35})$$

$$\zeta_1 = \sigma_4^* + \sigma_6^* Q_{xx} \quad (\text{A.36})$$

$$\zeta_2 = \frac{1}{2} \sigma_6^* Q_{xy} \quad (\text{A.37})$$

$$\zeta_3 = \frac{1}{2} \sigma_6^* Q_{xz} \quad (\text{A.38})$$

$$\zeta_4 = -\frac{1}{2} \sigma_4^* - \sigma_6^* (Q_{xx} + Q_{yy}) \quad (\text{A.39})$$

$$\zeta_5 = -\sigma_6^* Q_{yz} \quad (\text{A.40})$$

The non-dimensional parameters σ_4^* , σ_6^* , and τ_6^* are given by :

$$\sigma_4^* = \frac{\sigma_4}{\tau_4}; \quad \sigma_6^* = \frac{\sigma_6}{\tau_4}; \quad \tau_6^* = \frac{\tau_6}{\tau_4}. \quad (\text{A.41})$$

4.7. Appendix B

The reactive parameter set ($\lambda_n^n, \lambda_{mix}^n, \lambda_1^1, \lambda_{mix}^1$), the ordering function set ($\beta_{1,S}^n, \beta_{1,S}^m, \beta_{1,P}^n, \beta_{1,P}^m$), and the elastic functions set ($\beta_{2,S}, \beta_{2,P}$) are given by :

$$\lambda_n^n = -\frac{\gamma_{2,n}^n}{\gamma_1^n} = -\frac{9\sigma_4^* + 3\sigma_6^*(S-P)}{3S(3+\tau_6^*S) + 3P(3-\tau_6^*P) - 2\tau_6^*SP} \quad (B.1)$$

$$\lambda_{mix}^n = -\frac{\gamma_{2,mix}^n}{\gamma_1^n} = -\frac{6\sigma_6^*P}{3S(3+\tau_6^*S) + 3P(3-\tau_6^*P) - 2\tau_6^*SP} \quad (B.2)$$

$$\lambda_1^1 = -\frac{\gamma_{2,1}^1}{\gamma_1^1} = \frac{\gamma_{2,1}^1}{\gamma_1^n} = \frac{9\sigma_4^* + 3\sigma_6^*(S-P)}{3S(3+\tau_6^*S) + 3P(3-\tau_6^*P) - 2\tau_6^*SP} \quad (B.3)$$

$$\lambda_{mix}^1 = -\frac{\gamma_{2,mix}^1}{\gamma_1^1} = \frac{\gamma_{2,mix}^1}{\gamma_1^n} = \frac{3\sigma_6^*(3P-S)}{3S(3+\tau_6^*S) + 3P(3-\tau_6^*P) - 2\tau_6^*SP} \quad (B.4)$$

$$\beta_{1,S}^n = -\frac{8\sigma_6^*\tau_6^*(3S+P)P - (9\sigma_4^* + 2\sigma_6^*(3S-P))(9-2\tau_6^*(3S-P))}{4\tau_6^*(3+2\tau_6^*(S+P))P - (6+4\tau_6^*S)(9-2\tau_6^*(3S-P))} \quad (B.5)$$

$$\beta_{1,S}^m = \frac{4\tau_6^*(9\sigma_4^* - 2\sigma_6^*(3S-P))P - 4\sigma_6^*(9-2\tau_6^*(3S-P))P}{4\tau_6^*(3+2\tau_6^*(S+P))P - (6+4\tau_6^*S)(9-2\tau_6^*(3S-P))} \quad (B.6)$$

$$\beta_{1,P}^n = -\frac{6\sigma_6^*(3S+P)(6+4\tau_6^*S) - 3(9\sigma_4^* + 2\sigma_6^*(3S-P))(3+2\tau_6^*(S+P))}{4\tau_6^*(3+2\tau_6^*(S+P))P - (6+4\tau_6^*S)(9-2\tau_6^*(3S-P))} \quad (B.7)$$

$$\beta_{1,P}^m = \frac{3(9\sigma_4^* - 2\sigma_6^*(3S-P))(6+4\tau_6^*S) - 12\sigma_6^*(3+2\tau_6^*(S+P))P}{4\tau_6^*(3+2\tau_6^*(S+P))P - (6+4\tau_6^*S)(9-2\tau_6^*(3S-P))} \quad (B.8)$$

$$\beta_{2,S} = \frac{\chi_1 + \chi_2}{\chi_5} \quad (B.9)$$

$$\beta_{2,P} = \frac{\chi_3 + \chi_4}{\chi_5} \quad (B.10)$$

$$\chi_1 = \frac{(-9(S-P) + U(-3P - P^2 + 2P^3 + (3+6P-2P^2)S + (3+6P)S^2 - 6S^3))}{\left(\frac{4}{81} \tau_6^* P\right)} \quad (\text{B.11})$$

$$\chi_2 = \left(3 - \frac{2}{3} \tau_6^* (3S - P)\right) (18S + U(2P^2 + (4P^2 - 6)S - 6S^2 + 12S^3)) \quad (\text{B.12})$$

$$\chi_3 = \frac{(-9(S-P) + U(-3P - P^2 + 2P^3 + (3+6P-2P^2)S + (3+6P)S^2 - 6S^3))}{(6 + 4 \tau_6^* S)} \quad (\text{B.13})$$

$$\chi_4 = (3 + 2 \tau_6^* (S + P)) (18S + U(2P^2 + (4P^2 - 6)S - 6S^2 + 12S^3)) \quad (\text{B.14})$$

$$\chi_5 = 4 \tau_6^* (3 + 2 \tau_6^* (S + P)) P - (6 + 4 \tau_6^* S) (9 - 2 \tau_6^* (3S - P)) \quad (\text{B.15})$$

4.8. References

- [1] Otani S., *Mol. Cryst. Liq. Cryst.* **63** (1981) 249-264.
- [2] Zimmer J. E., White J. L., *Disclination Structures in the Carbonaceous Mesophase.* In: Brown H. G. (ed.), *Advances in liquid Crystals*, Vol. 5, 1982, Academic Press, New York.
- [3] Singer L. S., "The Mesophase in Carbonaceous Pitches", *Faraday Discuss. Chem. Soc.* **73** (1985) 265-272.
- [4] Gasparoux H., *Mol. Cryst. Liq. Cryst.* **63** (1981) 231-248.
- [5] Chandrashekhar S., *Mol. Cryst. Liq. Cryst.* **63** (1981) 171-179.
- [6] Destrade C., Tinh N.H., Gasparoux H., Malthete J., Levelut A. M., *Mol. Cryst. Liq. Cryst.*, **71** (1981) 111-135.
- [7] de Gennes P. G., "The Physics of Liquid Crystals", Oxford University Press, London, (1975) p 153-165.
- [8] Bird R., Armstrong R.C. and Hassager O., "Dynamics of Polymeric Liquids", Wiley, New York, 1987.
- [9] Ericksen J. L., "Liquid Crystals with variable degree of Orientation," *IMA Preprint Series No. 559* (1989).
- [10] Imura H. and Okano K., *Jpn. J. Appl. Phys.*, **11** (1972) 1440-1445.
- [11] Diogo A. C. and Martins A. F., *J. Phys.*, **43** (1982), 779-786.
- [12] Edwards B.J., Beris A.N. and Grmela M., *Mol. Cryst. Liq. Cryst.* **201** (1991) 51-86.
- [13] Farhoudi Y. and Rey A.D., *J. Rheol.*, **37** (1993) 289-314.

- [14] Singh A.P. and Rey A.D., *J. Phys. II France*, **4** (1994) 645-665.
- [15] Singh A.P. and Rey A.D., *Liq. Cryst.*, in press, (1994).
- [16] Dunmer D.A., Szumilin K. and Waterworth T.F., *Mol. Cryst. Liq. Cryst.*, **149** (1987) 385-392.
- [17] Gramsbergen E.F., Longa L. and de Jeu W. H., *Physics Reports*, **135**, (1986) 195-257.
- [18] Lubensky T.C., *Phys. Rev. A*, **2** (1970) 2497
- [19] Galame Y., *Mol. Cryst. Liq. Cryst.*, **165** (1988) 131-149.
- [20] Marrucci G, in "Liquid Crystallinity in Polymers", Ciferri A. (ed.), VCH Publishers, New York, 1991.
- [21] Thurston R.N., *J. Physique* **42** (1981) 413-417.
- [22] Thurston R.N., *J. Appl. Phys.*, **52** (1981), 3040-3052.
- [23] Porte G. and Jadot J.P., *J. Physique*, **39** (1978) 213-223
- [24] Carlsson T., *Phys. Rev A*, **34** (1986) 3393-3404
- [25] Weinstock R., "Calculus of Variations", McGraw-Hill, New York, 1954, p 26-28.
- [26] Farhoudi Y. and Rey A.D., *Rheol. Acta*, **32** (1993) 207-217.
- [27] Doi M. and Edwards S.F., *The theory of polymer dynamics* (Oxford university Press, New York, 1986) 358-362.
- [28] Finlayson B.A., "Nonlinear Analysis in Chemical Engineering", McGraw-Hill, New York, 1980, p 28-31.
- [29] Ericksen J.L., *Koll. Zeit.*, **173** (1960) 117-122.
- [30] Ruelle D., "Chance and Chaos", Princeton University Press, New Jersey, (1991) p47.
- [31] Volovik G. E., *JETP Lett.*, **31** (1980) 273-275.
- [32] Carlsson T., *Mol. Cryst. Liq. Cryst.*, **89** (1982) 57-66.
- [33] Carlsson T., *J. Physique*, **44** (1983) 909-911.
- [34] Baals H. and Hess S., *Z. Naturforsch.*, **43A** (1988) 662-670.
- [35] de Gennes P. G., "The Physics of Liquid Crystals", Oxford University Press, London, (1975).
- [36] Fathollahi B. and White J.L., *J. of Rheology*, in press, (1994).
- [37] Honda H., *Mol. Cryst. Liq. Cryst.*, **94**, (1983) 97-108.

Chapter 5

Thesis Summary, Conclusions and Recommendations

This chapter is divided into three sections. The first section contains an overall summary of this thesis, the second section gives the conclusions of this thesis, and the last section presents recommendations on further work.

5.1. Thesis Summary

Naturally occurring carbonaceous mesophases are derived from the pyrolysis of coal or petroleum pitches, and display discotic nematic behavior. These low cost discotic mesophases are used as precursor materials for the manufacture of high performance mesophase pitch-based carbon fibers. The fiber morphology, that is the molecular arrangement in the cross-section of fiber, governs the mechanical properties of the fiber. Thus the understanding of the behavior of these materials under the effect of spinning flows is essential. This was the goal of this thesis.

Chapter 1 contains the introduction to the basic concepts of discotic nematodynamics which are used in the later part of the thesis. A description of carbonaceous mesophases, mesophase carbon fiber morphology, and elongational flows is also presented.

In chapter 2 an approximate phenomenological theory governing the orientation and alignment of a model uniaxial discotic nematic liquid crystal of variable order was formulated. The theory was used to derive the governing equations that describe the behavior of uniaxial discotics under isothermal, incompressible, irrotational, three-dimensional, uniaxial extensional flow. The unit sphere description of the director is used to analyze the analytical and numerical orientation and alignment relaxations. Computations of tensor order parameter relaxations and flow-induced birefringence are also given. Flow-induced melting of the nematic phase is also discussed in this chapter.

In chapter 3 the application of the theory developed in chapter 2 was generalized

to describe all types of isothermal, incompressible, irrotational, three dimensional, extensional flows. Computations corresponding to uniaxial extensional flow, biaxial extensional flow, and planar extensional flow are presented. A flow classification based on the orienting strength and aligning strength of the three flows is given. The unit sphere description of the director is used to discuss and analyze the sensitivity of the director paths and the alignment relaxations to the initial orientation and alignment conditions, to the Deborah number, and to the flow type. The tensor order parameter relaxations and flow-induced birefringence for the three extensional flows are given.

Chapter 4 models the uniaxial extensional flow-induced biaxiality in a uniaxial discotic nematic crystal. Numerical and analytical solutions of the director triad and uniaxial and biaxial alignments are presented. The dependency of the uniaxial and biaxial alignments on the initial uniaxial orientation is identified using unit sphere description of the director. The analytical and numerical results of the director triad, and of the uniaxial and biaxial alignments relaxations are given. An alignment triangle is identified and is used to capture the couplings between uniaxial and biaxial orderings. The tensor order parameter relaxations, and computed scientific visualizations of biaxial molecular orientation distributions are presented in this chapter.

5.2. Thesis Conclusions

Chapter 2

- (1) The behavior of uniaxial discotic nematics was studied under the influence of a constant uniaxial, isothermal, incompressible, irrotational, extensional, three dimensional flow.
- (2) The sensitivity of the director trajectories, director steady states, scalar order parameter, tensor order parameter and flow-induced birefringence was analyzed with respect to the nematic potential, the alignment Deborah number, and the initial director orientation.
- (3) The director trajectories belong to geodesic meridian flow.
- (4) The director aligns, at steady state, anywhere in a plane normal to the extension direction and predictability is lost when initial director orientation is along the extension direction.

- (5) The governing parameter (alignment Deborah number) was used to classify the different elastic and viscous dominated relaxations of the director and the scalar order parameter.
- (6) For large Deborah number, the temporary flow-induced melting of the nematic phase may occur when the initial orientation of the director is near the extension direction.
- (7) The stable steady state value of the scalar order parameter is independent of the initial director orientation and is only a function of the alignment Deborah number and the nematic potential.
- (8) The presented unified view of the relaxation of discotic nematic under extension may be used to explain the characteristic pattern found in the cross-section of melt spun mesophase carbon fibers.

Chapter 3

- (1) The investigation of the nematorheology of uniaxial discotic nematics subjected to various extensional flows was performed.
- (2) The characterization of the sensitivity of the director paths, director steady states, scalar order parameter, tensor order parameter, and flow-induced birefringence was performed with respect to the flow types, alignment Deborah number, the nematic potential, and initial director orientation.
- (3) Using the unit sphere description, the director dynamics of uniaxial extensional and biaxial extensional flows were identified as geodesic meridian and non-geodesic (except for one special case) for planar extension.
- (4) The number of strains required to achieve steady state is governed by whether the flow is geodesic or non-geodesic. The number of strain units needed to reach steady state director orientation is larger in the case of planar extensional flow than for uniaxial extensional or biaxial extensional flows.
- (5) Some microstructural features of discotic nematic liquid crystals subjected to uniaxial, biaxial, and planar extensional flows exhibit sensitive dependence to the initial director orientation.

- (6) Biaxial extensional and planar extensional flows are strongly orienting flows as they have one stable director orientation (since $\mathbf{n} = -\mathbf{n}$); whereas uniaxial extensional flow is a weakly orienting flow since the stable states represent a degenerate circle.
- (7) The alignment strength $(|\tilde{\mathbf{A}}:\mathbf{nn}|)_{ss}$ of the flow scales with the magnitude of the ambient strain rate $(\mathbf{A}:\mathbf{nn})$.
- (8) Uniaxial extensional flow is a weakly aligning flow, whereas biaxial extensional and planar extensional flows are strongly aligning flows.

Chapter 4

- (1) Flow-induced biaxiality is simulated for a uniaxial discotic nematic liquid crystal subjected to a constant uniaxial, isothermal, irrotational, extensional, three dimensional flow.
- (2) A useful characterization of the sensitivity of the director triad $(\mathbf{n}, \mathbf{m}, \mathbf{l})$ trajectories, director triad steady states, uniaxial and biaxial scalar order parameters, and tensor order relaxations was performed with respect to the strength of the uniaxial nematic potential, the alignment Deborah number, and the initial director orientation.
- (3) The uniaxial director \mathbf{n} and the biaxial director \mathbf{l} trajectories exhibit geodesic meridian flow and belong to the same meridian, whereas the constant orientation of the biaxial director \mathbf{m} always lie on the equator.
- (4) The steady state orientations of the uniaxial director \mathbf{n} and the biaxial director \mathbf{m} lie on the compression plane (the equator); whereas the stable orientation of the biaxial director \mathbf{l} is the extension axis (along the poles).
- (5) The uniaxial alignment undergoes an initial decrease whereas the biaxial alignment shows an initial lag when the initial uniaxial director orientation is close to the extension axis.
- (6) Computed scientific visualizations of biaxial molecular orientation distributions are used to correlate the director triad dynamics and alignments dynamics.

5.3. Recommendations

The following modifications to the model presented in chapter 2 are recommended :

- (1) The description of the microstructure of the discotic nematic liquid crystal should be refined by constraining the (uniaxial) scalar order parameter S to a realistic range ($-\frac{1}{2} \leq S \leq 1$).
- (2) Frank elasticity should be included in the model to capture spatial variations of the microstructure.

After these modifications the model should be first applied to transient conical flows encountered in the converging spinneret of the fiber spinning process.